SID 66-286

A STUDY OF PROPELLANT BEHAVIOR AT ZERO GRAVITY

- Final Report -
(Contract NAS8-11097)

15 April 1966

Prepared by

E. T. Benedikt, Principal Investigator

Approved by

F. C. Hung
Assistant Director, Structures and Dynamics

NORTH AMERICAN AVIATION, INC.
SPACE and INFORMATION SYSTEMS DIVISION

081

SID 66-286

A STUDY OF PROPELLANT BEHAVIOR AT ZERO GRAVITY

- Final Report -
(Contract NAS8-11097)

15 April 1966

Prepared by

E. T. Benedikt, Principal Investigator

Approved by

F. C. Hung
Assistant Director, Structures and Dynamics

NORTH AMERICAN AVIATION, INC.
SPACE and INFORMATION SYSTEMS DIVISION

FOREWORD

This report was prepared by the Space and Information Systems Division of North American Aviation, Inc., for the George C. Marshall Space Flight Center, National Aeronautics and Space Administration, Huntsville, Alabama, under Contract NAS8-11097, "A Study of Propellant Behavior at Zero Gravity."

This work was performed under the direction of Dr. F. C. Hung, Program Manager, and Dr. E. T. Benedikt, Principal Investigator, assisted by R. Halliburton, B. Glicksberg, and P. Welch. The experimental phase of the study was supported by M. Suppanz, D. Fessett, J. Hall, J. Spurbeck, and M. C. Osimo. The contract was monitored by R. Ryan of the Aero-Astrodynamics Laboratory, MSFC.

ABSTRACT

Results of an analytical and experimental study of the behavior of liquids under conditions of zero gravity are presented.

A general analytical method has been formulated for the prediction of the kinematics of a liquid having a free surface and subjected to the joint action of gravitational, surface, and interfacial tension forces, as well as to the effects of an arbitrary translational motion imparted to the tank. The general formulas were specialized for application to the case of liquid in a cylinder subjected to axial and lateral forced translations. An automatic numerical procedure was developed for the integration of the equations of motion of the liquid. A concurrent experimental program provided data for verification of the analytical method.

A comparison of observed and computed results provides, satisfactory agreement within the computational accuracy maintained. Problems of heat transfer and boiling are discussed.

CONTENTS

ILLUSTRATIONS

INTRODUCTION

This report describes a method to predict the behavior of a liquid contained in a tank and subjected to the joint action of gravitational, surface, and interfacial tension forces, a situation which obtains typically in the case of space vehicle propellants.

The procedure consists of expanding the equation of the surface of the liquid in an appropriate series of orthogonal functions, and regarding its coefficients as generalized dynamical coordinates of the liquid system. The potential of the flow is similarly expressed by means of appropriate transformations as a series of these coefficients. It is thus possible to obtain the kinetic and potential (gravitational and surface) energy of the liquid and its Lagrangian function, modified by the requirement of the constancy of the volume of the liquid. From the knowledge of this function, the Lagrangian equations of motion are set up. Their integration provides the time history of the above dynamical coordinates. The behavior of the liquid, in particular the shape of the surface and the distribution of the pressure, can thus be determined. The effect of an arbitrary motion of the tank can also be easily taken into account by a slight modification of the Lagrangian function.

This procedure was applied in particular to the liquid contained in a vertical cylinder initially at rest under the action of terrestrial gravity and from which the latter is suddenly removed.

An automatic numerical procedure was developed for the integration of the equations of motion of the liquid; from it, the shape of the surface of the liquid in motion was synthetized for various instants of time.

A device to provide accurate experimentation with a liquid under conditions of zero or near-zero gravity was developed, employing the principle of the encapsulated cell. To implement this principle, a 100-foot tower was utilized to provide an effective free-fall time of 2.1 seconds. The encapsulated cell consists of a falling outer capsule, and an enclosed specimen cell in its evacuated interior. The outer capsule is 1 foot in diameter and 6 feet in height. The inner capsule is 6 inches in diameter and 1 foot in height. The liquid is contained in a quartz cylinder having an inside diameter of 1 inch and a height of 1 inch. For the duration of the experiment, this specimen cell falls freely inside the outer capsule. Since it is falling in a vacuum, it is free of aerodynamic drag, and falls faster than the outer capsule.

Data were registered by appropriate cinematographic equipment, which reproduced the theoretical situation, enabling a comparison to be made. Comparison of theoretical and experimental results have, so far, indicated a satisfactory agreement.

SECTION 1. DYNAMICS OF LIQUID MASSES PARTIALLY BOUNDED BY FREE SURFACES

In problems considered here, the liquid systems occupy a finite region of space. The geometry of the closed surface bounding such a region can be identified with sufficient generality by one or more functions of the type

$$F(x, y, z; a_1, a_2, \ldots, a_i; \ldots) = 0 \qquad (1\text{-}1)$$

in terms of a finite or countably infinite number of parameters a_i. These parameters which define the external configuration of the system can be used, as will energy from the following discussion, as generalized coordinates apt to define the dynamics of the system in most cases of interest. Such problems are most directly handled by the Lagrangian methods of analytical mechanics. Application of the method gives a definition of the constraints acting upon the system, its potential and kinetic energy, and the rate at which energy is dissipated. These contributions will be discussed separately.

CONSTRAINTS

The volume V occupied by the liquid in a given configuration is fully defined by the value of the parameters defining this configuration. Therefore, these parameters must be subjected to the constraint expressing the constancy of the volume. This constraint can be expressed in the differential form

$$\sum_k G_k \dot{a}_k = 0 \qquad (1\text{-}2)$$

where

$$G_k = \partial V / \partial a_k .$$

POTENTIAL ENERGY

Surface Energy

The free surface energy[1] of the system will be given by

$$U_* = \sum_a \sigma_a S_a \tag{1-3}$$

where S_a represents the areas of the various portions of the surface bounding the liquid and σ_a the coefficients of surface or interfacial tension, defining the energy required to increase the area of the given portion to the surface. This increase is brought about by the transfer of molecules from interior regions of the liquid to locations on or near the surface. The transfer involves a change in the energy of the intermolecular field to which the particles are subjected.

The areas S_i and, consequently, the potential energy are also identified by the values of the parameter, a_i.

Inertial or Gravitational Energy

The gravitational or inertial energy can be generally expressed in the form

$$U_o = \frac{1}{2} \rho \, ng_o \int_v z \, dv = \frac{1}{2} \rho \, ng_o \, \bar{z} \tag{1-4}$$

where z is a coordinate measuring distances along the direction and in the sense in which the intensity of the gravitational or inertial field (supposed to be uniform) and of intensity ng_o is acting, and $\bar{z}$ is the value of this coordinate pertaining to the center of mass of the system.

---

[1] These considerations must be regarded as restricted to cases in which the temperature of the liquid remains constant.

In this connection, the intermolecular forces responsible for surface tension phenomena are quite small as compared to ordinary gravitation or inertial forces. Hence, it is to be expected that the intensity of these forces must be quite small for intermolecular actions to be capable of significantly affecting the behavior of the liquid.

It has been estimated (Reference 2) that the effects of surface tension and those of a gravitational or inertial acceleration upon a liquid may become comparable when the load factor assumes a value

$$n_* = (\sigma/\rho\, g)\, L^2$$

where σ and ρ are, respectively, the coefficient of surface tension and the density of the liquid, and L the linear dimension of the region of space occupied by the liquid.[1]

RATE OF DISSIPATION OF ENERGY

The relative importance of surface tension as compared to viscous forces is found to be given by (Reference 1)

$$\frac{1}{\nu}\sqrt{\sigma L/\rho}$$

where ν is the kinematic viscosity. The largest physical dimension of the system for which viscous phenomena become important is given by

$$r_* = \nu^2/(\sigma\rho)$$

[1] In the case of surface tension phenomena, L is best defined as the radius $\sqrt{V/4\pi/3}$ of the sphere having a volume equal to that of the liquid mass. This sphere represents the configuration of minimum energy of the liquid system.

zero in the most common case where the boundaries are rigid) and continuous normal derivatives on the boundaries between two liquids. On the free surface, assumed to be defined by an equation of the type (1-1), we have

$$\frac{\partial F}{\partial x}\frac{\partial \phi}{\partial x} + \frac{\partial F}{\partial y}\frac{\partial \phi}{\partial y} + \frac{\partial F}{\partial z}\frac{\partial \phi}{\partial z} = -\frac{\partial F}{\partial t} = -\sum F_k \dot{a}_k \qquad (1\text{-}6)$$

where

$$F_k = \partial F / \partial a_k$$

The function ϕ can be generally represented as a linear combination

$$\phi = \sum \psi_k \dot{a}_k \qquad (1\text{-}7)$$

of the generalized velocities and certain functions ψ_k which must be subjected to the condition

$$\sum \Delta\psi \dot{a}_k = 0$$

In view of Equation (1-2), this relation will be satisfied if we take

$$\Delta\psi_k = \chi G_k, \qquad (1\text{-}8)$$

χ being a factor of proportionality. The boundary condition will be satisfied on a rigid boundary by requiring the normal derivative of ψ_k to vanish.

Condition (1-6) on a free boundary can be satisfied by requiring the ψ_k's to fulfill the condition

$$\frac{\partial F}{\partial x}\frac{\partial \psi_k}{\partial x} + \frac{\partial F}{\partial y}\frac{\partial \psi_k}{\partial y} + \frac{\partial F}{\partial z}\frac{\partial \psi_k}{\partial z} = -F_k \qquad (1-9)$$

The ψ_k's will thus be a function of the a_i's, but not of their derivatives.

In this development, as the solution to the continuity equation, $\text{div}\,\vec{v} = 0$, the gradient of a velocity potential has been chosen primarily for convenience in developing a general method for solving dynamical problems. The expression

$$\vec{v} = \text{grad}\,\phi + \text{curl}\,\vec{A}$$

where $\vec{A}$ is the vector potential could have been chosen for greater generality; however, in view of the analytical complications this involves, it is proposed to postpone analysis of this generalization.

Kinetic Energy

The kinetic energy of the system will be given by

$$\mathcal{T} = \frac{1}{2}\rho\int_v (\vec{v} + \vec{u})^2\, dv$$

where $\vec{u}$ is the velocity of the translatory motion of the container, and $\vec{v}$ the velocity of the liquid relative to the latter. Since the addition of an arbitrary function of the time to the Lagrangian leaves the equations unaffected, the expression for $\mathcal{T}$ can be replaced by the equivalent one

$$\mathcal{T} = \frac{1}{2}\rho\int_v (\vec{v}^2 + 2\,\vec{u}\cdot\vec{v})\, dv$$

If again we specialize the motion to be irrotational, applying well-known integral transformations and taking into account the appropriate boundary conditions, we obtain the identities

$$\int_v v^2 \, dv = \int_v (\text{grad } \Phi)^2 \, dv = \int_S \Phi \, \text{grad } \Phi \cdot \vec{n} dS = \int_{S_*} \Phi \, \text{grad } \Phi \cdot \vec{n} dS_*$$

and

$$\int_v \vec{u} \cdot \vec{v} dv = \vec{u} \cdot \int_v \text{grad } \Phi dv = \vec{u} \cdot \int_S \Phi \vec{n} dS$$

Making use of (1-7) and (1-9), it follows that the kinetic energy can be expressed as the quadratic form

$$\tau = \frac{1}{2} \rho \left(\sum_i \sum_k V_{ik} \dot{a}_i \dot{a}_k + 2 \sum_j \beta_j \dot{a}_j \right) \tag{1-10}$$

whose coefficients are given by

$$V_{ik} = - \int_S \frac{\psi_i F_k}{\sqrt{(\text{grad } F)^2}} dS \tag{1-11}$$

$$\beta_j = \vec{u} \cdot \int \psi_j \vec{n} dS$$

Using equations (1-10), (1-4), and (1-3), we can write the Lagrangian function

$$\mathcal{L} = \mathcal{T} - U - U_* + \lambda v$$

(λ indicating a Lagrangian multiplier) in the form

$$\mathcal{L} = \frac{1}{2}\rho \sum_{i,k}\left[V_{ik}\,\dot{a}_i\,\dot{a}_k + 2\sum_j \beta_j\,\dot{a}_j\right] + \frac{1}{2}\rho\, ng_o\,\bar{z} - \sum_\alpha \sigma_\alpha S_\alpha + \lambda\dot{v} \tag{1-12}$$

With the Lagrangian, we can immediately obtain the equations of motion in the form

$$\frac{d}{dt}\frac{\partial \mathcal{L}}{\partial \dot{a}_j} - \frac{\partial \mathcal{L}}{\partial a_j} = 0 \tag{1-13}$$

if the motion is conservative, or employing Equation (1-5)

$$\frac{d}{dt}\frac{\partial \mathcal{L}}{\partial \dot{a}_j} - \frac{\partial \mathcal{L}}{\partial a_j} + \frac{\partial \mathcal{R}}{\partial \dot{a}_j} = 0 \tag{1-13}$$

if dissipation is taken into account. It should be clear that if $\mathcal{L}$ is a known function of the a_i and $\dot{a}_i$, integration of these equations completely determines the motion. As will be pointed out in a subsequent article, the difficulty lies in obtaining the Lagrangian function.

Once the kinematics of the system are determined, the pressure distribution can be obtained immediately from the Bernoulli integral in the form

$$p = \rho \sum_i \left[\psi_i\right]_* \ddot{a}_i + \frac{1}{2}\rho \sum_{ik} \left[\text{grad}\,\psi_i \cdot \text{grad}\,\psi_k\right]_* \dot{a}_i\,\dot{a}_k + n g_o \left[\bar{z}\right]_* + \sigma\left(\frac{1}{R_1} + \frac{1}{R_2}\right)_* \tag{1-14}$$

where $(f)_*$ indicates the difference between the values which a function assumes on an arbitrary point of the surface and the point at which the pressure is derived. R_1 and R_2 are the principal radii of curvature of the liquid surface of this point.

Impulsive Motion

The case in which motion is imparted to the tank impulsively at a time $t = t_o$ is of particular interest. This implies that the translatory velocity imparted to the tank is 0, except for an infinitesimal duration τ, during which it becomes infinite in such a manner that the integral

$$\int_{t_o}^{t_o+\tau} \vec{u}(\tau)\,dt = \vec{u}_o$$

remains finite.

Integrating the various terms of equations of motion from t_o to $t_o + \tau$, we obtain

$$\int_{t_o}^{t_o+\tau} \frac{d}{dt}\frac{\partial \mathcal{T}}{\partial \dot{a}_i}\,dt = \left[\frac{\partial \mathcal{T}}{\partial \dot{a}_i}\right]_{t_o}$$

where the brackets indicate the discontinuity of a function at the instant of time t_o and

$$\int_{t_o}^{t_o+\tau} \frac{\partial \mathcal{T}}{\partial a_i}\,dt = \vec{u}^o \cdot \left(\frac{\partial}{\partial a_i}\sum_j \int \psi_j \vec{n}\,dS\right)_{t=t_o}$$

the remaining terms disappearing upon integration. Thus, we obtain the system of linear equations

$$\left(\sum_k V_{ik}\,\dot{a}_k + \beta_i\right)_{t=t_o} = \vec{u}^{\,o} \cdot \left(\frac{\partial}{\partial a_i}\sum_j \int \psi_j\,\vec{n}\,dS\right)_{t=t_o} \qquad (1\text{-}15)$$

for the determination in the discontinuities in the generalized velocities.

SECTION 2. DIFFERENTIAL EQUATIONS OF EPIHYDRODYNAMICS FOR A RIGHT CIRCULAR CYLINDER

The prediction of the kinematics of a liquid subject to gravity, surface, and interface tension (a situation that obtains typically in space vehicles), is based upon the so-called equation of epihydrodynamics derived in the previous section.

The initial task consists of integrating the preceding equations for the special case of a circular tank of semi-infinite height, with the idealizing assumption that the motion of the liquid is identical for all normal cross-sections of the tank.

It is further assumed that the motion is irrotational. The coefficients of the Fourier-Bessel series describing the free surface of the liquid will be taken as generalized (or Lagrangian) coordinates of the system. For the purpose of the present development, we shall assume that the surface is symmetrical about the vertical axis of symmetry of the tank. The position of points of the liquid will be referred to a cylindrical system of coordinates r, z having origin at the center of the bottom of the tank and vertical z axis.

The free surface of the liquid is describable by the equation

$$z = \sum_k A_k(t)\, J_o(\lambda_k r) \tag{2-1}$$

where

$$A_k(t) = \frac{2}{[RJ_o(\lambda_k R)]^2} \int_0^R f(r, t)\, J_o(\lambda_k r)\, r\, dr \tag{2-1'}$$

DETERMINATION OF THE KINEMATICS OF THE LIQUID

Since the motion of the liquid is assumed to be irrotational, the velocity can be derived from a potential Φ by means of the relation

$$\vec{v} = \text{grad}\ \Phi \tag{2-2}$$

In this case, the equation of continuity becomes

$$\text{div}\ \vec{v} = \Delta\Phi = 0 \tag{2-3}$$

indicating that Φ must be a harmonic function. The relations

$$\left(\frac{\partial \Phi}{\partial r}\right)_{r=R} = 0\ ; \tag{2-4}$$

$$\left(\frac{\partial \Phi}{\partial z}\right)_{z=0} = 0 \tag{2-4'}$$

must be fulfilled at the wall ($r = R$) and bottom ($z = 0$), respectively, of the tank. In addition, Lord Kelvin's condition,

$$\text{grad}\ f \cdot \text{grad}\ \Phi = -\frac{\partial f}{\partial t} \tag{2-5}$$

must be fulfilled upon the free surface of the liquid.

The function

$$\Phi = \sum_k C_k(t)\, J_o(\lambda_k r) \cosh \lambda_k z \qquad (2\text{-}6)$$

will be harmonic and will fulfill boundary conditions (2-4), (2-4′), whence the λ_k are roots of $J_1(\lambda_j R) = 0$. In order to fulfill the required boundary condition on the free surface, we must have

$$\sum_{k=1} \lambda_k C_k(t)\, J_1(\lambda_k r) \cosh \lambda_k f(r) \cdot \frac{\partial f}{\partial r}$$

$$+ \sum_{k=1} \lambda_k C_k(t)\, J_o(\lambda_k r) \sinh \lambda_k f(r) = \sum_{k=1} \dot{A}_k(t)\, J_o(\lambda_k r)$$

This relation can be expressed in the form

$$\frac{d}{dr} \sum_{k=1} C_k(t)\, J_1(\lambda_k r) \sinh \lambda_k f(r)$$

$$+ \sum_{k=1} C_k(t) \frac{J_1(\lambda_k r)}{r} \sinh \lambda_k f(r) = \sum_{k=1} \dot{A}_k(t)\, J_o(\lambda_k r)$$

where we have put

$$J_o = \frac{1}{\lambda_k}\left(\frac{dJ_1}{dr} - \frac{J_1}{r}\right)$$

so that, integrating both sides, we get equivalently

$$\sum_{k=1} C_k(t)\, J_1(\lambda_k r) \sinh \lambda_k f(r) = \sum_{k=1} \frac{1}{\lambda_k^2}\, \dot{A}_k(t)\, J_1(\lambda_k r)$$

Multiplying both members of this relation by $r J_1(\lambda_j r)$, and integrating over the interval $0 \le r \le R$, we obtain the system of linear equations

$$\sum_{k=1} C_k B_{jk} = \dot{A}_j \qquad (2\text{-}7)$$

with

$$B_{jk} = \frac{2\lambda_j^2}{[RJ_o(\lambda_j R)]^2} \int_0^R r J_1(\lambda_j r)\, J_1(\lambda_k r) \sinh \lambda_k f(r)\, dr \qquad (2\text{-}7')$$

If the transformation (2-7) has an inverse, it may also be written in the form

$$C_k = \sum_h \Gamma_{hk}\, \dot{A}_k$$

where we have put

$$\Gamma_{hk} = B^{-1}_{hk}$$

DYNAMICS OF LIQUID

Kinetic Energy

The kinetic energy of the laminar flow of the liquid will be given by

$$\mathcal{T} = \frac{1}{2} \rho \sum_{i,k} V_{ik} \dot{A}_i \dot{A}_k \tag{2-8}$$

where

$$V_{ik} = 2\pi \int_0^R \sum_h \Gamma_{hk} r J_o(\lambda_i r) J_o(\lambda_k r) \cosh \lambda_{k_1} f(r) \, dr \tag{2-8'}$$

Potential Energy

Gravitational (or Inertial) Energy

The gravitational energy of the system will be given by

$$U_o = \pi \rho n g_o \int_0^R z^2 r dr = \frac{\pi}{2} \rho n g_o R^2 \sum_i [A_i J_o(\lambda_i R)]^2 \tag{2-9}$$

where g_o represents the position-dependent terrestrial acceleration of gravity, n the load factor.

Surface Energy

The surface energy of the liquid will be given by

$$U_* = \int_S \sigma \, d\, S \tag{2-10}$$

where S indicates the surface bounding the liquid, and σ indicates the surface or interfacial tension typical of the pertinent surface/vapor or surface (solid) wall boundary. When the inessential constant contribution of the interfacial energy of the bottom of the tank is suppressed, Equation (2-10) becomes

$$U_* = 2\pi \sigma_o \int_0^R \sqrt{1 + \left(\frac{dz}{dr}\right)^2} \, rdr + 2\pi\sigma_1 z_1 R$$

$$= 2\pi \sigma_o \int_0^R \left\{ 1 + \left[\sum_k \lambda_k A_k J_1(\lambda_k r) \right]^2 \right\}^{1/2} rdr$$

$$+ 2\pi\sigma_1 R \sum_{i=0} A_i J_o(\lambda_i R) \tag{2-10'}$$

where we have put

$$z_1 = f(R)$$

and $\sigma = \sigma_o$ on free surface of the liquid, and $\sigma = \sigma_1$ on the solid boundary.

Kinetic Potential

Collecting Equations (2-8), (2-9), and (2-10'), the kinetic potential (or Lagrangian function) of the dynamic process here considered will thus be given by

$$\mathcal{L} = \mathcal{T} - U_o - U_* = 1/2\ \rho \sum_{i,k} V_{ik} \dot{A}_i \dot{A}_k - \frac{\pi}{2} \rho n g_o R^2 \sum_i \left[A_i J_o(\lambda_i R)\right]^2$$

$$- 2\pi \sigma_o \int_0^R \left\{ 1 + \left[\sum_k \lambda_k A_k J_1(\lambda_k r) \right]^2 \right\}^{1/2} r\,dr$$

According to Hamilton's principle, the motion of the liquid must occur in such a manner that

$$\delta \left[\int_0^t \mathcal{L}\, dt + 2\pi \sigma_1 f_1 R \right] = 0 \qquad (2\text{-}11)$$

In addition, the mass or, in our case, the volume (v) of the liquid must be constant, thus requiring the introduction of the constraint

$$\dot{v} = \sum_j G_j \dot{A}_j = 0 \qquad (2\text{-}12)$$

where

$$G_j = \frac{\partial v}{\partial A_j} = 2\pi \int_0^R r J_o(\lambda_j r)\, dr = \pi R^2 \delta_{jo} \qquad (2\text{-}12')$$

upon the values of the coordinates A_j. This requirement can be fulfilled by replacing Equation (2-12) with the condition

$$\delta \left(\int_0^t \mathcal{J} \, dt + 2 \sigma_1 f_1 R \right) = 0 \qquad (2\text{-}13)$$

where

$$\mathcal{J} = \mathcal{L} + \Lambda \dot{v} \qquad (2\text{-}13')$$

Λ being a Lagrangian multiplier, ultimately determinable on the basis of Equation (2-12).

EQUATIONS OF MOTION

It immediately follows that, if Equation (2-13) is to be an extremum, $\mathcal{J}$ must satisfy the system of differential equations

$$\frac{d}{dt} \frac{\partial \mathcal{J}}{\partial \dot{A}_i} - \frac{\partial \mathcal{J}}{\partial A_i} = -2\pi \sigma_1 R \frac{\partial f_1}{\partial A_i} \qquad (2\text{-}14)$$

which provide after the indicated operations are performed, equations of motion in the form

$$\sum_k (V_{ik} + V_{ki}) \ddot{A}_k + \sum_{jk} \left[\left(\frac{\partial V_{ik}}{\partial \dot{A}_j} + \frac{\partial V_{ki}}{\partial \dot{A}_j} \right) - \left(\frac{\partial V_{jk}}{\partial \dot{A}_i} + \frac{\partial V_{kj}}{\partial \dot{A}_i} \right) \right] \dot{A}_j \dot{A}_k - \pi n g_o [R J_o(\lambda_j R)]^2 \dot{A}_j$$

$$- \frac{4\pi \sigma_o}{\rho} \sum_k \int^R \frac{\lambda_j \lambda_k J_1(\lambda_j r) J_1(\lambda_k r)}{\left| 1 + \left[\sum_j \lambda_j A_j J_1(\lambda_j r) \right]^2 \right|^{1/2}} \, dr - \frac{2\pi}{\rho} \Lambda R \dot{A}_o = - \frac{4\pi}{\rho} R \sigma_1 \frac{\partial f_1}{\partial \dot{A}_j} \qquad (2\text{-}15)$$

Differentiating Equation (2-8′) with respect to A_i, we obtain

$$\frac{\partial V_{jk}}{\partial A_i} = \sum_h \int_0^R \left\{ \frac{\partial \Gamma_{hk}}{\partial A_i} J_o(\lambda_j r) J_o(\lambda_k r) \cosh \lambda_k f(z) \right.$$

$$\left. + \lambda_h \Gamma_{hk} J_o(\lambda_j r) J_o(\lambda_k r) \sinh [\lambda_k f(z)] \frac{\partial f(z)}{\partial A_i} \right\} r dr \qquad (2-16)$$

The derivative of Γ_{hk} can be obtained in the following manner. Since Γ is the inverse of the matrix B,

$$\sum_\ell B_{j\ell} \Gamma_{\ell k} = \delta_{jk} \qquad (2-17)$$

and

$$\sum_\ell \frac{\partial B_{j\ell}}{\partial A_i} \Gamma_{\ell k} + B_{j\ell} \frac{\partial \Gamma_{\ell k}}{\partial A_i} = 0 \qquad (2-17')$$

Hence, by premultiplying relation (2-17′) by Γ_{hj} and using relation (2-17) we get

$$\frac{\partial \Gamma_{hk}}{\partial A_i} = -\sum_j \Gamma_{hj} \frac{\partial B_{j\ell}}{\partial A_i} \Gamma_{\ell k} \qquad (2-18)$$

where

$$\frac{\partial B_{j\ell}}{\partial A_i} = \frac{2\lambda_j^2}{[R J_o(\lambda_j R)]^2} \int_0^R \lambda_\ell r J_1(\lambda_j r) J_1(\lambda_\ell r) J_o(\lambda_i r) \cosh [\lambda_\ell f(z)] dr \qquad (2-18')$$

Using the adimensional variables,

$$r = \ell\xi\,;\; z = r\zeta\,;\; A_k = \ell a_k\,;\; t = t_o\tau\,;\; \gamma_{ik} = \Gamma_{ik}\ell\,;\; \lambda = \Lambda R\,;\; \lambda_k = a_k\ell$$

where

$$\ell = \sqrt{\frac{\sigma}{\rho n g_o}}\,; \qquad t_o = \sqrt{\frac{\sigma L^3}{\rho}}\,; L = \sqrt[3]{\frac{\nu}{(4/3)\pi}}$$

and employing the notation,

$$F' = \frac{\partial F}{\partial \tau}$$

the previous equations are later put into a nondimensional form that is more amenable to calculation.

CONVERGENCE OF SERIES AND RESCALING OF THE INVERSION MATRIX[1]

The classical Riesz-Fischer theorem gives the following criterion for convergence of the Fourier-Bessel series (2-1). This series will converge only if the series

$$\sum_{k=0}^{\infty} \left[A_k J_o(\lambda_k R)\right]^2 \qquad (2\text{-}19)$$

where $\lambda_k R$ is the kth root of J_1, converges. Furthermore, if the initial free surface f(r, 0) is continuous in r from 0 to R and has only a finite number of maxima and minima in this interval, the series (2-1) will converge to f(r, 0), the coefficients being given by (2-1). Then, to demonstrate convergence for $t > 0$, a bound on the time derivatives of the sequence $\{A_k\}$ is required. In

[1] Work discussed in this section and in parts of the next section was done under subcontract to Measurement Analysis Corporation and is reported in Reference 5.

particular, if the series $\Sigma(\dot{A}_k)^2/(2k+1)$ converges for some range of time, $0 \le t \le t_*$, the series will converge for this same time range.

But, from the asymptotic forms, for large k we have

$$\lambda_k R \sim (k + 1/4)\pi \tag{2-20}$$

and

$$J_o(\lambda_k R) \sim \frac{2(-1)^k}{\pi\sqrt{2k+1}} \tag{2-21}$$

Introducing expressions (2-20) and (2-21) into the expression (2-19) if is found that the necessary and sufficient condition for the convergence of series (2-1) is that

$$\sum_{k=0}^{\infty} \frac{A_k^2}{2k+1} \tag{2-22}$$

converges. By the same reasoning, the series of Equations (2-6) will converge for $0 \le r \le R$ and $0 \le z \le z_*$, only if the series

$$\sum_{k=1}^{\infty} \frac{C_k^2 (\cosh \lambda_k z_*)^2}{2k+1} \tag{2-23}$$

converges. But $(\cosh \lambda_k z_*)^2 \sim 1/4 \exp\{(2\pi + 1/2)kz_*\}$, and so C_k must be at least exponentially decreasing in k to maintain the convergence. Thus, the numbers $c_k = C_k \cosh \lambda_k z$, which may be of intermediate size, are written awkwardly as the product of a very large number and a very small number. This is also the case in the inversion of the matrix B_{jk} given by Equation (2-7').

[1]Work discussed in this section and in parts of the next section was done under subcontract to Measurement Analysis Corporation and is reported in Reference 5.

These difficulties may be circumvented by rewriting the potential in the form

$$\phi = \Sigma c_k e^{-\lambda_k z_*} J_o(\lambda_k r) \cosh \lambda_k z \qquad (2\text{-}24)$$

where z_* should be regarded as slightly larger than the maximum value of z expected on the free surface. The substitution,

$$C_k = c_k e^{-\lambda_k z_*} \qquad (2\text{-}25)$$

replaced in Equation (2-7) provides the determination,

$$\dot{A}_j = \Sigma B_{jk} e^{-\lambda_k z_*} Ck \qquad (2\text{-}26)$$

$$= \Sigma D_{jk} c_k \qquad (2\text{-}26)$$

where

$$D_{jk} = \frac{2\lambda_j^2}{R^2 J_o^2(\lambda_j R)} \int_0^R r J_1(\lambda_j r) J_1(\lambda_k r)$$

$$\cdot e^{-\lambda_k z_*} \sinh(\lambda_k f)\, dr \qquad (2\text{-}27)$$

In the process of the numerical integration, the factor $e^{-\lambda_k z_*} \sinh \lambda_k f$ should be computed as

$$\frac{1}{2}\left(e^{\lambda_k (f - z_*)} - e^{-\lambda_k (f + z_*)}\right) \qquad (2\text{-}28)$$

where the first term will be the dominant one; and since $z_* > f$, the entire expression will be smaller than 1, thus avoiding the aforementioned scaling difficulties.

Since the elements, D_{jk}, will be moderate in size, the inversion of matrix D presents no particular difficulties, and a standard elimination scheme is adequate up to at least order 70.

AUTOMATIC NUMERICAL DETERMINATION OF TRANSIENT MENISCI OF LIQUID CONTAINED IN A CYLINDRICAL TANK

The velocity potential, ϕ, will be written in terms of the series

$$\phi = \Sigma C_k J_o(\lambda_k r) \cosh \lambda_k r \, e^{-\lambda_k z_*} \tag{2-29}$$

where $C_k = c_k e^{-\lambda_k z_*}$, as introduced earlier. This change will introduce the term $e^{-\lambda_k z_*}$ into the equations of motion (2-15).

The nondimensional form of the equations of motion are

$$\sum_k \left(\hat{V}_{jk} + \hat{V}_{kj}\right) a_k'' + \sum_k \left(\dot{\hat{V}}_{jk} + \dot{\hat{V}}_{kj}\right) a_k' +$$

$$-\sum_{jk} \frac{\partial \hat{V}_{ik}}{\partial a_j} a_j' a_k' + J + P + H = 0 \tag{2-30}$$

where

$$\hat{V},\ \dot{\hat{V}},\ \frac{\partial \hat{V}}{\partial a_j},\ J,\ P,\ \text{and } H$$

are defined as the following:

$$\hat{V} = M\gamma$$

$$M_{jk} = + 2\pi \ell_o \int_o^{\xi_1} J_o(a_j \xi)\, J_o(a_k \xi) \cosh\left[a_k \Sigma_n a_n J_o(a_n \xi)\right] e^{-a_k \xi} \xi\, d\xi$$

$$\hat{V} = M\dot{\gamma} + \dot{M}\gamma \qquad (2\text{-}31)$$

$$\dot{M}_{jk} = + \frac{2\pi \ell_o}{\tau_o} \int_o^{\xi_1} J_o(a_j \xi)\, J_o(a_k \xi) \sinh\left[a_k \sum_n a_n J_o(a_n \xi)\right] \cdot \qquad (2\text{-}32)$$

$$\cdot\, a_k \sum_n a'_n J_o(a_n \xi)\, e^{-a_k \xi} \xi\, d\xi \qquad (2\text{-}32)$$

$$\gamma = D^{-1}$$

$$D_{jk} = \frac{2a_j}{\ell_o \left[\xi_1 J_o(a_j \xi_1)\right]^2} \int_o^{\xi_1} J_1(a_j \xi)\, J_1(a_k \xi) \sinh\left[a_k \sum_n a_n J_o(a_n \xi)\right] \cdot$$

$$\cdot\, e^{-a_k \xi} \xi\, d\xi \qquad (2\text{-}33)$$

$$\dot{\gamma} = -\gamma \dot{D} \gamma$$

$$\dot{D} = \frac{2 a_j a_k}{\xi_1^2 \ell_o^2 J_o^2 (a_j \xi_1)} \int_o^{\xi_1} J_1 (a_j \xi) J_1 (a_k \xi) \cosh \left[a_k \sum_n a_n J_o (a_n \xi) \right] \cdot$$

$$\cdot \sum_n a'_n J_o (a_n \xi) e^{-a_k \xi} \xi \, d\xi \qquad (2\text{-}34)$$

$$\frac{\partial \bar{V}_{ji}}{\partial a_m} = E\gamma - M\gamma \, F\gamma$$

$$E_{jk} = +2\pi \ell_o a_k \int J_o (a_j \xi) J_o (a_k \xi) J_o (a_m \xi) \cdot$$

$$\cdot \sinh \left[a_k \sum_n a_n J_o (a_n \xi) \right] e^{-a_k \xi} \xi d\xi \qquad (2\text{-}35)$$

$$F_{jk} = \frac{2 a_j a_k}{\ell_o^2 \xi_1^2 J_o^2 (a_j \xi_1)} \int_o^{\xi_1} J_1 (a_j \xi) J_1 (a_k \xi) J_o (a_m \xi) \cdot$$

$$\cdot \cosh \left[a_k \sum_n a_n J_o (a_n \xi) \right] e^{-a\xi} \xi \, d\xi \qquad (2\text{-}36)$$

$$J = -\pi n g_o \left[\xi_1 J_o (a_j \xi_1)\right]^2 a_j \tag{2-37}$$

$$P = -\frac{4\pi\sigma_o \ell_o}{\rho} \sum_k \int_o^{\xi_1} \frac{a_k a_j a_k J_1 (a_k \xi) J_1 (a_j \xi) \xi \, d\xi}{\left\{1 + \left[\sum_n a_n a_n J_1 (a_n \xi)\right]^2\right\}^{1/2}} \tag{2-38}$$

$$H = \frac{4\pi \xi_1}{\rho} \sigma_1 J_o (a_j \xi) \tag{2-39}$$

Let

$$\hat{V}_{jk} + \hat{V}_{kj} = W$$

$$\dot{\hat{V}}_{jk} + \dot{\hat{V}}_{kj} = \dot{W}$$

$$U = E - M\gamma F\gamma$$

The equations of motion then become

$$Wa'' + \dot{W}a' - Ua'^2 + J + P + H = 0 \tag{2-40}$$

or

$$a'' = W^{-1} \left[-\dot{W}a' + G - J - P - H\right] \tag{2-41}$$

The initial conditions are obtained from

$$a_k(0) = \frac{2}{\left[\xi_1 J_o(a_k \xi_1)\right]^2} \int^{\xi_1} f(\xi, 0)\, J_o(a_k \xi)\, \xi\, d\xi \qquad (2\text{-}42)$$

where $f(\xi, 0)$ is the equation of the free surface at time (t) = zero. At time zero, the surface is in equilibrium, and so $a'_k(0) = 0$. The flow chart for the computer program used is shown in Figure 1. The number of generalized coordinates used to obtain a solution for the free surface was determined by the two following primary facts:

1. The number of coordinates necessary to represent the free surface to some degree of accuracy, and

2. Choice of the least number of coordinates that can be used to maintain accuracy and keep the time required for one time interval a minimum.

Under the first consideration, it was found that a maximum of 20 coordinates could be used before there were introduced machine errors that were more significant that the error in truncating the series representation for the free surface.

$$F(\xi, t) = \sum_k a_k(t)\, J_o(a_k \xi)$$

The time required for one time interval is a function of the number of generalized coordinates used and the integration error criteria. There are approximately $(5+2n)n^3$ (n = number of generalized coordinates) integrations to be performed in one time interval. The number of integrations is of the order of $2n^3$. The time required for one integration depends on the error criteria.

An Adams-Moulton six-point predictor-corrector routine was used to perform the integrations in the program. This routine enables the integrals to be obtained to a high degree of accuracy.

The integrals being evaluated are all products of Bessel functions of the first and second kind. These functions are sinusoidal in nature, with

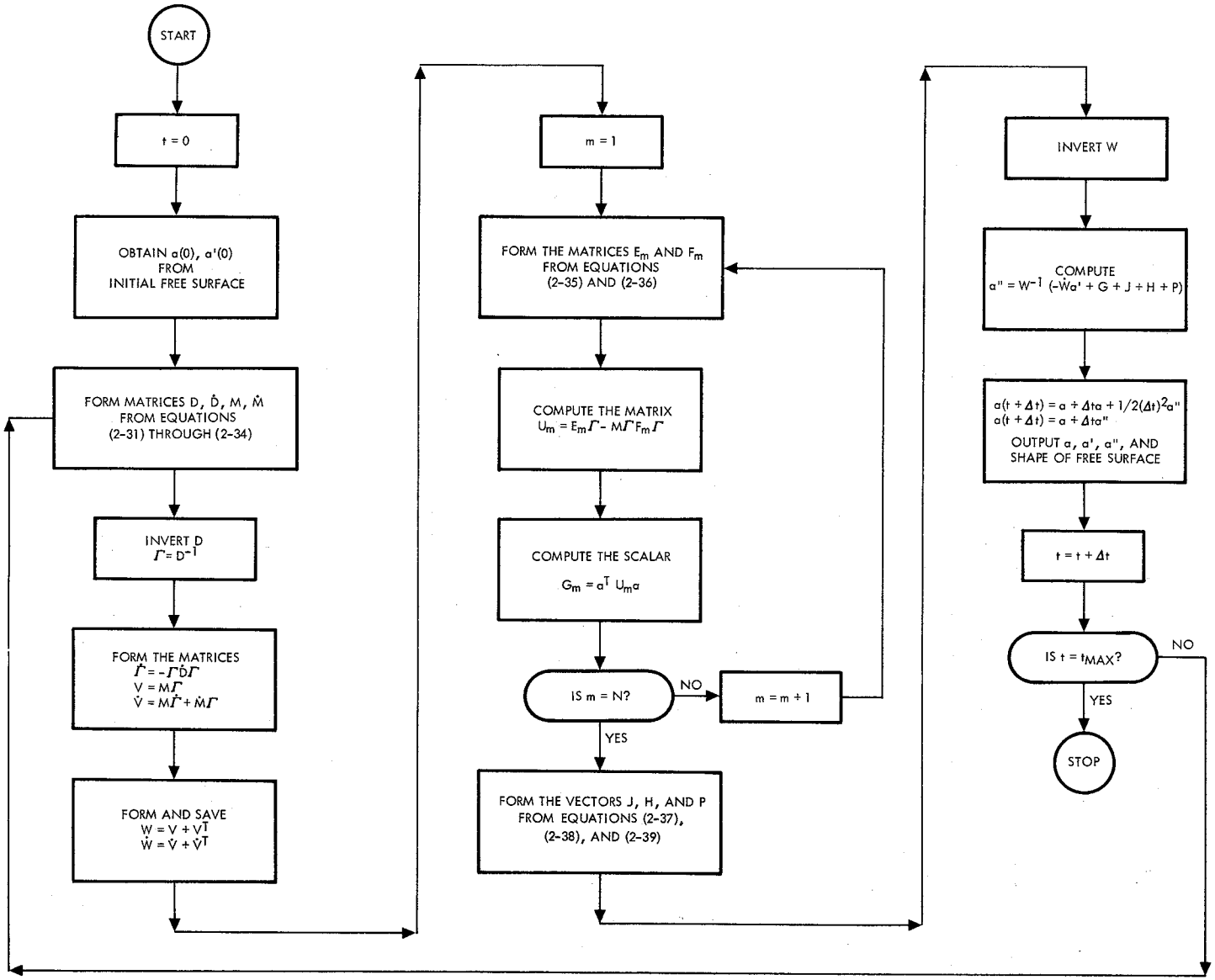

Figure 1 . Flow Chart of Computer Program

amplitude decreasing as the number of roots considered increases, thus requiring the use of a very good integration routine.

The error criteria used for the integration routine will yield answers to a ± tolerance per integrated step. This tolerance can be as low as 10^{-7}, i.e., at least seven significant digits per integrated step. All integrals that were considered required from 50 to 300 integrated steps. Since the errors tend to compensate in oscillatory functions, the accuracy of each integral could be obtained to 5 to 6 significant digits. The problem is that the time to evaluate each integral is a function of the error. Generally speaking, for the functions used, an increase in the error by two orders of magnitude will double the integration time. This is true if the number of coordinates, n, (the number of roots used in the Bessel functions) is 10 or less. When the number of coordinates is greater than 10, the time more than doubles when the error limit is increased by two orders of magnitude. For this reason, 10 coordinates were selected as the maximum. (The partial completion of one time interval for 15 coordinates indicated that it would require about 2-1/2 hours of IBM 7094 time for one complete time increment.)

Further investigation revealed that it was better to use a smaller number of coordinates with a small error limit than a greater number of coordinates with a larger error limit. When the time required for these two cases was the same, the answers were more stable when the smaller tolerance was used.

In the final production runs of the program, six coordinates with the error limit of 10^{-3} to 10^{-5} are used. It requires 25 minutes of IBM 7094 time to complete one time increment. The choice of Δt (time increment) size is governed by ensuring that neglected terms in the Taylor series expansion ($\Delta t^3/3!$) for the new generalized coordinates are smaller than the least significant digit of the last good generalized coordinates.

Visual verification is also possible because, if the time increment is too large, instability of the free surface becomes apparent. A maximum time step of 0.05τ, where τ is the approximate length of the period (given in Reference 1), has been used.

The integrations involved in obtaining D and W have the smallest error limits since these matrices must be inverted in the subsequent calculations for the generalized accelerations. The routine for inverting these matrices uses double precision and the logarithm of the pivotal values to increase the accuracy of the inversion process. Double precision integration routines are not used because no additional accuracy can be obtained unless an error limit less than 10^{-7} is used.

The results obtained for the first fifth of the period are contained in Section 5. The graphs indicate that the free surface rounds off at the wall of the tank. This round-off is a good measure of the truncation error and the total numerical error. At time t = 0 (initial configuration), if the smallest error and largest number of generalized coordinates are used, this error decreases appreciably but does not vanish. By neglecting the round-off and extending the curve of the free surface near the wall until it intersects the latter, the curve is a good representation of the correct contact angle to within ±0.5 percent. Therefore, it is evident that the prediction of the constancy and magnitude of the contact angle, as established in Reference 1, is confirmed. Hence, the rounding off of the menisci at the container wall is, in reality, the contact angle calculated to an accuracy of approximately 5 percent.

The total error introduced in the calculation of the free surface is approximately five percent, indicating that the value of the free surface at any point is within five percent of a smooth curve representation of the free surface. This five-percent error exists in the numerical calculation and truncation. It does not mean the method used to obtain the results is incorrect.

EFFECT OF FORCED TRANSLATORY MOTION OF TANK

If the cylindrical tank is moving at a uniform time-dependent velocity $\vec{u} = \vec{u}(t)$ relative to an absolute system of reference, the motion cannot, in general, be cylindrically symmetrical, and the general expression of the kinetic energy (2-10) will have to be used in the derivation of the Lagrangian equations of motion.

Dynamic Coordinates

The surface of the liquid will be expressed in the form of the series

$$z = f(r,\theta) = \sum_{j,\,h=0}^{\infty} J_j(\lambda_{jh} r)\left[A_{jh}^{(1)} \cos j\theta + A_{jh}^{(2)} \sin j\theta\right] \qquad (2\text{-}43)$$

where the λ_{jh}'s are the roots of the equation

$$J_j'(\lambda R) = 0$$

The $A_{jh}^{(1)}$, $A_{jh}^{(2)}$ now constitute the generalized coordinates of the liquid system. If another functional expression of $z = f(r, \theta)$ is known, these coordinates can be determined by means of the expressions

$$A_{jh}^{(1)} = \frac{2\lambda_{jh}^2}{\epsilon_j \pi \left[\lambda_{jh}^2 R^2 - j^2\right] \left[J_j(\lambda_{jh} R)\right]^2} \int_o^R r J_j(\lambda_{jh} r) \int_o^{2\pi} f(r, \theta) \cos j\theta \, d\theta \, dr \qquad (2\text{-}43')$$

$$\left(\epsilon_j = \begin{cases} 2 \text{ for } j = 0 \\ 1 \text{ for } j \neq 0 \end{cases}\right)$$

$$A_{jh}^{(2)} = \frac{2\lambda_{jh}^2}{\pi \left[\lambda_{jh} R^2 - j^2\right] \left[J_j(\lambda_{jh} R)\right]^2} \int_o^R r J_j(\lambda_{jh} r) \int_o^{2\pi} f(r, \theta) \sin j\theta \, d\theta \, dr \qquad (2\text{-}43'')$$

Velocity Potential and Kelvin's Condition

The velocity potential must now have the form

$$\Phi = \sum_{n,k=0}^{\infty} J_n(\lambda_{nk} r) \cosh \lambda_{nk} z \left[C_{nk}^{(1)} \cos n\theta + C_{nk}^{(2)} \sin n\theta\right] \qquad (2\text{-}44)$$

fulfilling the required boundary conditions on the sides and bottom of the tank. Their expression, in terms of the dynamical coordinates, can be obtained from Lord Kelvin's relation which, in this case, assumes the form

$$\frac{\partial f}{\partial r}\left(\frac{\partial \Phi}{\partial r}\right)_* + \frac{1}{r^2}\frac{\partial f}{\partial \theta}\left(\frac{\partial \Phi}{\partial \theta}\right)_* - \left(\frac{\partial \Phi}{\partial z}\right)_* = -\frac{\partial f}{\partial t}$$

where $\left(\quad\right)_*$ indicates values which the function in parenthesis assumes on the free liquid surface, determined for $z = f(r, \theta)$. Inserting Equation (2-43) into this formula, we obtain after some transformation

$$\sum_{n,k=0}^{\infty} \frac{1}{\lambda_{nk}} C_{nk}^{(1)} \left[J_n'(\lambda_{nk} r) \frac{\partial}{\partial r} \sinh(\lambda_{nk} f) \cos n\theta \right.$$

$$\left. - \frac{n}{r} J_n(\lambda_{nk} r) \frac{\partial}{\partial \theta} \sinh(\lambda_{nk} f) \sin n\theta - \lambda_{nk}^2 J_n(\lambda_{nk} r) \sinh(\lambda_{nk} f) \cos n\theta \right]$$

$$+ \sum_{n,k} \frac{1}{\lambda_{nk}} C_{nk}^{(2)} \left[J_n'(\lambda_{nk} r) \frac{\partial}{\partial r} \sinh(\lambda_{nk} f) \sin n\theta + \right.$$

$$\left. + \frac{n}{r} J_n(\lambda_{nk} r) \frac{\partial}{\partial \theta} \sinh(\lambda_{nk} f) \cos n\theta - \lambda_{nk}^2 J_n(\lambda_{nk} r) \sinh(\lambda_{nk} f) \sin n\theta \right]$$

$$= - \sum_{\ell,j=0}^{\infty} J_\ell(\lambda_{\ell j} r) \left[\dot{A}_{\ell j}^{(1)} \cos \ell\theta + \dot{A}_{\ell j}^{(2)} \sin \ell\theta \right]$$

Multiplying both sides of the relation, respectively, by $r J_m(\lambda_{mj} r) \cos m\theta$ and $r J_m(\lambda_{mj} r) \sin m\theta$, we obtain the system of linear equations

$$\sum_{n,k} \left(B_{nk\ell j}^{(1,1)} C_{nk}^{(1)} + B_{nk\ell j}^{(1,2)} C_{nk}^{(2)} \right) = \dot{A}_{\ell j}^{(1)} \qquad (2\text{-}45)$$

$$\sum_{nk} \left(B_{nk\ell j}^{(2,1)} C_{nk}^{(1)} + B_{nk\ell j}^{(2,2)} C_{nk}^{(2)} \right) = \dot{A}_{\ell j}^{(2)} \qquad (2\text{-}45')$$

for the determination of the $\dot{A}_{\ell j}$ in terms of the C_{nk}'s

where

$$B_{nk\ell j}^{(\alpha,\beta)} = \frac{2\lambda_{\ell j}^2 / \lambda_{nk}}{\epsilon_\ell \pi \left[\lambda_{\ell j}^2 R^2 - \ell^2 \right] \left[J_\ell(\lambda_{\ell j} R) \right]^2}$$

(continued on next page)

$$\cdot \int_o^R \int_o^{2\pi} r \Bigg[J_n' (\lambda_{nk} r)\, J_\ell (\lambda_{\ell j} r)\, \frac{\partial}{\partial r} \sinh \lambda_{nk} f\, {}^{(I)}Q^{(\alpha,\beta)}_{n\ell}$$

$$+ n J_n (\lambda_{nk} r)\, J_\ell (\lambda_{\ell j} r)\, \frac{\partial}{\partial \theta} \sinh \lambda_{nk} f\, {}^{(II)}Q^{(\alpha,\beta)}_{n\ell}$$

$$- \lambda^2_{nk} r\, J_n (\lambda_{nk} r)\, J_\ell (\lambda_{\ell j} r) \sinh \lambda_{nk} f\, {}^{(I)}Q^{(\alpha,\beta)}_{nf} \Bigg] d\theta\, dr \qquad (2\text{-}46)$$

with $\alpha, \beta = 1, 2$ and

$${}^{(I)}Q^{(1,1)}_{n\ell} = \cos n\theta \cos \ell\theta \qquad {}^{(II)}Q^{(1,1)}_{n\ell} = -\sin n\theta \cos \ell\theta$$

$${}^{(I)}Q^{(1,2)}_{n\ell} = \sin n\theta \cos \ell\theta \qquad {}^{(II)}Q^{(2,2)}_{n\ell} = \cos n\theta \cos \ell\theta$$

$${}^{(I)}Q^{(2,1)}_{n_\ell} = \cos n\theta \sin \ell\theta \qquad {}^{(II)}Q^{(2,1)}_{n\ell} = -\sin n\theta \sin \ell\theta$$

$${}^{(I)}Q^{(2,2)}_{n\ell} = \sin n\theta \sin \ell\theta \qquad {}^{(II)}Q^{(2,2)}_{n_\ell} = \cos n\theta \sin \ell\theta$$

By inverting the matrix formed by the $B^{(\alpha,\beta)}_{nk\ell j}$ (regarded as a square matrix with respect to the indexes (nk), (ℓj)), and putting $\Psi^{(\alpha)}_{ik} = \sum_{\ell m} J_i (\lambda_{ik} r) \cdot \cdot \left[\Gamma^{(\alpha,1)}_{ik\ell m} \cos i\theta + \Gamma^{(\alpha,2)}_{ik\ell m} \sin i\theta \right] \cosh \lambda_{ik} f$, we obtain the required expression

$$\Phi = \sum_{ik} \left(\psi^{(1)}_{ik}\, \dot{A}^{(1)}_{ik} + \psi^{(2)}_{ik}\, \dot{A}^{(2)}_{ik} \right) \qquad (2\text{-}47)$$

of the potential in terms of the generalized coordinates, where

$$C^{(\alpha)}_{nk} = \sum_{\ell j} \sum_{\beta=1}^{2} \Gamma^{(\beta,\alpha)}_{nk\ell j}\, \dot{A}^{(\beta)}_{nk} \qquad (2\text{-}48)$$

Kinetic Energy

In terms of the generalized coordinates introduced here, the kinetic energy of the system will assume the form

$$\mathcal{T} = \frac{1}{2}\rho \left[\sum_{ikjh} \sum_{\alpha,\beta=1}^{2} \left(V_{ikjh}^{(\alpha,\beta)} + V_{jhik}^{(\alpha,\beta)} \right) \dot{A}_{ik}^{(\alpha)} \, A_{jh}^{(\beta)} + 2 \sum_{jh} \sum_{\alpha=1}^{2} \beta_{jh}^{(\alpha)} \dot{A}_{jh}^{(\alpha)} \right] \quad (2\text{-}49)$$

Using S_o to indicate the bottom of the tank, we have $dS_o = dS \cos(\vec{n}, z) = dS / \sqrt{|\text{grad } F|^2}$. Since $F = -f(r,\theta) + z$, formula (2-11) gives

$$V_{ikjh}^{(\alpha,\beta)} = \int_{S_o} \psi_{ik}^{(\alpha)} f_{jh}^{(\beta)} \, dS_o \quad (2\text{-}50)$$

where we have put

$$f_{jk}^{(1)} = \frac{\partial f}{\partial A_{jk}^{(1)}} = J_j(\lambda_{ih} r) \cos j\theta, \quad f_{jh}^{(2)} = \frac{\partial f}{\partial A_{jk}^{(2)}} = J_j(\lambda_{jh} r) \sin j\theta \quad (2\text{-}51)$$

Equation (2-11) can be written now in the form

$$\beta_{ik}^{(\alpha)} = u_r \, a_{ik}^{(\alpha)} + u_\theta \, b_{ik}^{(\alpha)} + u_z \, c_{ik}^{(\alpha)} \quad (2\text{-}52)$$

where u_r, u_θ, u_z are the radial, longitudinal, and axial components, respectively, of $\vec{u}$ and

$$a_{ik}^{(\alpha)} = \int_{S_o} \psi_{ik}^{(\alpha)} \frac{\partial f}{\partial r} \, dS_o + \int_{S_1} \psi_{ik}^{(\alpha)} \, dS_1; \quad b_{ik}^{(\alpha)} = \int_{S_o} \psi_{ik} \frac{\partial f}{r \partial \theta} \, dS_o;$$

$$c_{ik}^{(\alpha)} = -2 \int_{S_o} \psi_{ik}^{(\alpha)} \, dS_o \quad (2\text{-}53)$$

S_1 indicating the lateral surface of the tank

Gravitational Energy

The gravitational energy of the liquid will be given by

$$U_o = \frac{1}{2}\rho n g_o \int_o^R \int_o^{2\pi} r z^2 \, d\theta \, dr =$$

$$= \frac{1}{2}\rho n g_o \int_o^R \int_o^{2\pi} r \left\{ J_j(\lambda_{jh} r) \left[A_{jh}^{(1)} \cos j\theta + A_{jh}^{(2)} \sin j\theta \right] \right\}^2 d\theta \, dr =$$

$$= \rho n g_o \, \epsilon_j \pi \sum_{j,h} \frac{\lambda_{jh}^2}{\left[\lambda_{jh}^2 R^2 - j^2\right] \left[J_j(\lambda_{jh} R)\right]^2} \left[\left(A_{jh}^{(1)}\right)^2 + \left(A_{jh}^{(2)}\right)^2 \right] \qquad (2\text{-}54)$$

Surface Energy

The surface energy of the system will be given by

$$U_* + U_*' = \sigma_o \int_o^R \int_o^{2\pi} r \sqrt{1 + \left(\frac{\partial f}{\partial r}\right)^2 + \left(\frac{1}{r}\frac{\partial f}{\partial \theta}\right)^2} \, d\theta \, dr + \sigma_1 \int_o^{2\pi} R f(R,\theta) \, d\theta$$

and

$$U_* = \sigma_o \int_o^R \int_o^{2\pi} r \left\{ 1 + \left[\sum_{j,h} J_j'(\lambda_{jh} r) \left(A_{jh}^{(1)} \cos j\theta + A_{jh}^{(2)} \sin j\theta \right) \right]^2 + \right.$$

$$\left. + \frac{1}{r^2} \left[\sum_{j,h} j \, J_j(\lambda_{jh} r) \left(-A_{jh}^{(1)} \sin j\theta + A_{jh}^{(2)} \cos j\theta \right) \right]^2 \right\}^{1/2} d\theta \, dr \qquad (2\text{-}55)$$

while

$$U_*' = \sigma_1 R \sum_{j,h} J_j(\lambda_j R) \int_o^{2\pi} \left(A_{jh}^{(1)} \cos j\theta + A_{jh}^{(2)} \sin j\theta \right) d\theta = 2\pi \sigma_1 R A_{oo}^{(1)} \qquad (2\text{-}55')$$

Volume of Liquid

The volume of the liquid is given as

$$\mathcal{V} = \int_o^R \int_o^{2\pi} r\, z\, d\theta\, dr = \sum_{j,k} \int_o^R \int_o^{2\pi} r\, J_j(\lambda_{jh} r) \left(A_{jh}^{(1)} \cos j\theta + A_{jh}^{(2)} \sin j\theta \right) d\theta\, dr$$

$$= \pi R^2 A_{oo}^{(1)} \qquad (2\text{-}56)$$

EQUATIONS OF MOTION

The extended kinetic potential or Lagrangian function of the system will be given by

$$\mathcal{F} = \mathcal{T} - U_o - U_* + \lambda \dot{\mathcal{V}}$$

whose terms are given by Equations (2-54), (2-55), and (2-56). The equations of motion will be obtained, as before, from the variational principle

$$\delta \left[\int_o^t \mathcal{F}\, dt + U_*' \right] = 0$$

and, hence, will assume the form

$$\sum_{j,h} \sum_{\beta=1}^{2} \left\{ \left(V_{ikjh}^{(\beta,\alpha)} + V_{jhik}^{(\beta,\alpha)} \right) \ddot{A}_{jh}^{(\beta)} + \sum_{\ell,m} \sum_{\beta,\gamma=1}^{2} \left[\left(\frac{\partial V_{ikjh}^{(\beta,\alpha)}}{\partial A_{\ell m}^{(\gamma)}} + \frac{\partial V_{jhik}^{(\beta,\alpha)}}{\partial A_{\ell m}^{(\gamma)}} \right) \right.\right.$$

$$\left.\left. - \left(\frac{\partial V_{\ell mjh}^{(\beta,\alpha)}}{\partial A_{ik}^{(\alpha)}} + \frac{\partial V_{jh\ell m}^{(\beta,\alpha)}}{\partial A_{ik}^{(\alpha)}} \right) \right] \dot{A}_{jh}^{(\beta)} \dot{A}_{\ell m}^{(\gamma)} \right\} + \sum_{j,h} \sum_{\beta=1}^{2} \left(\frac{\partial \beta_{ik}^{(\alpha)}}{\partial A_{jh}^{(\beta)}} - \frac{\partial \beta_{jh}^{(\beta)}}{\partial A_{ik}^{(\alpha)}} \right) \dot{A}_{jh}^{(\beta)} +$$

$$- 4\pi n g_o \epsilon_i \frac{\lambda_{ik}^2 A_{ik}^{(\alpha)}}{\left[\lambda_{ik}^2 R^2 - i^2 \right] \left[J_i(\lambda_{ik} R) \right]^2} - 2\sigma_o / \rho \sum_{j,h} \sum_{\beta=1}^{2} K_{ikjh}^{(\alpha,\beta)} A_{jh}^{(\beta)} +$$

$$+ \frac{2\pi R^2}{P} \frac{\partial A_{oo}^{(1)}}{\partial A_{ik}^{(\alpha)}} \delta_{oi} \delta_{ok} \delta_{\alpha 1} = - \frac{4\pi\sigma 1}{\rho} R \frac{\partial A_{oo}^{(1)}}{\partial A_{ik}^{(\alpha)}} \delta_{oi} \delta_{ok} \delta_{\alpha i} \qquad (2\text{-}57)$$

where $V_{ikjh}^{(\alpha,\beta)}$ is given by Equations (2-48), (2-50), (2-51), $\beta_{ik}^{(\alpha)}$ by Equations (2-52), (2-53) and

$$K_{ikjh}^{(\alpha,\beta)} = \int_o^R \int_o^{2\pi} \frac{\left[J_i'(\lambda_{ik} r) J_j'(\lambda_{jh} r) {}^{(I)}Q_{ij}^{(\alpha,\beta)} + \frac{ij}{r^2} J_i(\lambda_{ik} r) J_j(\lambda_{jh} r) {}^{(III)}Q_{ij}^{(\alpha,\beta)} \right]}{\sqrt{1 + \left(\frac{\partial f}{\partial r}\right)^2 + \left(\frac{1}{r}\frac{\partial f}{\partial \theta}\right)^2}} A_{jh}^{(\alpha)} \, r d\theta dr$$

with ${}^{(I)}Q_{ij}^{(\alpha,\beta)}$ being given by (2-46') and, in addition,

$${}^{(III)}Q_{ij}^{(1,1)} = \sin i\theta \sin j\theta \quad ; \quad {}^{(III)}Q_{ij}^{(1,2)} = - \sin i\theta \cos j\theta$$

$${}^{(III)}Q_{ij}^{(2,1)} = - \cos i\theta \sin j\theta \; ; \quad {}^{(III)}Q_{ij}^{(2,2)} = \cos i\theta \cos j\theta .$$

EQUATIONS OF IMPULSIVE MOTION

The equation of impulsive motion (1-16) can readily be specialized to the case of unsymmetrical motion in a cylindrical tank for, from the above equations (2-49), and (2-52), we obtain

$$\frac{1}{2}\rho \left[\sum_{j,h} \sum_{\beta=1}^{2} \left(V_{ikjh}^{(\beta,\alpha)} + V_{jhik}^{(\beta,\alpha)} \right) \dot{A}_{jh}^{(\beta)} + 2\beta_{ik}^{(\alpha)} \right]_{t=t_o} = \left(\alpha \beta_{jh}^{(\alpha)} \right)_{t=t_o}$$

SECTION 3. HEAT TRANSFER IN A LIQUID IN A LOW OR ZERO GRAVITY ENVIRONMENT

In the absence of gravity or, equivalently, of inertial forces, heat can be propagated in a stationary fluid only by the mildly efficient mechanism of molecular conduction. Under such conditions, the temperature distribution and, consequently, the flow of heat can be determined by the same well-known methods used for conduction in solids; that is, by integration of the heat transfer equation with the required boundary conditions. If the liquid is in motion under these weightless conditions, i.e., under the exclusive action of surface and interface tension forces, the velocity of the flow must be determined. The temperature distribution can then be obtained by adding a convective term (linear in the above velocity) to the heat transfer equation.

If an initially stationary but not isothermal liquid is acted upon by a low gravitational field, [1] the ensuing difference in density will give rise to buoyancy and to motion of the liquid. Heat will be transferred jointly by conduction and convection. The determination of the temperature distribution involves the simultaneous determination of the density, pressure, and velocity distributions. This requires the integration of the system of equations formed by the equations of motion of the liquid, the equation of continuity, the equation of joint convective and conductive heat transfer, and the knowledge of the equation of state of the liquid. In view of the slowness of the motion, the nonlinear inertial terms can be disregarded; however, the terms representing the components of the viscous forces must be retained. The corresponding equations will thus be linear. For the small temperature differences involved, the equation of state can be replaced with excellent approximation by a linear relation between the density and the temperature. This situation has been treated in detail in Reference 2. It was planned to subject the results of this analysis, and its generalization to a cylindrical case, to experimental verification. Construction of instrumentation for this purpose has been initiated; however, some important components could not be procured to date.

If the liquid has a free surface, the situation is complicated by the nonlinear boundary conditions at this surface (Kelvin's condition) as well as the dependence of the surface and interface tension upon the temperature. However, if the velocity of the motion of the liquid under the action is

[1] For quantitative estimate of the relative importance of the intensity of the gravitational or inertial field for the various heat transfer processes in a liquid, see Reference 1, Chapter 1.

sufficiently large so that the contribution of buoyancy can be ignored, the problem can be regarded as one of free convection. Only the two equations of nonviscous motion of the liquid and the equation of heat transfer might be required, with the possible addition of the formula expressing the dependence of the surface and interface tension upon the temperature.

SECTION 4. KINETIC THEORY OF BOILING UNDER WEIGHTLESS CONDITIONS

As is well known, nucleate[1] boiling of a liquid occurs by formation of vapor bubbles upon particular spots[2] of the heated surfaces of the container. Under reaction of gravity and/or hydrodynamic effect[3] (References 7 and 8), these bubbles detach from the site of their formation and rise to the surface of the liquid as a result of their buoyancy.

In the absence of gravity, the directive effect of the gravitational field is now absent and the bubble will move only under the action of the fluctuation in pressure along its boundary (i.e., perform a random Brownian motion). The root mean square of the displacement of the bubble of radius a in an interval of time t is given by

$$S = \sqrt{\frac{kT}{6\,\eta\,a}\,t} \qquad (1)$$

where

$k = 1.380 \times 10^{-16}$ erg/°K
= Boltzmann's constant
η = the viscosity of the liquid
T = temperature of the liquid

During their motion, two bubbles might meet and coalesce in a bubble of larger radius, which will be a function of the radii of the colliding bubbles as well as of the local pressure and temperature. The possibility also exists that the bubbles might collide with the surface, become attached and re-emitted. It is clear that this condition leads to the formation of fewer bubbles of increasing dimensions so that eventually the liquid will be evaporated into one bubble.

The initial kinetics of this procedure has been formulated mathematically for a model in which it is assumed that bubbles of equal radius

---

[1] A discussion of flash boiling that occurs under the action of extremely large heat fluxes and results in the formation of a layer of vapor on the heating surface will not be included.

[2] The formation of vapor bubbles inside a liquid requires an infinite amount of energy. Bubbles can be formed upon solid surfaces exhibiting a large curvature. Thus, the above spots probably correspond to microscopic bumps and depressions of the surface.

[3] The exact mechanism of the detachment of bubbles from heated surfaces has not been definitely stabilized.

a_o are emitted into the liquid at a certain rate ν and they are reflected upon collision with the boundary. This system of equations expresses the rate of change in concentration of bubbles of radius a_k as a balance between its augmentation due to collision of bubbles of radius a_j, a_h leading to the formation of bubbles of radius a_k, and its diminution due to collision of bubbles of radius a_k with other bubbles, as well as to their diffusion. This system of (nonlinear) partial differential equations has to be supplemented by the equation of heat transfer and the boundary condition requiring that the flux of N_k at the boundary be ν for k = o, o otherwise. Interpretation of the above differential problem has not been attempted to date; however, in view of the extremely low rate of diffusion of bubbles of other than microscopic ($\sim 10^{-5}$ centimeters) dimensions, the rate of evaporation of the liquid by the mechanism previously described is extremely low (it can be estimated to be of the order of several months for liquid masses of linear dimensions of the order of 10 centimeters).

SECTION 5. EXPERIMENTAL VERIFICATION OF THEORY

EXPERIMENTAL METHOD

The S&ID zero-gravity facility is based on the principle of the encapsulated cell (References 3 and 4). The device (Figure 2) consists of a falling outer capsule that contains an enclosed specimen cell in its evacuated interior. For the duration of the experiment, this specimen cell is falling freely inside the outer capsule. Since it is falling in a vacuum, it is free of aerodynamic drag, and falls faster than the outer capsule. The available time for experimentation is the duration of the free fall of the specimen cell.

Data are recorded by means of a motion picture camera mounted in the upper part of the outer capsule. Four mirrors, each set at an angle of 45 degrees to the vertical axis, are used to obtain four views of the specimen.

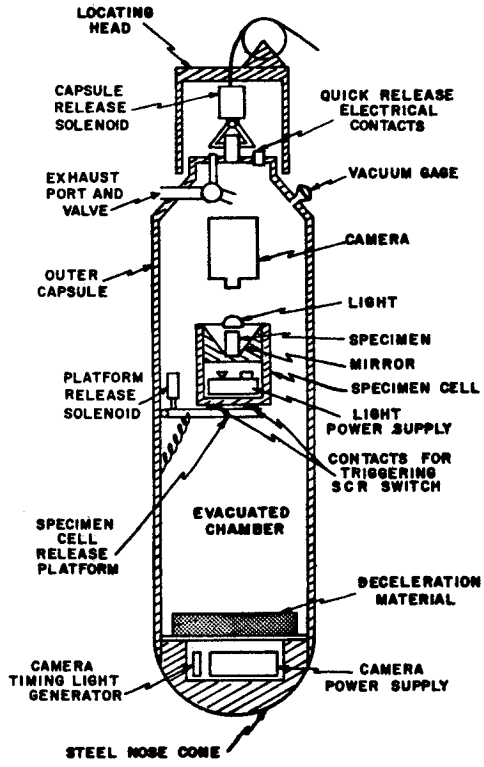

Figure 2. Diagram of Capsule Assembly

Drop Tower

Of the several structures available for use, the most stable structure was chosen. The drop tower (Figure 3) is 100 feet high; however, the capsule locating head had to be mounted 11 feet below the tower top, and the deceleration material projected 4 feet above ground level, so that the usable drop height was 85 feet.

A set of triaxially mounted accelerometers with a sensitivity of 0.005 g was located on the drop head. The accelerometers did not detect any disturbance of the tower, but analysis of the data indicated that there was some motion of the capsule prior to dropping. A crude device, utilizing a small pool of mercury, the size of the specimen used, resting on the drop head and reflecting a beam of light, showed that, in reality, the tower was never completely at rest; and the motion was sufficient to disturb the specimen. Efforts to isolate the drop head from these tower vibrations have not been successful to date. Periods of relative quiet were selected for drops.

Outer Capsule

The outer capsule is 1 foot in diameter by 6 feet high and weighs 220 pounds (Figure 4). It is composed of the following four sections:

1. A Nose Piece: Consists of a 12-inch diameter steel hemisphere, hollowed in the center to contain the camera battery and timing light generator, and open to the atmosphere (Figure 2).

2. The Lower Chamber Half: Contains the lower half of the evacuated inner chamber, and sealed on the bottom, with vacuum-tight electrical lead-through to connect to the camera battery, silicon-controlled rectifier (SCR) trigger, and timing light generator. The specimen cell release platform is mounted on the upper portion of this section.

3. The Upper Chamber Half: Forms the upper half of the evacuated inner chamber. The camera box is mounted in this section. A neoprene O-ring forms a vacuum-tight seal between the two chamber halves.

4. The Top Bonnet (Figure 6): Contains a 31-conductor vacuum-tight electrical feed-through, an evacuation port and valve, a thermocouple vacuum gage for monitoring the chamber pressure, and a release shackle stud. This forms the top cover of the evacuated chamber, and is sealed to the remainder of the chamber by a neoprene O-ring. The top of the bonnet mates with a locating ring in the drop head to accurately locate the capsule before dropping.

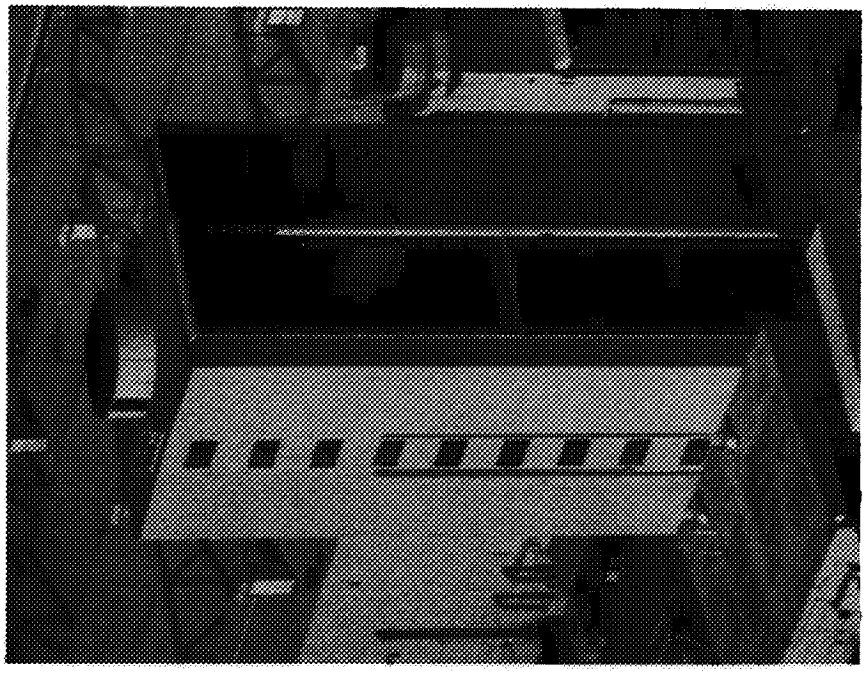

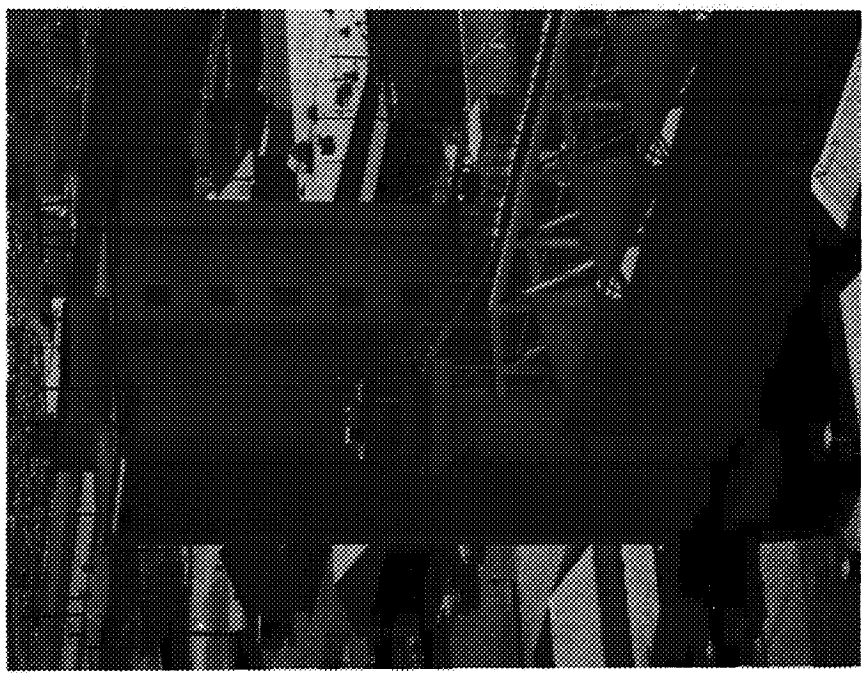

Figure 3. S&ID Gravidrome, Two Views

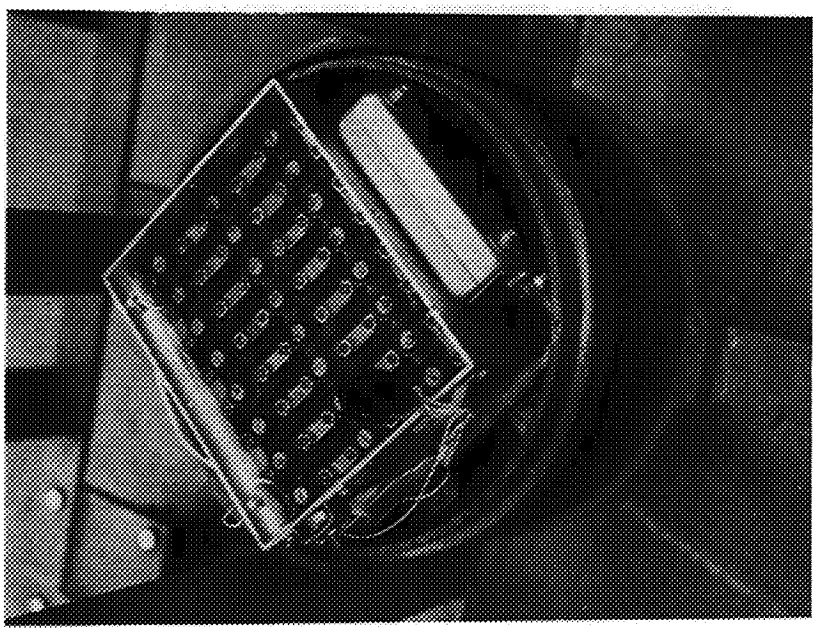

Figure 5. Nosepiece, Showing Camera Battery and Timing Light Generation

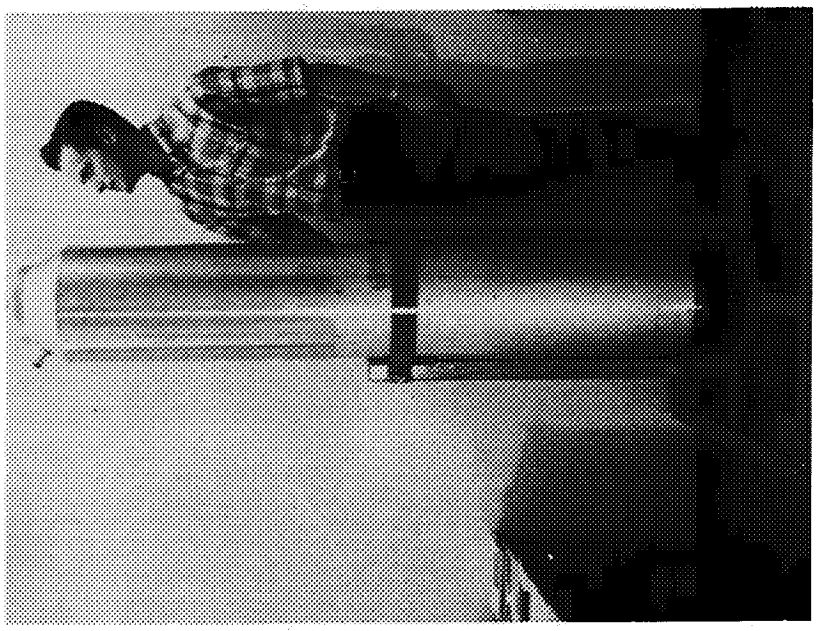

Figure 4. Assembled Outer Capsule

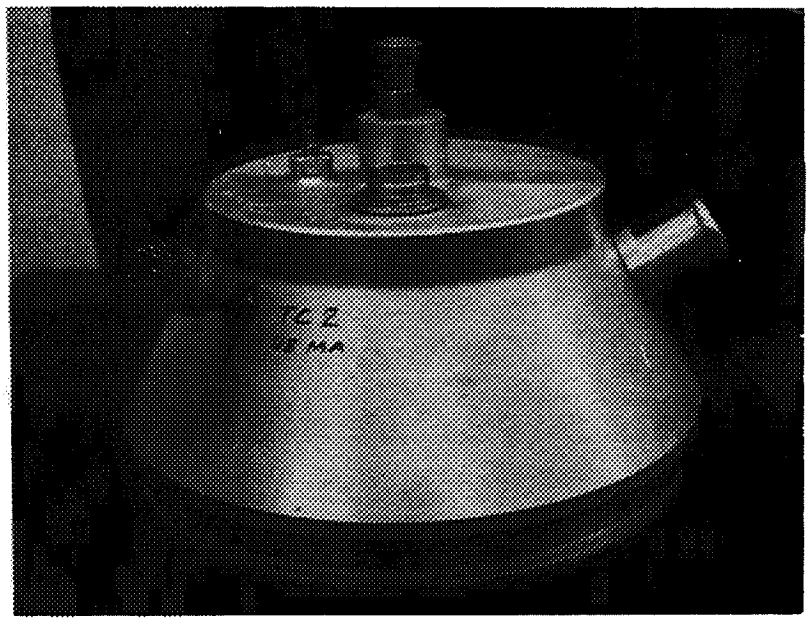

Figure 6. Top Bonnet

The difference in velocities of the inner specimen cell and the outer capsule causes the cell to travel 23 inches for a drop height of 85 feet. A pad of deceleration material is placed on the bottom of the chamber to protect the specimen cell at impact. Allowing a distance of 12 inches for the camera-to-subject distance, 10 inches for the camera length, and 12 inches for the nose piece, a total space of 60 inches is needed to permit the cell to travel the maximum distance.

Drop Head

The drop head incorporates a locating ring that fits around a shoulder on the capsule bonnet and guides the capsule for the first 1 inch of fall. Figure 7 shows the capsule located inside the drop head. A cable passes over a pulley located in the top center of the head and is used to haul the capsule up to the head. The capsule is located firmly within the locating ring and held in place by an electrically operated release shackle. A quick-release electrical plug is also held firmly in the drop head, and makes contact with the mating socket on top of the capsule bonnet (Figure 8). The first 1/8 inch of capsule motion disengages this plug.

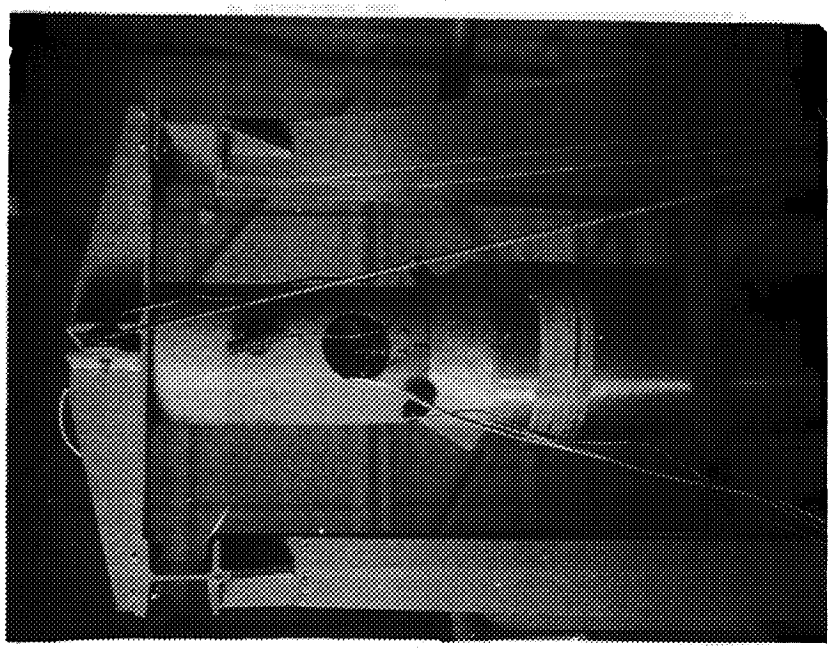

Figure 7b. Close-up View of Drop Head

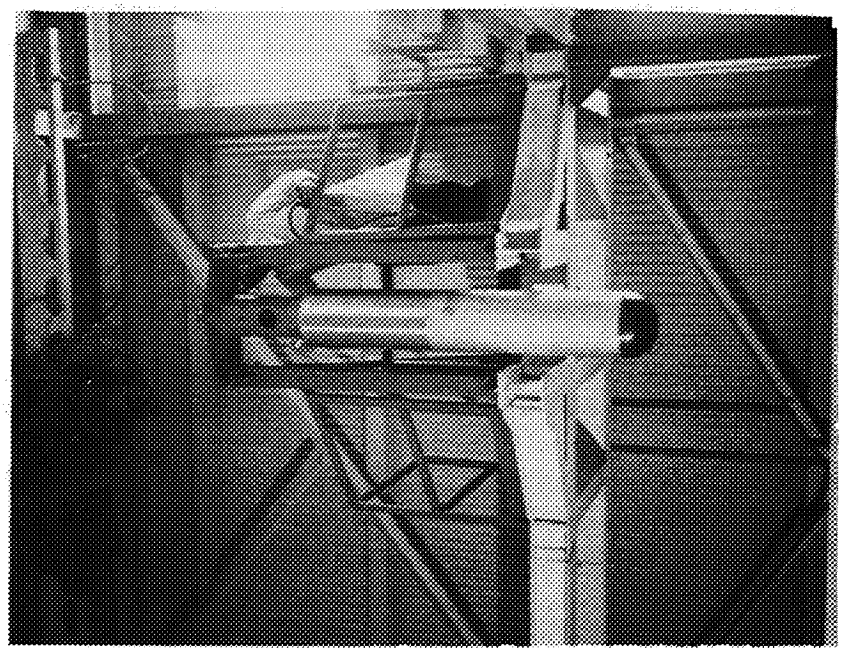

Figure 7a. Capsule Located in Drop Head

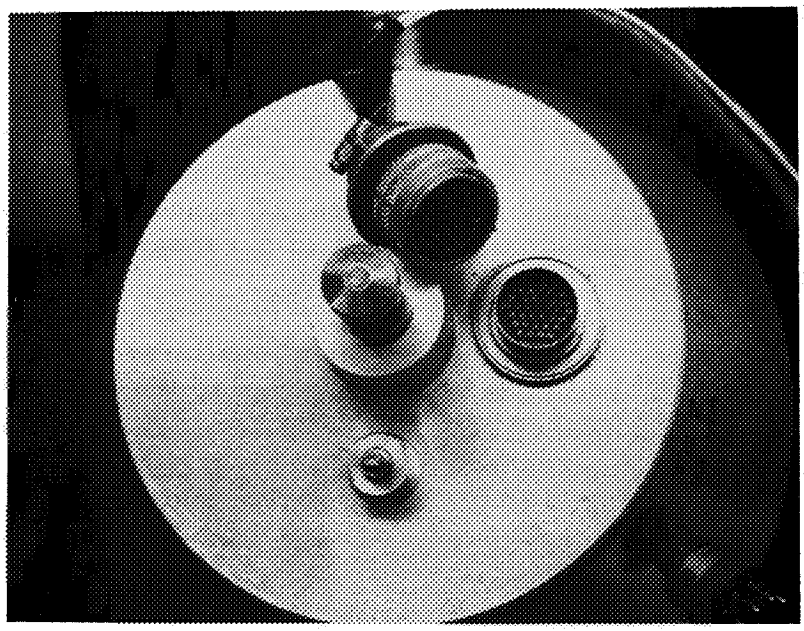

Figure 8. Quick-Release Plug and Socket Located in Top of Capsule Bonnet

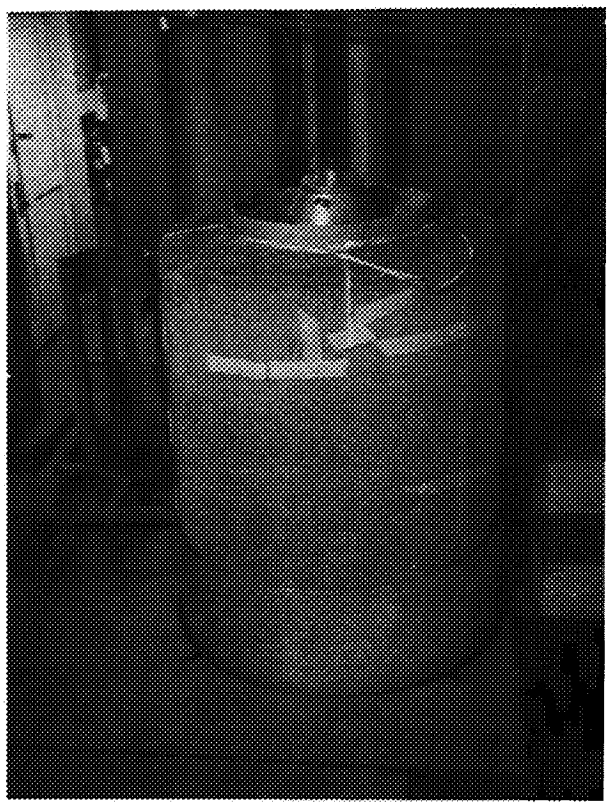

Figure 9. Capsule After Deceleration

Outer Capsule Deceleration

A roll of corrugated cardboard, with the corrugations parallel to the axis of fall, is used to stop the capsule upon impact. A roll of cardboard 6 feet high and 4 feet in diameter was first used, with an inner core 2 feet in diameter rolled to half density (alternating layers of spacer strips and cardboard), surrounded by an additional thickness of cardboard rolled at full density to a diameter of 4 feet.

Capsule penetration was originally 4 feet for a maximum deceleration of no more than 20 g. With the additional weights added to the capsule (as explained later), penetration increased to 5 feet (Figure 9). As a safety precaution, an additional roll of cardboard 3 feet high was placed beneath the 6-foot roll. The cardboard was held in place by an aluminum tank 5 feet high and 4 feet in diameter so that the cardboard extended 4 feet above ground level and 5 feet below.

The center core of the 6-foot-high roll had to be replaced after every drop (Figure 10). The 3-foot-high safety layer was replaced after 6 to 10 drops, and it was not necessary to replace the outer layer of cardboard.

Specimen Cell

The specimen cell is shown in Figure 11. Electrical signals for triggering the specimen cell lights and camera motor, operating the specimen cell release platform, and supplying the timing signal to start the experiment utilize eight of the electrical feed-throughs in the bonnet. The remainder can be used for operating additional devices inside the chamber as needed.

Primary requirements demand that the specimen cell be completely self-contained (no umbilical connections to external power sources), with no moving parts. The cell used is 6 inches in diameter and 12 inches high. The specimen container, made of fused quartz, 1 inch inside diameter by 1 inch high, is mounted in the uppermost portion. (See Figure 12.) Four first-surface mirrors, spaced 90 degrees apart and inclined at an angle of 45 degrees to the vertical surround this container (Figure 13). The specimen cell is sealed from the top by means of a lucite cover and O-ring, held in place from the side by six screws. Inside the cell are the batteries for operating the lights, a silicon-controlled rectifier (SCR) for switching the lights on, and an inertia switch for turning the lights off (Figure 14). Two foil strips, electrically insulated from the cell and resting on two similar strips on the cell release platform, are on the outside bottom of the cell (Figure 15). An electrical triggering signal is supplied through these

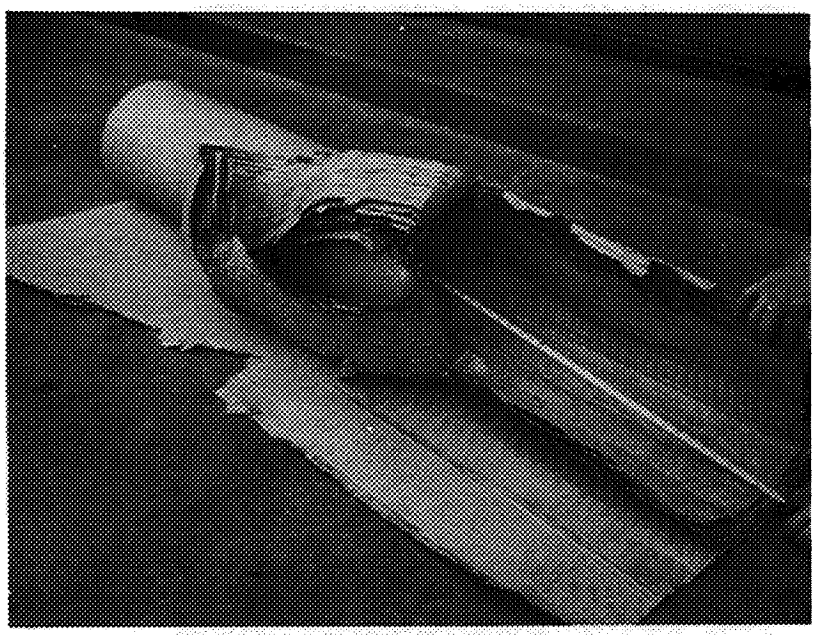

Figure 10a. Center Cardboard Core After Deceleration

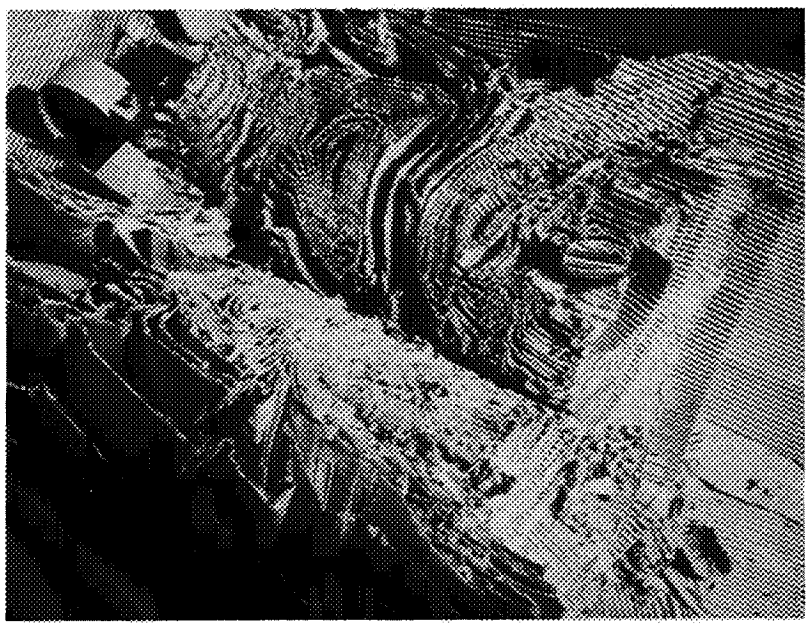

Figure 10b. Core Cut Away to Show Buckling of Cardboard

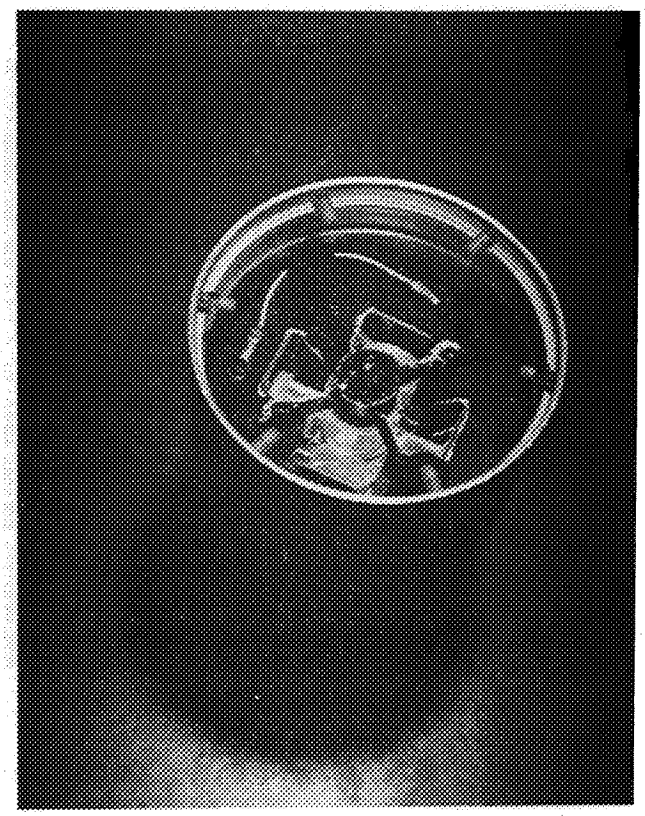

Figure 11. Specimen Cell

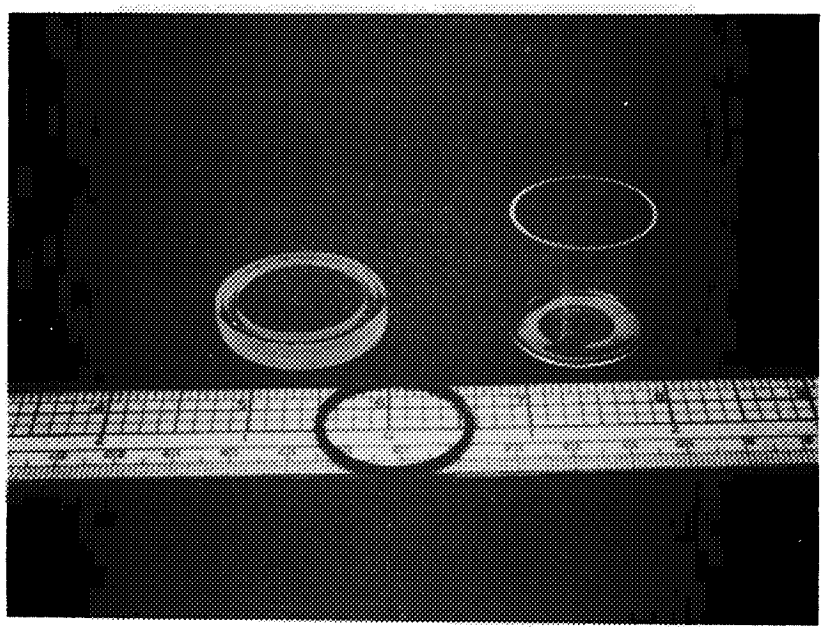

Figure 12. Specimen Container, Cover, and O-Ring

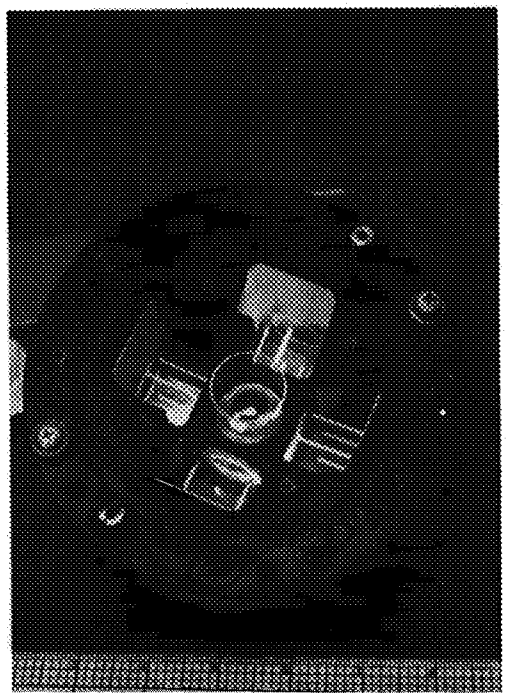

Figure 13. Top View of Specimen Container Showing Arrangement of Four Mirrors

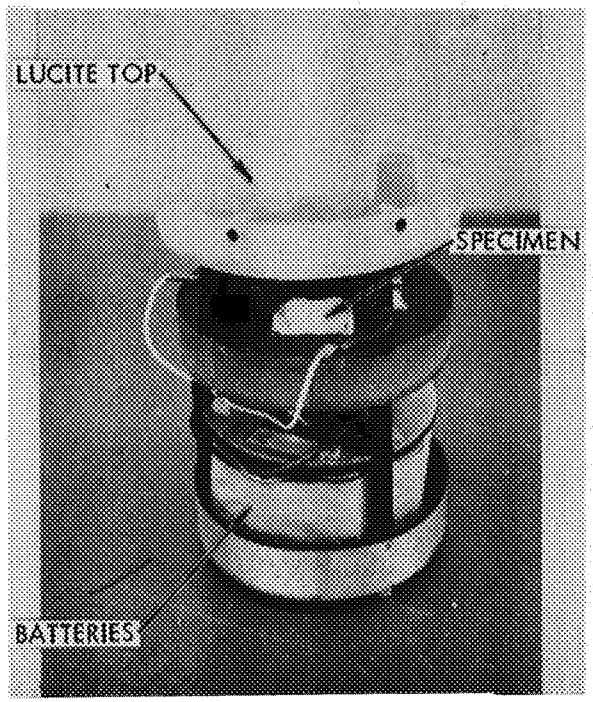

Figure 14. Location of Components Inside Specimen Cell

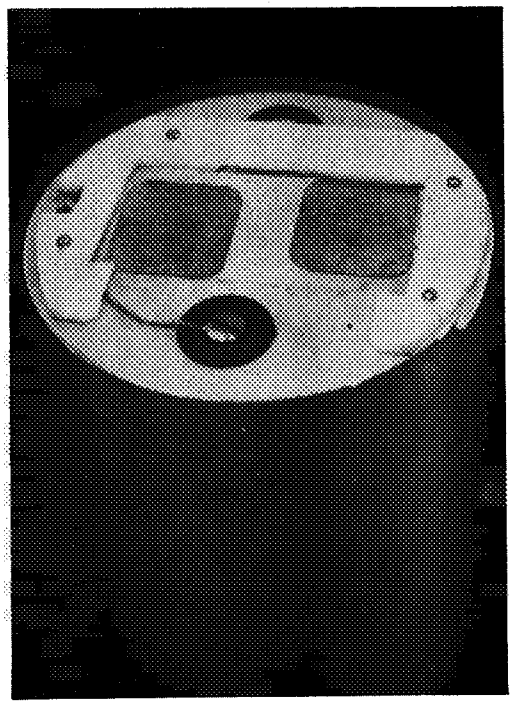

Figure 15. Bottom of Specimen Cell Showing Contacts for Triggering Cell Light SCR and Teflon Locating Collar

pads to two conductors leading to the SCR switch inside the cell to turn on the cell lights. With the operation of the release platform, the cell contacts are removed from the platform contacts. The SCR, a solid-state device, has no moving parts.

Several methods have been used to illuminate the specimens (Figure 16). First, bottom-lighting the specimen was tried. The liquid meniscus was not clearly defined, and this method could not be used for mercury.

Next, a light ring was used, consisting of 8 quartz-iodine lamps, mounted 4 inches above and on a radius of 2-1/2 inches around the specimen. Although this gave a flat, reflection-free lighting, imperfections in the specimen container walls tended to obscure the meniscus. In addition, the batteries required to operate so many lamps (needed to maintain the high-light level) were extremely heavy, imposing a severe load on the release platform.

Finally, a single quartz-iodine lamp, mounted in the retainer ring directly above the specimen, was used (Figure 17). This system gives excellent contrast, with the meniscus appearing as a sharply defined bright line against a totally black background, as shown at the end of this section. Since only one lamp is used, the number of batteries is reduced, and the release platform functions smoothly.

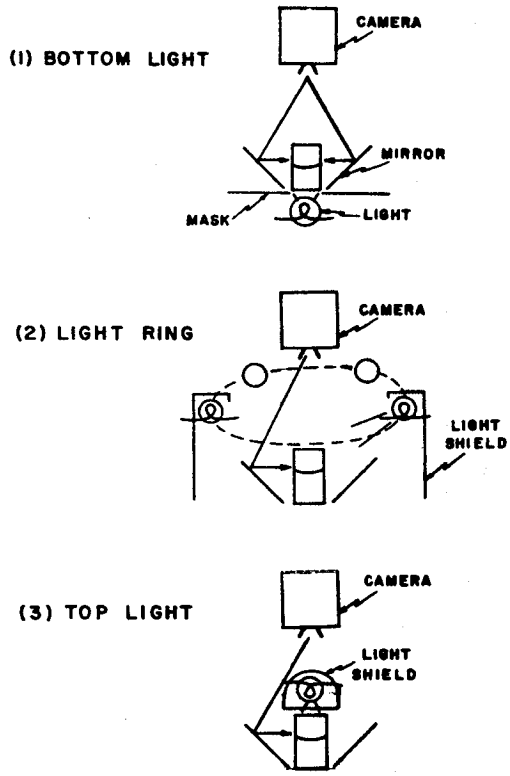

Figure 16. Lighting Arrangements

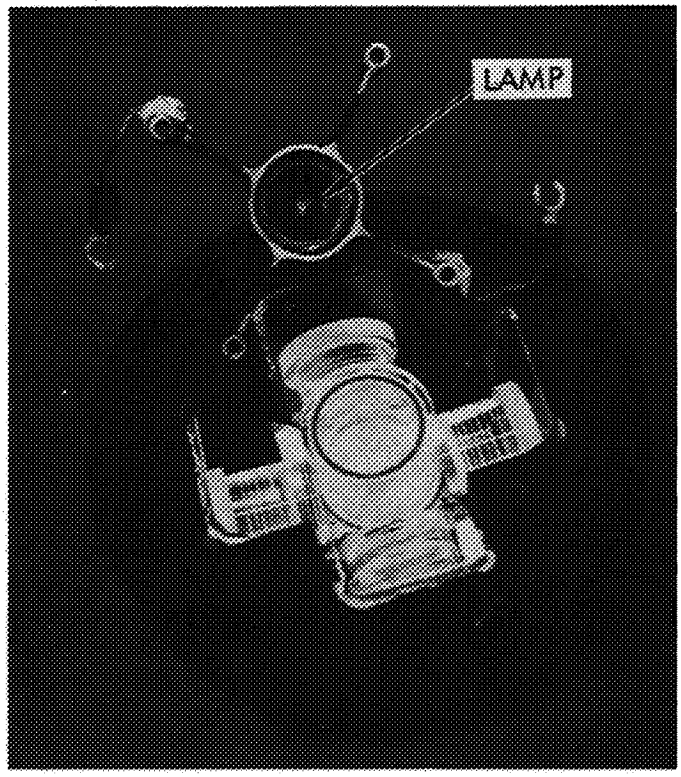

Figure 17. Quartz-Iodine Lamp Mounted in Center of Specimen Container Retaining Ring

Specimen Cell Release Platform

The specimen cell release platform is a critical part of the entire assembly. It must hold the specimen cell rigidly in place, level and centered in the capsule chamber, and move out of the specimen cell path of fall in a manner that will impart no motion to the cell other than free fall. The platform proper is supported in the raised position by a hinge joint, a release latch, and a roller resting on a cam guide (Figures 18 and 19).

Upon release, it is pulled straight down for a distance of 1/2 inch and then folded down and out of the way of the cell by two springs, one on either side of the platform. This motion is imparted by the roller support and cam guide (Figure 20). The platform is held in the raised position by a spring loaded latch lever that is held closed by a solenoid-activated plunger.

The outer capsule, during its fall, can be tilted by the latching of the platform, thus tilting the camera in relation to the specimen. To overcome this deficiency, the release platform was constructed in two halves, each with its own release mechanism located 180 degrees apart. It was hoped that in this manner the release actions would be equal and opposite and the capsule would remain vertical during its fall. Since it was not possible to synchronize the two platforms sufficiently to release the specimen cell with

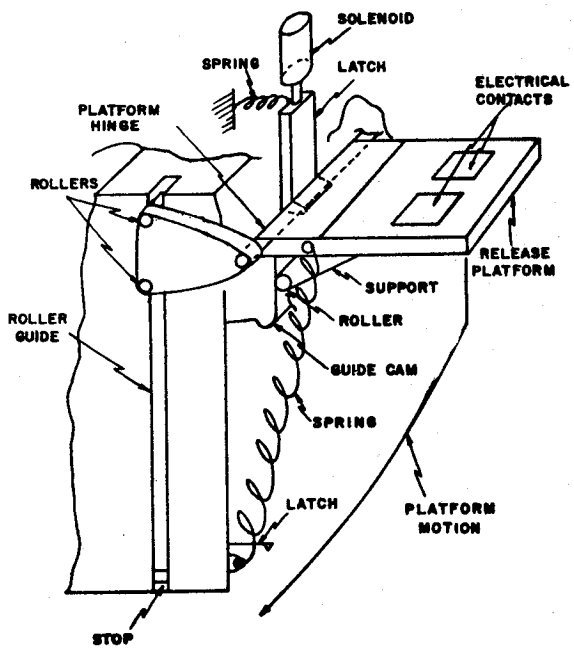

Figure 18. Release Platform Details

no tilting action, one platform was removed, and the remaining platform lengthened. A slight tilt was still imparted to the specimen cell upon release, however. The platform motion was analyzed with the aid of a high-speed (2,000 frames/sec) motion picture camera. While the inboard end of the platform (nearest the release mechanism) was operating properly, the outboard end was first rising and then falling. This was corrected by placing two stops above the platform to prevent any upward motion. The rigidity of the platform was not sufficient to ensure a dependable release action when using the heavy battery pack required for the ring lighting system mentioned earlier. Replacing this system with the single top light and the accompanying reduction in battery weight allowed the release platform to function as desired.

A further difficulty was experienced with the specimen cell slipping off the electrical contact pads when the capsule assembly was being transported and hoisted to the top of the tower. This was corrected by the addition of a 1/16-inch-thick teflon pad to the bottom of the specimen cell. The pad was cut to fit loosely around the outer perimeter of the release platform (shown in Figures 15 and 20).

The capsule tilt was almost entirely removed by adding 50 pounds of weight to the top of the capsule, thus raising the center of gravity to three

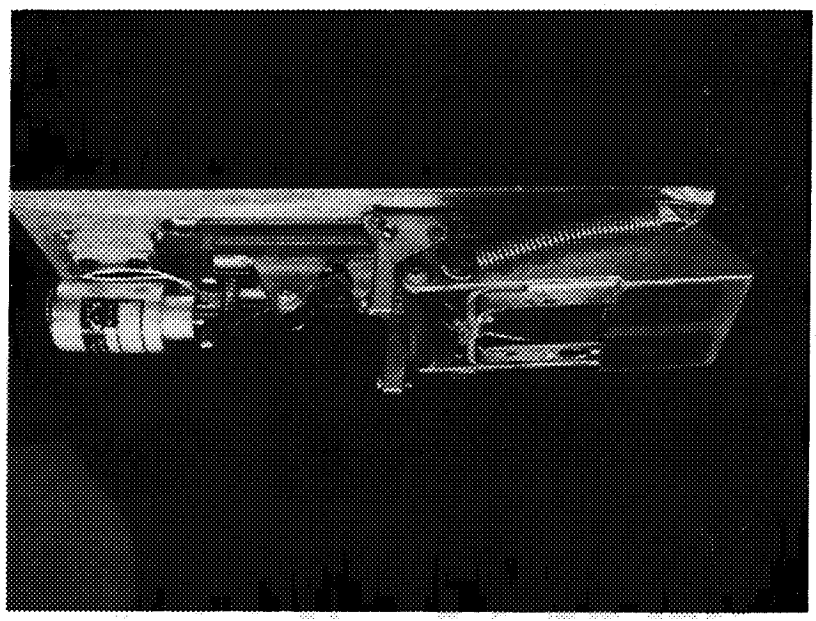

(Folded)

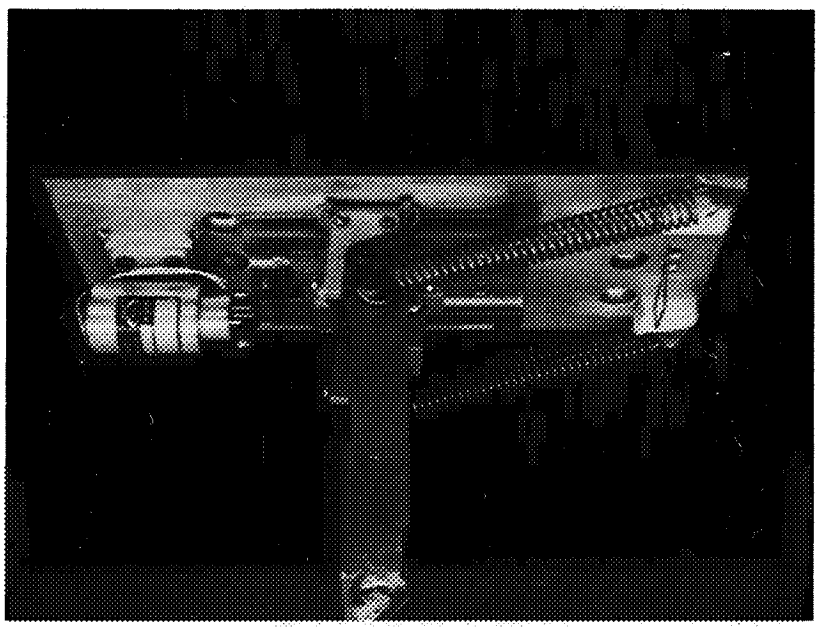

(Extended)

Figure 19. Release Platform

(Detail of Roller Support and Cam Guide)

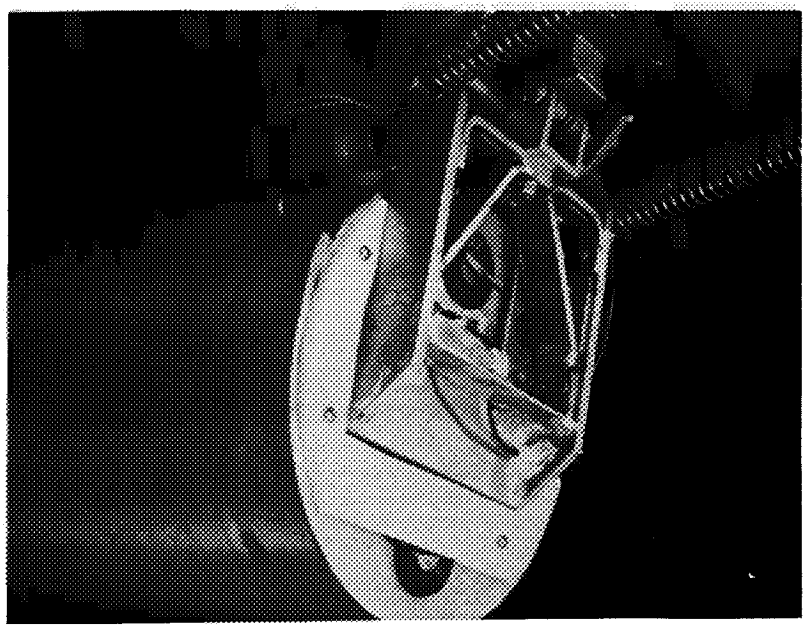

(Bottom View of Release Platform)

Figure 20. Release Platform

inches below the geometrical center of the capsule. While an additional mass might have removed the tilt entirely, it might have raised the center of gravity to a point that would endanger the aerodynamic stability of the capsule.

Camera

For the majority of specimens examined, the time of transition from a normal-gravity to a low-gravity configuration was in the range of 0.1 second. Since data registration was by means of a motion picture camera, it was desirable to use a camera with as high a framing rate as possible. The size of the apparatus and the high framing rate indicated that it would be necessary to use a 16 mm camera driven by an electric motor. In addition, the camera has to be able to withstand the shock of deceleration at the termination of the drop. Based on these considerations, a Milliken model DBM-4A camera, incorporating a wide range of framing rates, up to 400 frames per second, was used.

Since umbilical connections to the capsule during the actual drop would defeat the purpose of the apparatus, it was necessary to include a power supply and switching mechanism to turn the camera on and off. This was accomplished by incorporating a 28-volt nickel-cadmium battery and a solid-state switch (SCR) in the nose cone of the outer capsule.

The SCR is triggered by an electrical impulse applied through a set of electrical contacts at the top of the capsule. Originally, an inertia switch was used to turn the camera off. It proved to be more desirable, however, to allow the film to run out in the camera, at which time the camera turns itself off.

The camera also contains two timing lights, one over each edge of the film. One of these lights was connected to a 100-cycle-per-second timing generator that was also placed in the nose cone, thus establishing an accurate time base for analyzing the data. The other timing light was synchronized with the specimen cell platform release solenoid to accurately establish the start of the experiment.

The device described in Reference 3 incorporates a camera fixed in the outer capsule. The specimen cell is falling away from the camera during the experiment, causing the image size to decrease, and forcing the use of a very small lens opening to encompass a large depth of field. High camera framing rates with their accompanying extremely short exposure times demand a high light-level and/or high film-speed. The available light is limited by the size of the power source than can be incorporated in the specimen cell. High-speed films customarily have a large grain size and low resolution that, in

our case, results in an undesirable loss of picture detail. The added requirement of a small lens opening compounds an already difficult situation. In addition, the changing parallax between a fixed camera and the falling specimen makes data reduction more difficult.

There was an attempt made to overcome these difficulties by enclosing the camera in a vacuum-tight box (Figure 21) and then releasing it, together with the specimen cell. Teflon guides and tracks were used to keep the camera box aligned. Electrical connections were made by means of umbilical cords connected to the box. This design proved unworkable because the camera torque caused the box to bind in the locating tracks. Therefore, the camera box was fixed in place by means of spacer sleeves.

The inherent advantages of this system (e.g., shallow depth of field with the accompanying large lens opening and constant image size) indicate that further development along these lines may be advantageous. It is possible that the desired result could be obtained by the use of a positive-displacement device.

The final camera system used a one-inch lens stopped down to f22 and a camera-to-subject distance of 15-1/2 inches with the specimen cell in the raised position. The fastest film available at present that will render a fair amount of detail has a speed rating of 250 ASA. Using this setup, the image is sharp for the entire distance of specimen cell travel.

Experimental Procedures

Many of the liquids used for experimentation, and particularly water, are extremely sensitive to contamination. This demands that the fused quartz specimen containers be cleaned as thoroughly as possible. The procedure used consists of first cleaning the container in a hot concentrated solution of potassium hydroxide in a small ultrasonic cleaner. The container is rinsed well in running tap water and then placed in a bath of an acid glass cleaning solution. After being rinsed in tap water, the container is again placed in the ultrasonic cleaner and cleaned for several hours in a bath of hot Alconox solution. The container is then rinsed for several minutes in running tap water, again in distilled water, and is then allowed to dry and is examined for visual signs of contamination.

The burettes used for measuring the volume of the liquids are cleaned with similar solutions, which are drawn into the tip of the burettes and out the top with the aid of an aspirator and an aspirating flask. After drying, the burette is then rinsed well with the liquid to be used and filled.

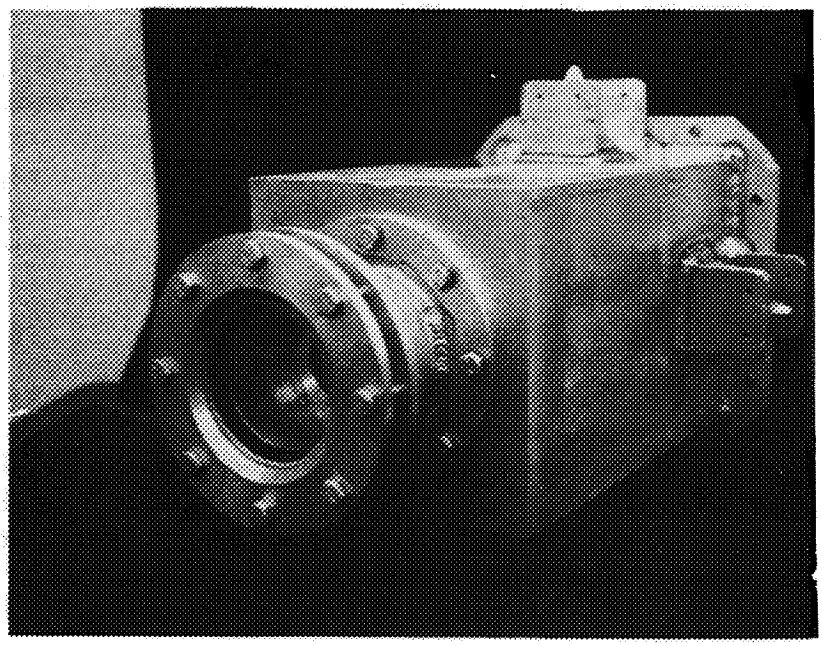

(Vacuum-Tight Camera Box)

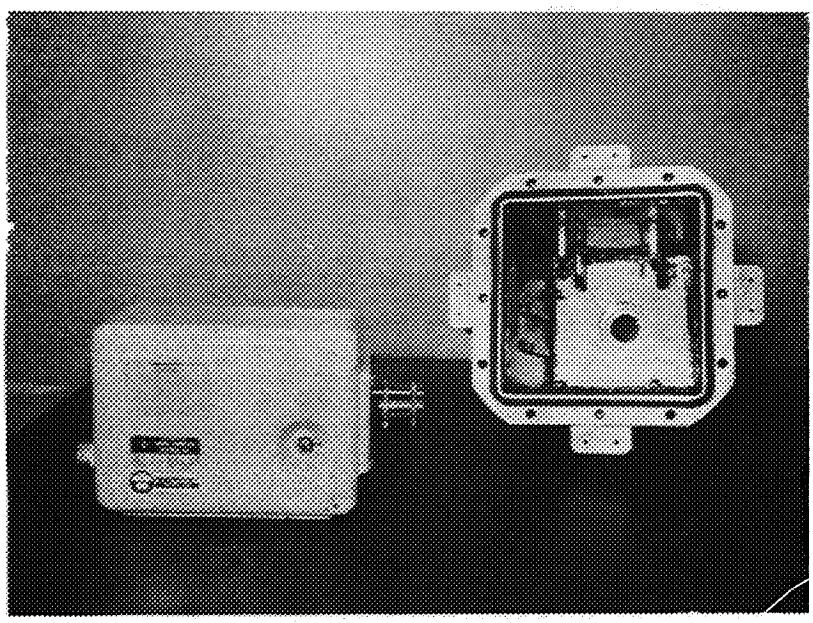

(Camera and Box, Disassembled)

Figure 21. Camera Assembly

The specimen container is then weighed on a chain balance, and the desired volume of liquid is measured into the container from the burette. The container is placed on the table of the epihydrogoniometer, an instrument that measures the contact angle between the liquid and the wall of the container. The meniscus is examined with a low-powered microscope. Container contamination will appear at this point in the form of a ragged meniscus. The container and specimen are weighed again to determine the mass of the specimen. The container is then placed in the specimen cell, and the cover plate and gasket, which have undergone the same cleaning process, are placed over it and clamped into place with the retaining ring.

The specimen cell is then assembled and placed on the cell release platform located in the lower half of the outer capsule, and the upper half of the capsule, which contains the camera, is assembled over it. The complete capsule assembly, which has been assembled in its special transport cart, is then brought to the vacuum pump where, with the aid of a 6-inch diffusion pump, the chamber pressure is reduced to no more than a few microns of mercury (Figure 22). The capsule is then wheeled out to the adjacent tower and hoisted to the drop head.

At this point, the specimen cell light-trigger circuit is checked for continuity. If the specimen cell has shifted its position on the release platform, it will be reflected in a loss of continuity in this circuit. The

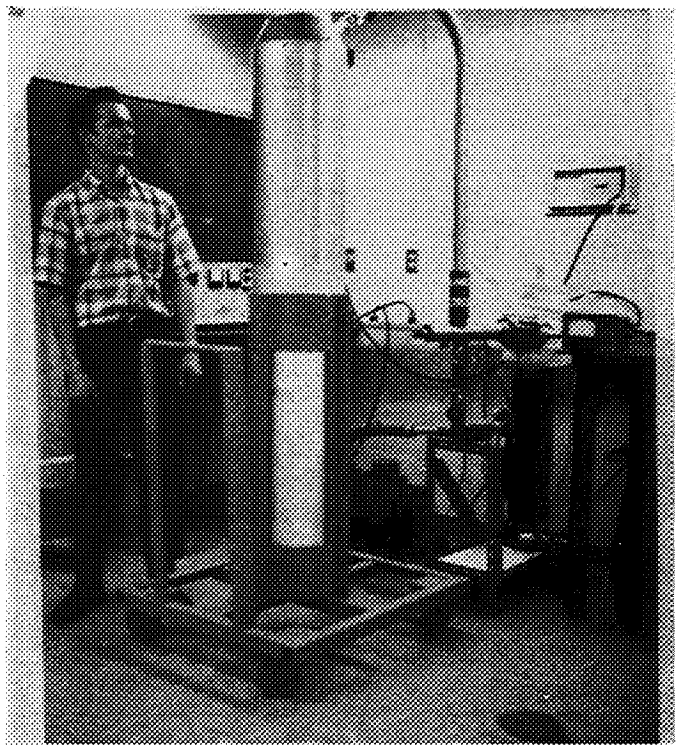

Figure 22. Evacuating the Assembled Capsule

capsule is then allowed to rest undisturbed for a period of at least a half hour so that the motion of the liquid may dissipate through viscous damping. During this rest period, to ensure that no disturbance has taken place, the drop head vibrations are monitored by means of accelerometers mounted on the head. The chamber pressure is also checked by means of a thermocouple vacuum gage mounted in the capsule bonnet. This gage is disconnected for the last few minutes of rest prior to the drop. After the rest period has elapsed, the drop sequence proper is started.

Sequence of Events During Drop

Figure 23 illustrates the sequence of events during a drop. A control box employing time-delay relays is used to obtain the needed timing of events prior to capsule release. The electrical impulses are fed from the control box, through the plug mounted in the drop head (31 conductors), to the socket mounted on the capsule bonnet, and then down through the bonnet to the various devices.

The drop sequence starts with the triggering of the SCR in the specimen cell to turn on the cell light. A one-second time-delay relay allows the light to come to operating voltage and then switches on the camera motor by triggering the SCR located in the capsule nose. The camera comes up to operating speed of 400 frames per second in 0.8 second. Since the camera

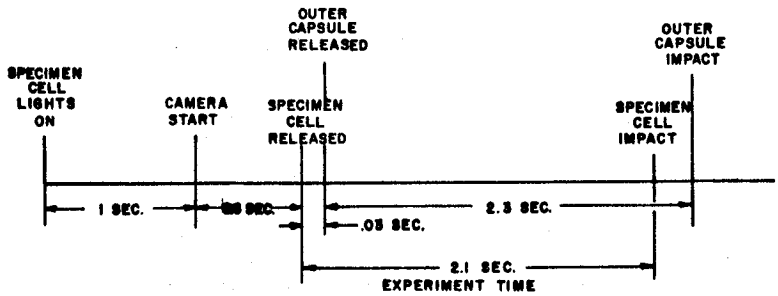

Figure 23. Sequence of Events During Drop

vibrations are transmitted to the specimen through the capsule wall and platform release mechanism, it is desirable to release the specimen cell as soon as possible after the camera starts. On the other hand, since the transition from the normal to the low-gravity configuration takes place in roughly 0.1 second (for the size of containers used) and since as much data as possible should be gathered during this period, some compromise between these two factors must be reached. A solid-state, variable time-delay relay is used to vary the time between the camera start and the specimen cell release. A time delay of 0.6 second between these two events is used at present. Another delay relay of 30 milliseconds duration then releases the outer capsule. This delay is to ensure that any irregularities in the outer capsule release motion will not be transmitted to the specimen.

The specimen cell hits the deceleration material at the bottom of the capsule chamber 2.1 seconds after release. This is the time available for experimentation. The inertia switch in the specimen cell turns off the cell light at this point. Two-tenths of a second later, the outer capsule hits the cardboard roll at the bottom of the tower and is brought to rest.

DATA COMPARISON

The experimental data selected for quantitative analysis were obtained with 6.145 cubic centimeters of distilled water contained in a quartz cylinder having an inner diameter of 2.54 centimeters. The angle of contact between the liquid and the container was determined to be 14 degrees.

A comparison of experimental data with the computed menisci was made photographically. The frames on the motion picture film corresponding to the time intervals of the computed curves were selected. The image size was then enlarged so that the inner diameter dimension of the specimen container corresponded to the wall dimension on the computed curve. The shape of the meniscus was then photographed on a transparent lithograph film. This film was then superimposed on the computed graphs, and the two curves were examined for correspondence. These results are shown in Figure 24. The computed graphs are repeated in Figure 25.

Due to optical distortion of the cylindrical specimen container, the outer edges of the image are not usable. The central portion (about three-fourths of the cylinder diameter), however, has only a negligible amount of distortion. This was demonstrated by choosing three arbitrary points on the meniscus curve and constructing a circle to pass through them. The correspondence of the circle to the edge of the meniscus was excellent for the aforementioned portion of the image. This also provides an additional check for the presence of a true zero-gravity configuration.

Figure 26 shows results obtained by computation with an error of less than one percent. Figure 27 is a series of unretouched photos of the test specimen during a drop test.

Figure 24

Comparison of Computed and Observed Menisci
(9 Sheets)

In the following illustrations, the nondimensional variables ξ and ζ are employed.

$$\xi = r/\ell$$

$$\zeta = z/\ell$$

where $\ell = \sqrt{\sigma/\rho g n_o}$

r = radius of the container; g_o = standard terrestrial gravity; n = load factor; and σ and ρ = surface tension and density of the liquid, respectively.

Figure 24

Comparison of Computed and Observed Menisci
(9 Sheets)

In the following illustrations, the nondimensional variables ξ and ζ are employed.

$$\xi = r/\ell$$

$$\zeta = z/\ell$$

where $\ell = \sqrt{\sigma/\rho g n_o}$

r = radius of the container; g_o = standard terrestrial gravity; n = load factor; and σ and ρ = surface tension and density of the liquid, respectively.

PRECEDING PAGE BLANK NOT FILMED.

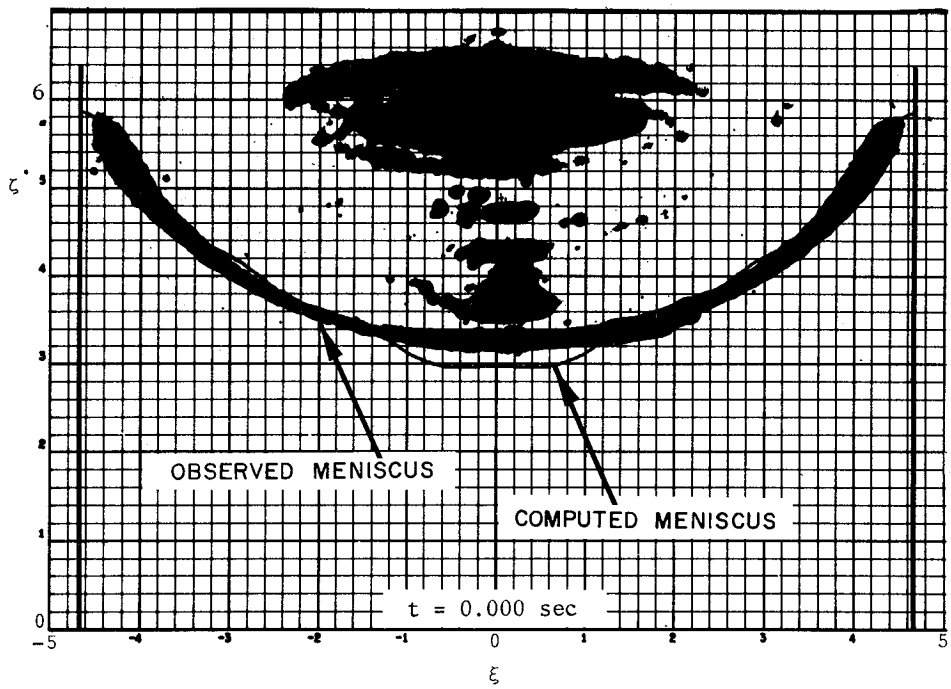

LIQUID CONFIGURATION AT ZERO GRAVITY

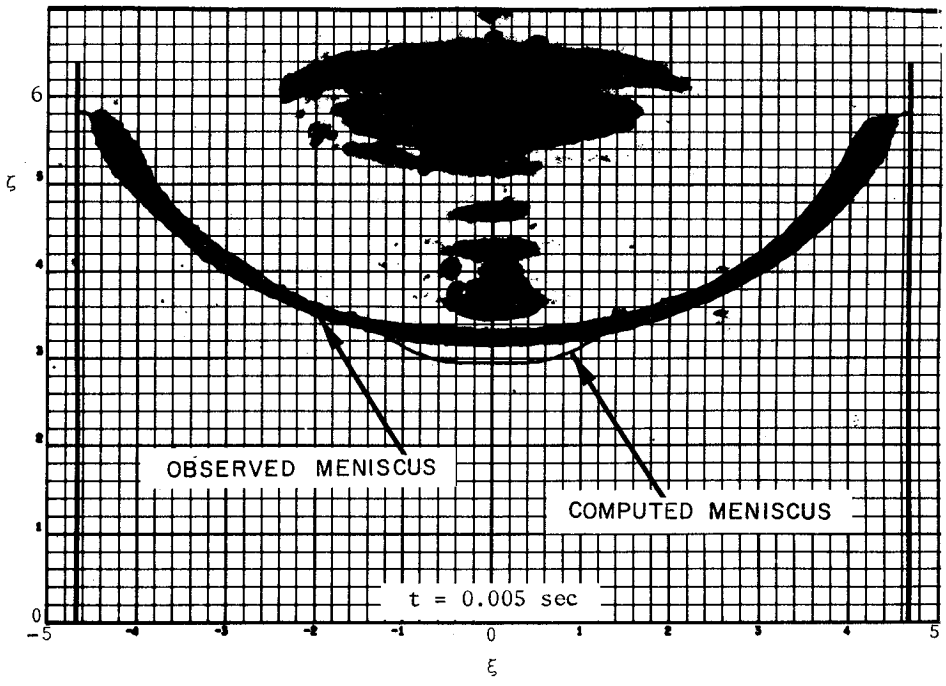

FIGURE 24 a

PRECEDING PAGE BLANK NOT FILMED

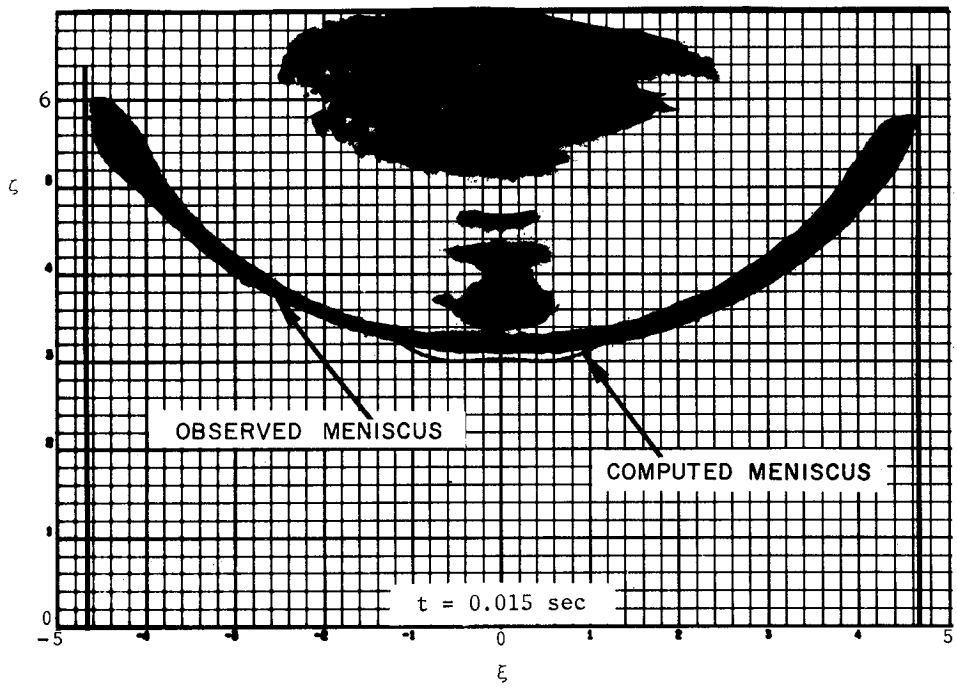
OBSERVED MENISCUS
COMPUTED MENISCUS
t = 0.015 sec
ζ
ξ

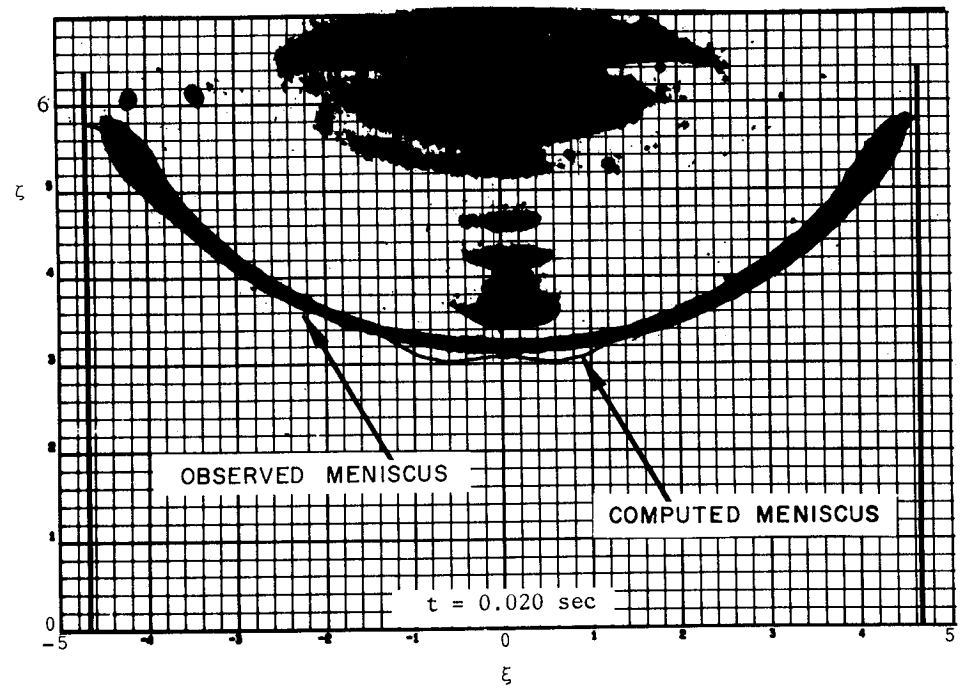
OBSERVED MENISCUS
COMPUTED MENISCUS
t = 0.020 sec
ζ
ξ

FIGURE 24 b

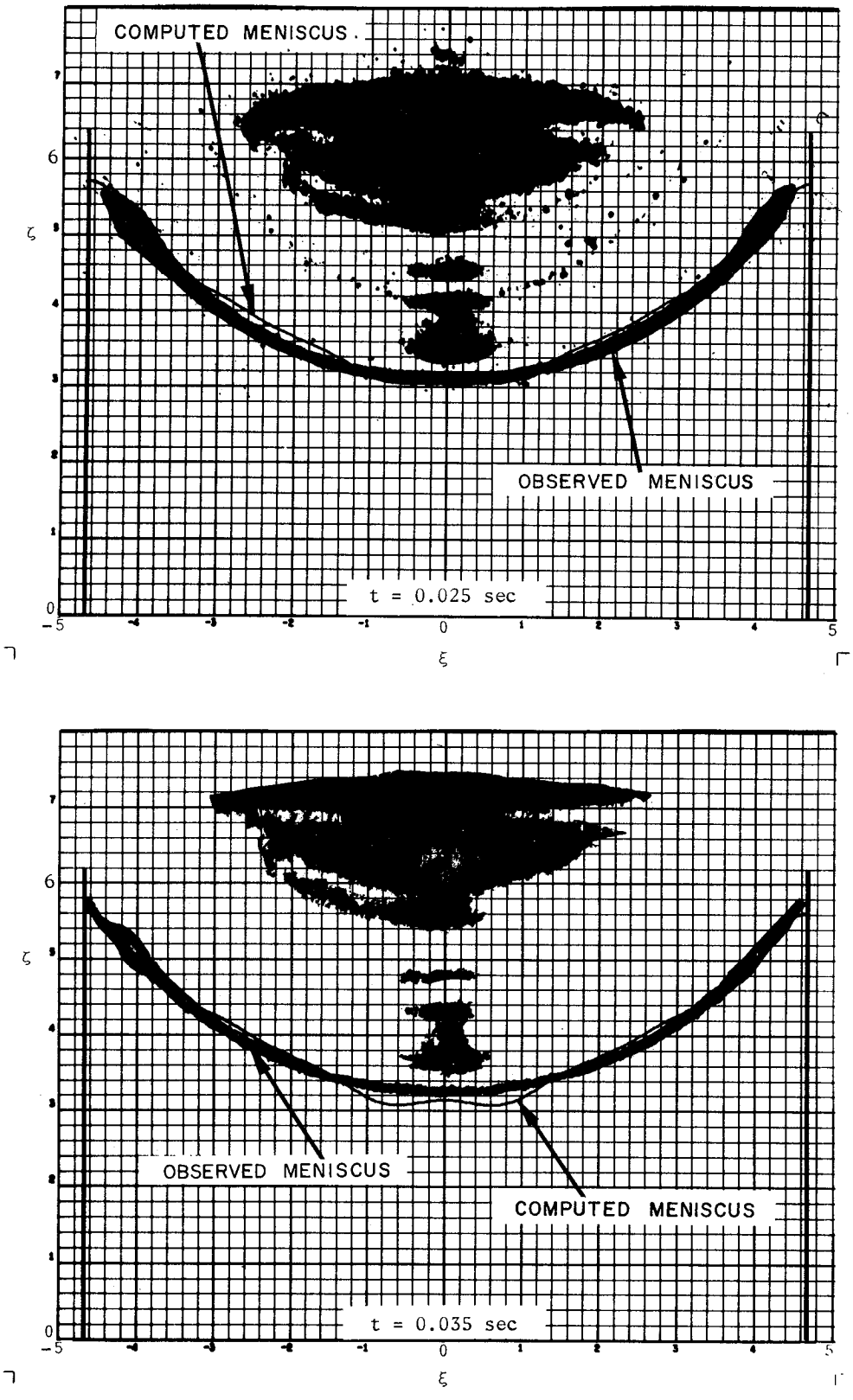
COMPUTED MENISCUS
OBSERVED MENISCUS
t = 0.025 sec
ζ
ξ
OBSERVED MENISCUS
COMPUTED MENISCUS
t = 0.035 sec
ζ
ξ

FIGURE 24 c

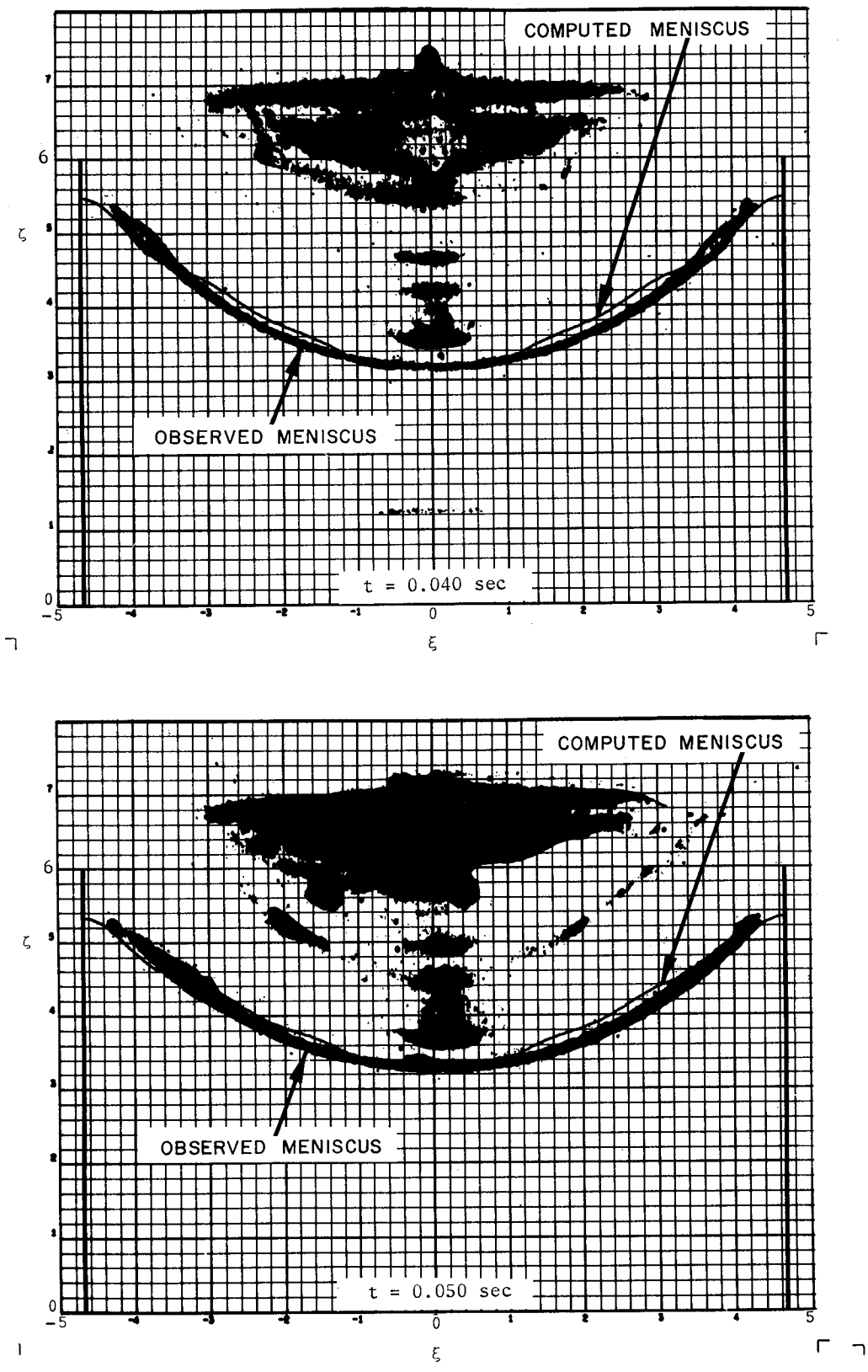
COMPUTED MENISCUS
OBSERVED MENISCUS
t = 0.040 sec
ζ
ξ
COMPUTED MENISCUS
OBSERVED MENISCUS
t = 0.050 sec
ζ
ξ

FIGURE 24 d

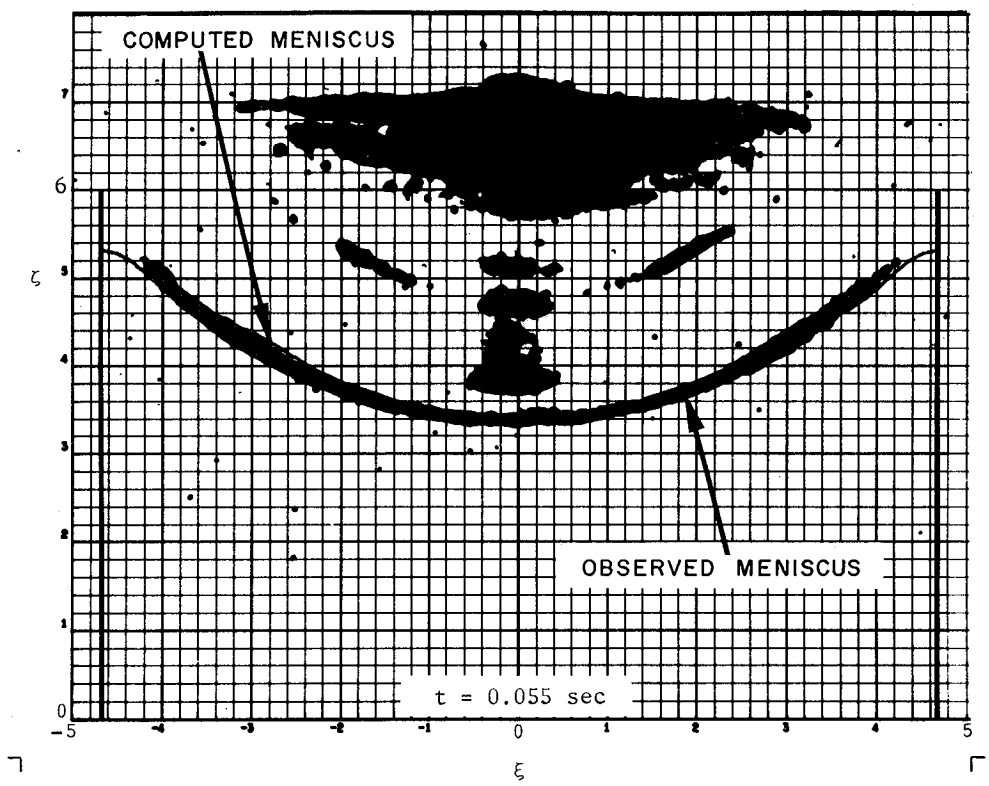
COMPUTED MENISCUS
OBSERVED MENISCUS
t = 0.055 sec
ζ
ξ

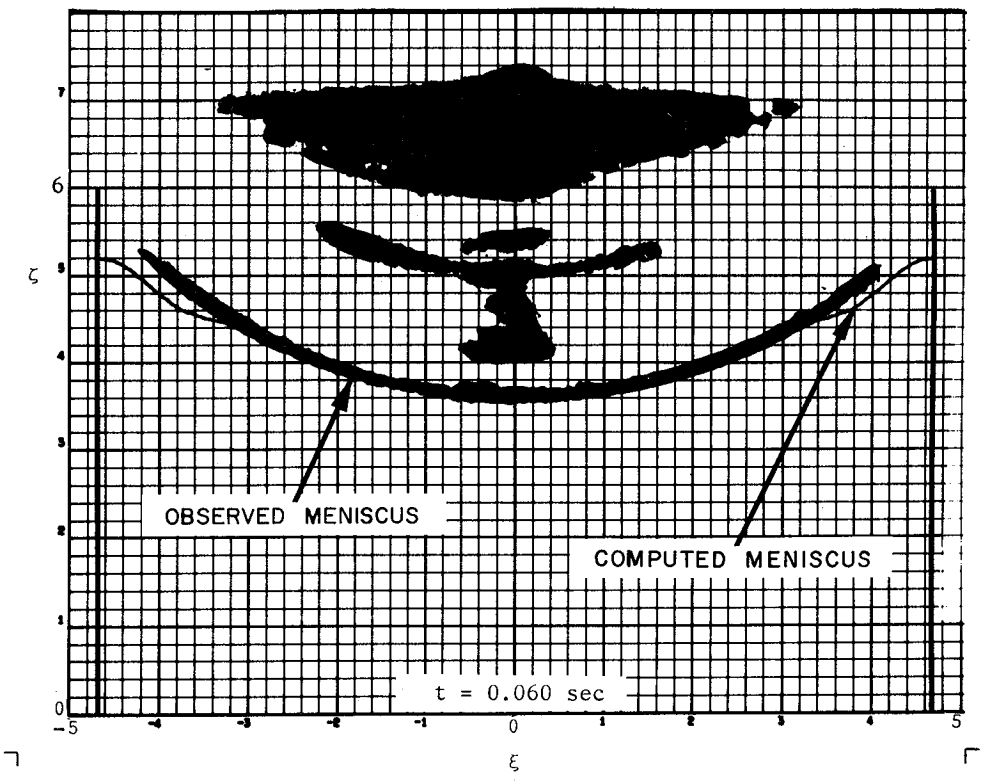
OBSERVED MENISCUS
COMPUTED MENISCUS
t = 0.060 sec
ζ
ξ

FIGURE 24e

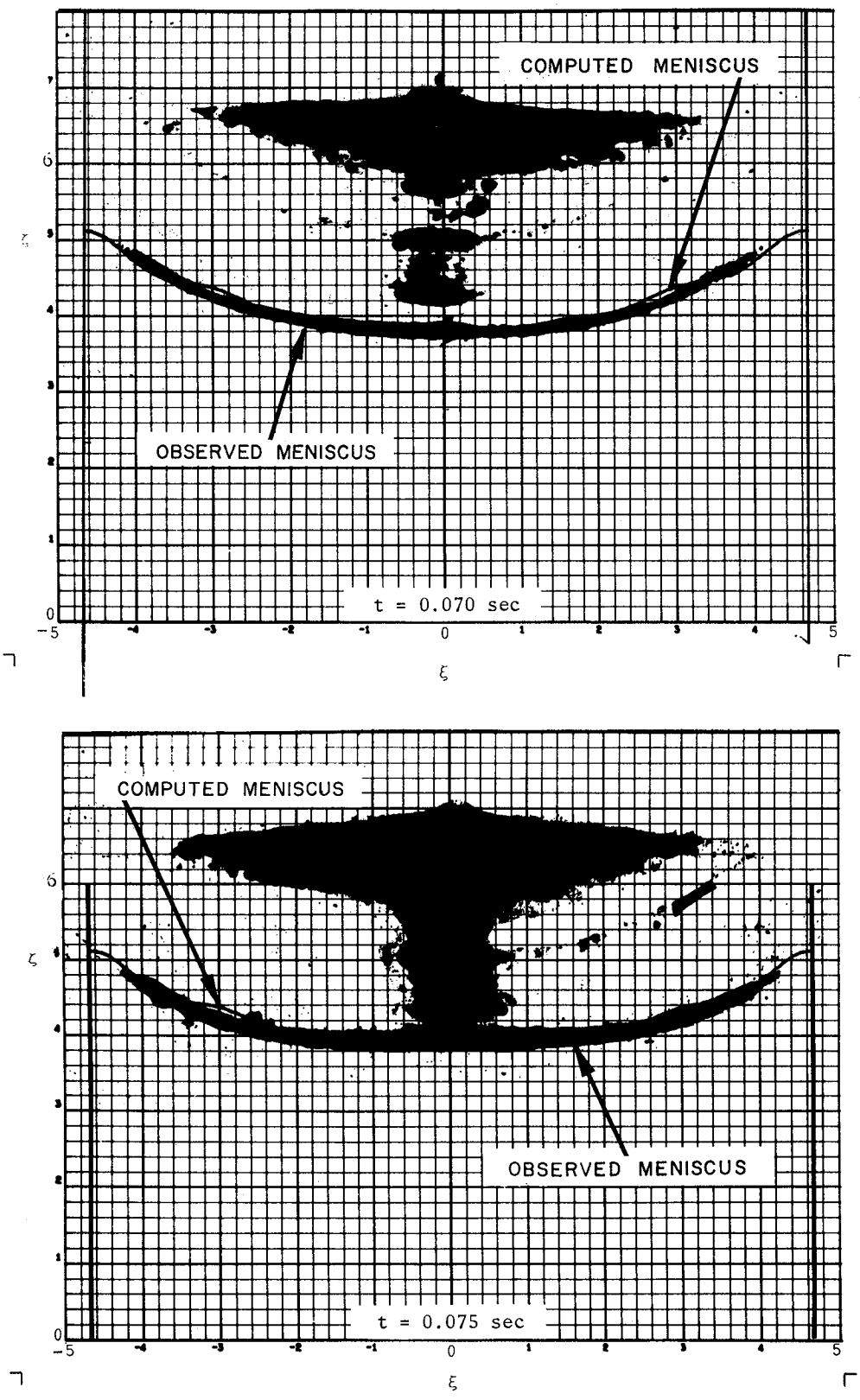
COMPUTED MENISCUS
OBSERVED MENISCUS
t = 0.070 sec
ζ
ξ
COMPUTED MENISCUS
OBSERVED MENISCUS
t = 0.075 sec
ζ
ξ

FIGURE 24f

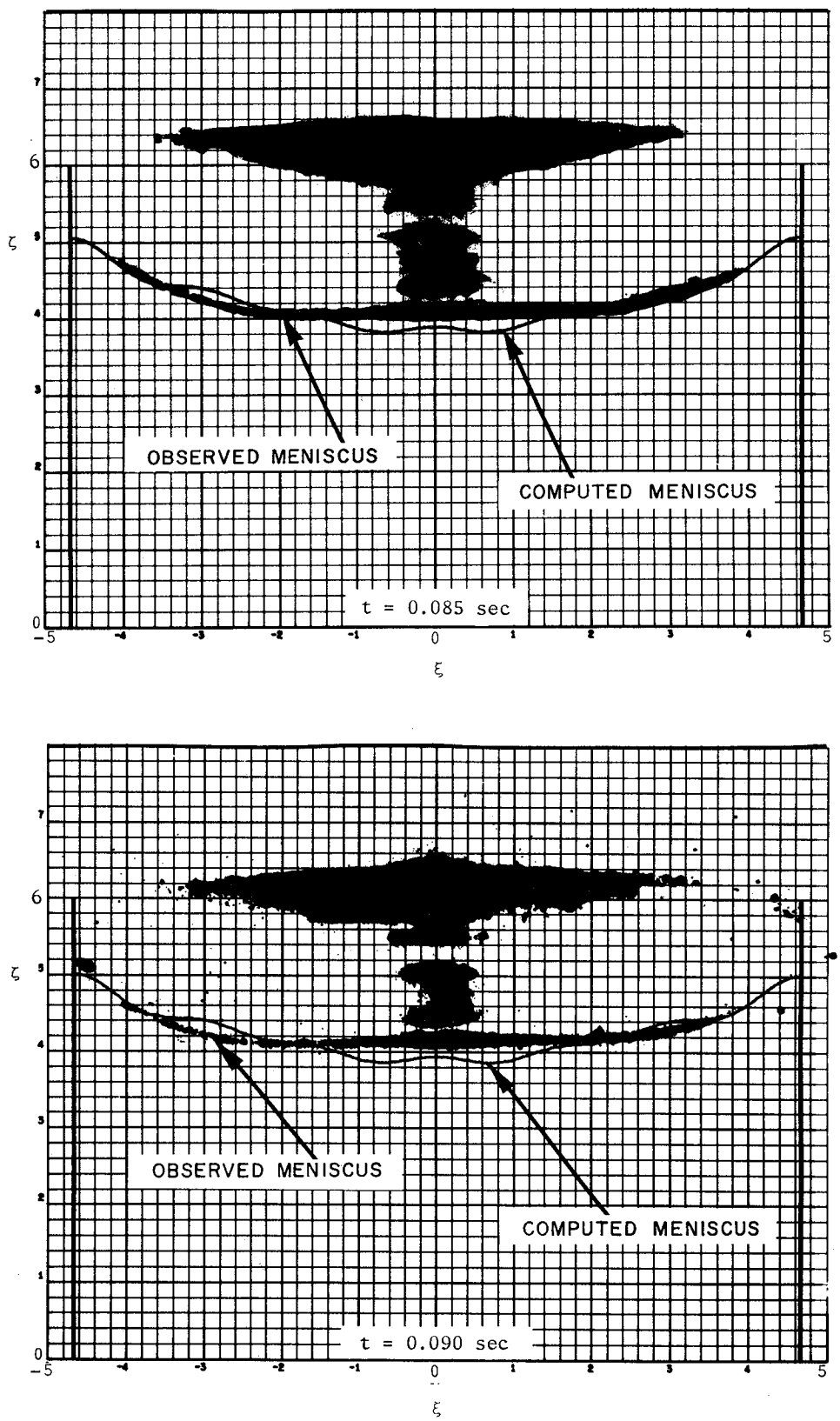
OBSERVED MENISCUS
COMPUTED MENISCUS
t = 0.085 sec
t = 0.090 sec
ζ
ξ

FIGURE 24g

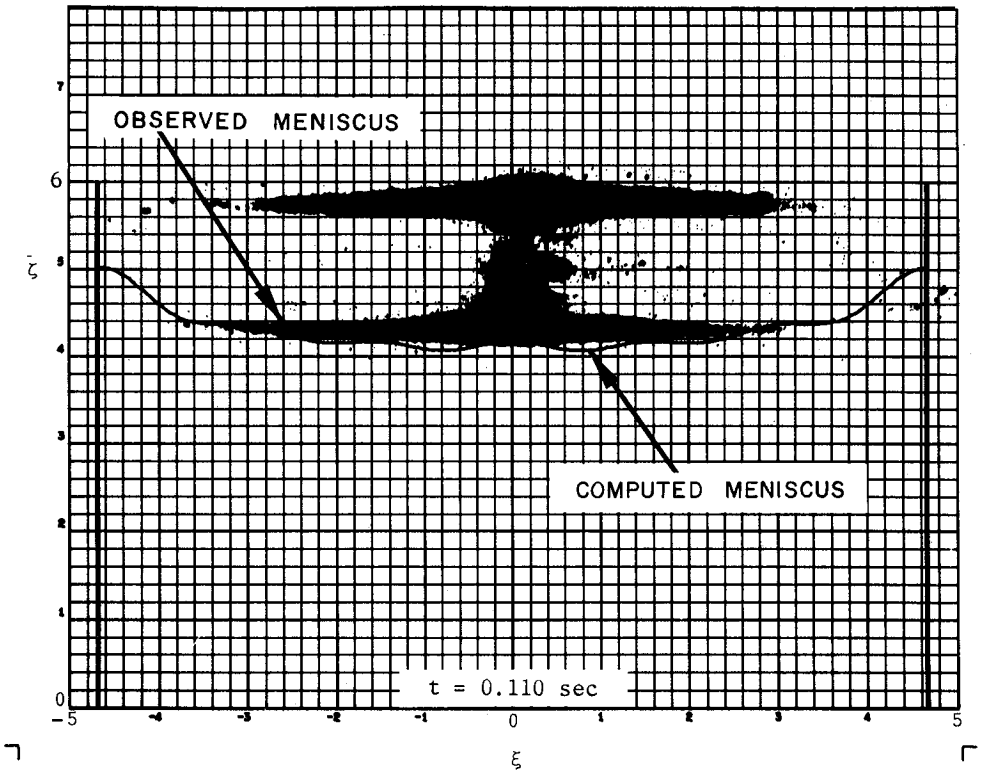
OBSERVED MENISCUS
COMPUTED MENISCUS
t = 0.110 sec
ζ
ξ

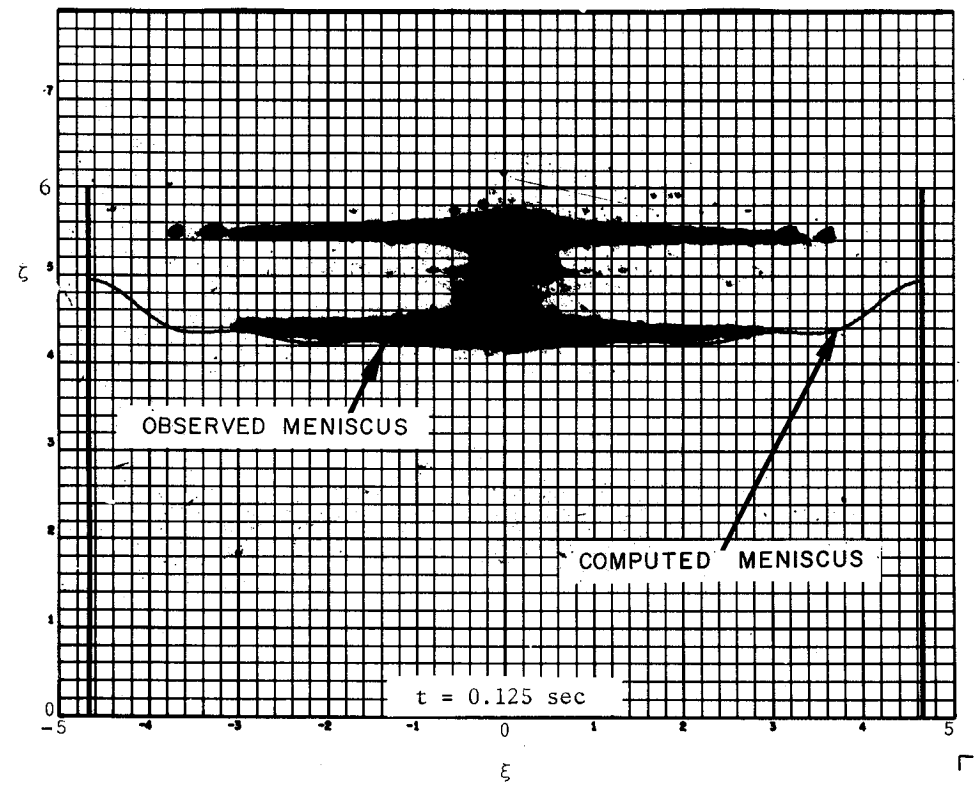
OBSERVED MENISCUS
COMPUTED MENISCUS
t = 0.125 sec
ζ
ξ

FIGURE 24 h

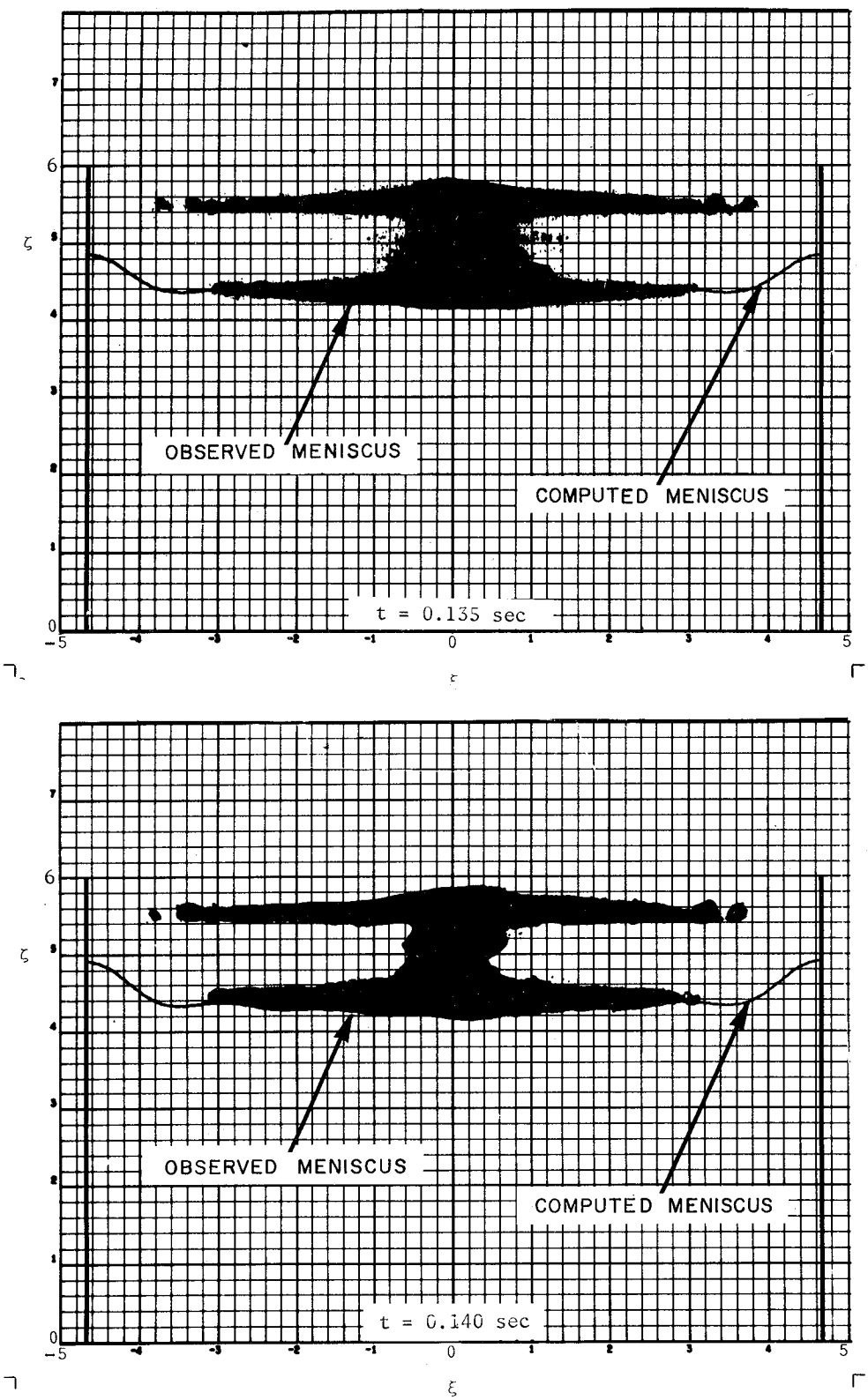

LIQUID CONFIGURATION AT TERRESTRIAL GRAVITY

FIGURE 24 i

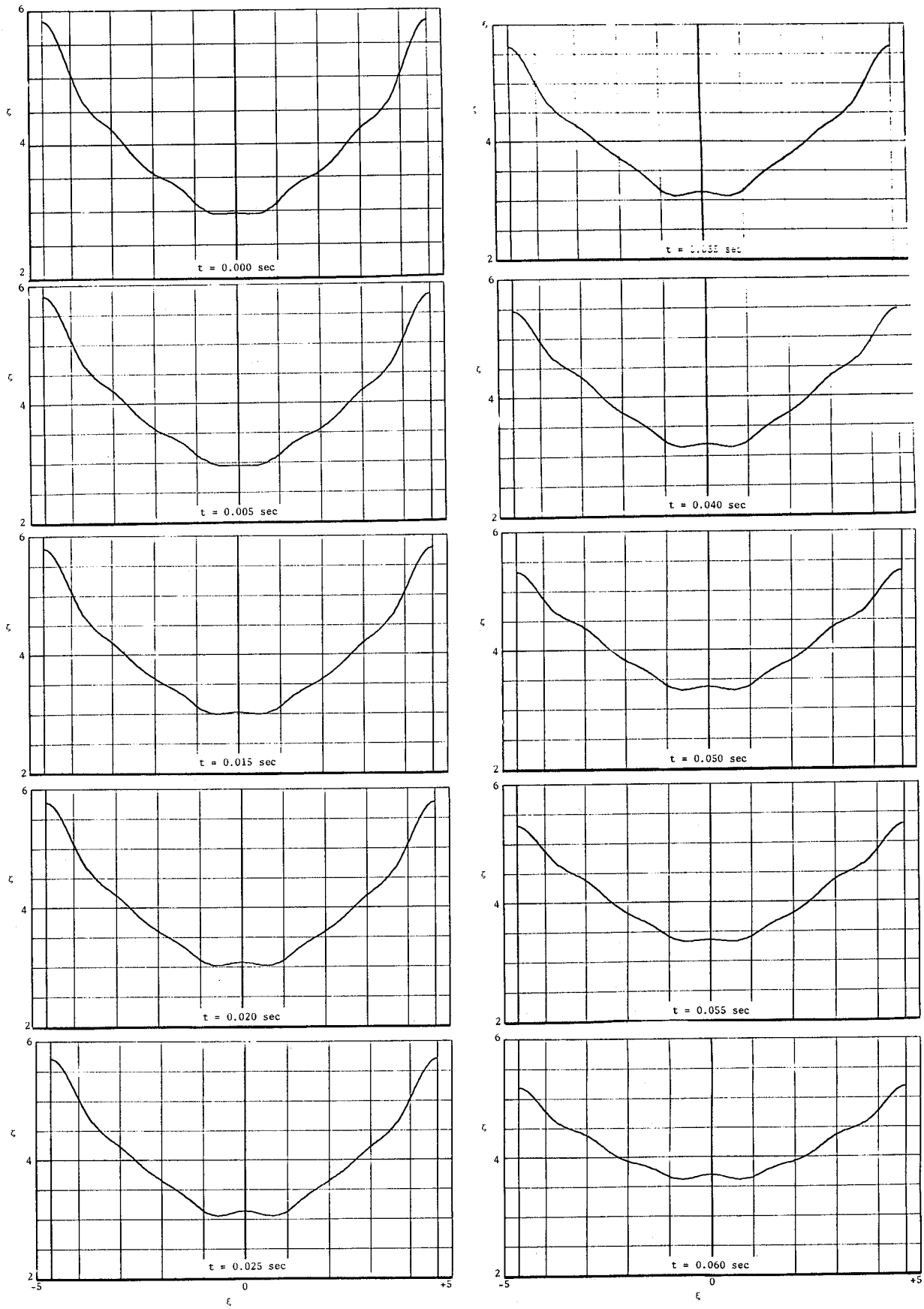
t = 0.000 sec
t = 0.005 sec
t = 0.015 sec
t = 0.020 sec
t = 0.025 sec
t = 0.035 sec
t = 0.040 sec
t = 0.050 sec
t = 0.055 sec
t = 0.060 sec
ζ
ξ
6
4
2
-5
0
+5

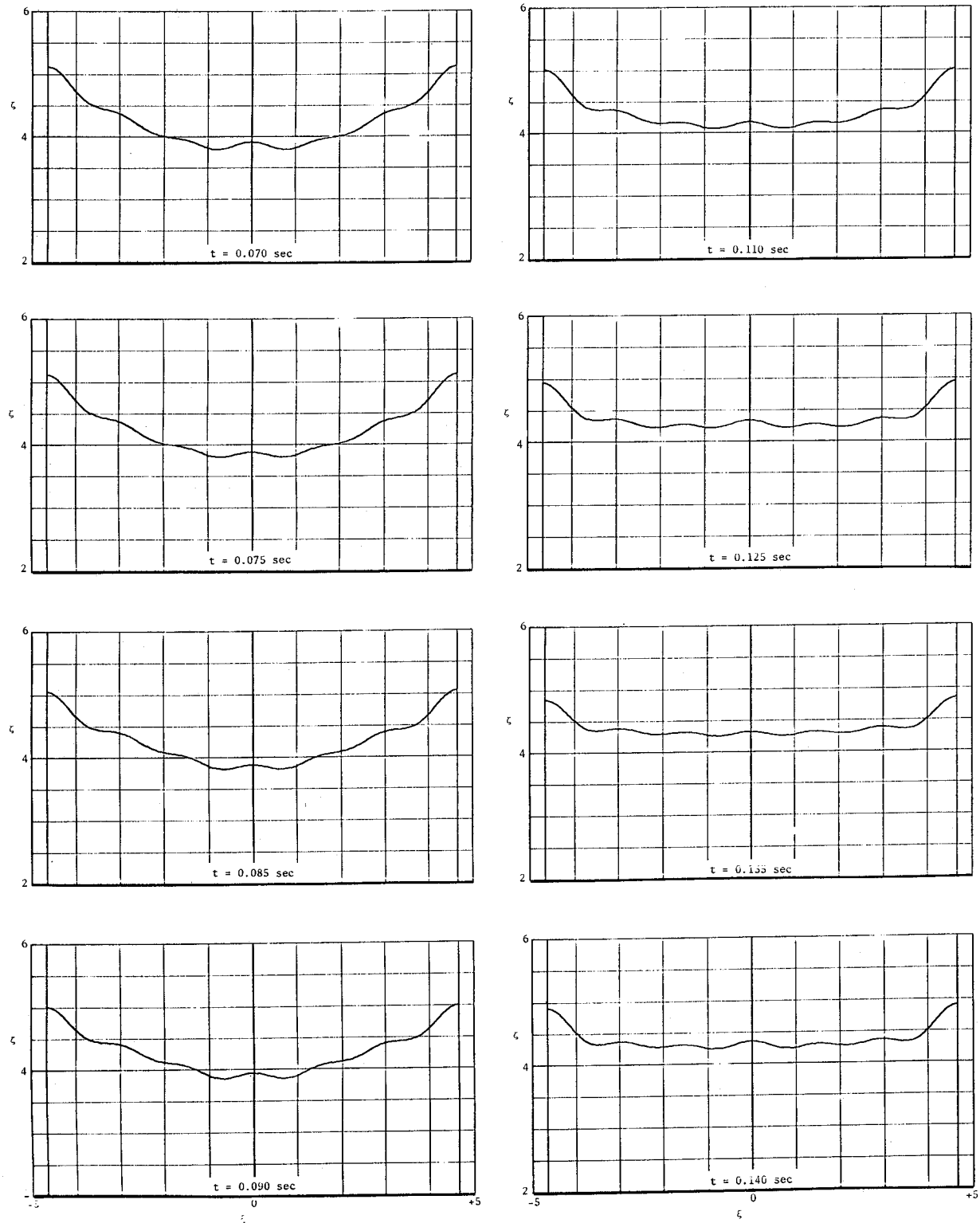

Figure 25. Computed Menisci Used for Comparisons in Figure 24
(2 Sheets)

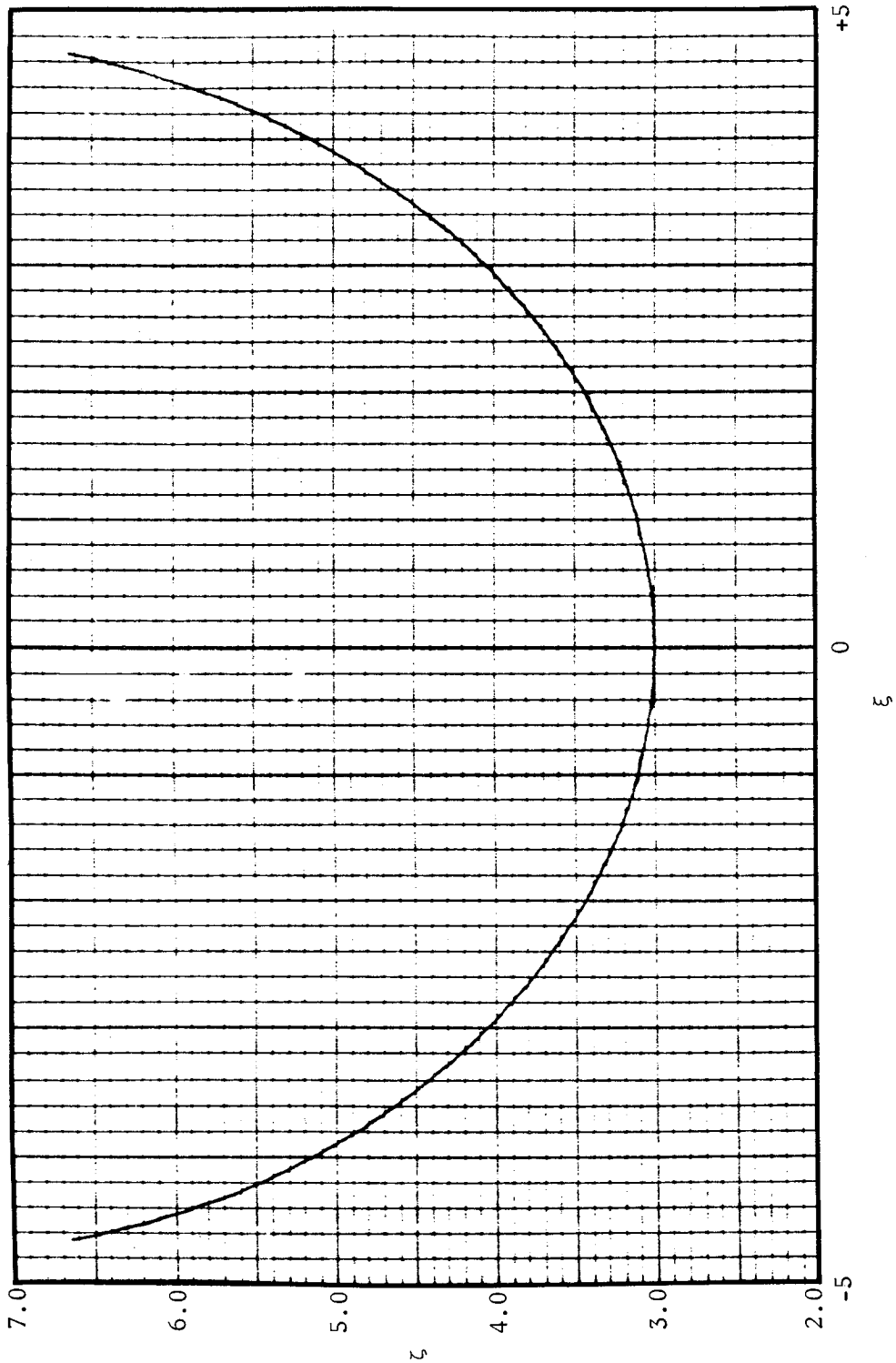

Figure 26. Surface Configuration at Zero g, Computed With an Error of Less Than One Percent

PRECEDING PAGE BLANK NOT FILMED.

Figure 27

Surface Configuration During Drop Test

The photographs on the following sixteen pages show the behavior of the specimen liquid during the transition from normal to zero gravity for various values of the time, t, reckoned from the instant of activation of the platform release solenoid.

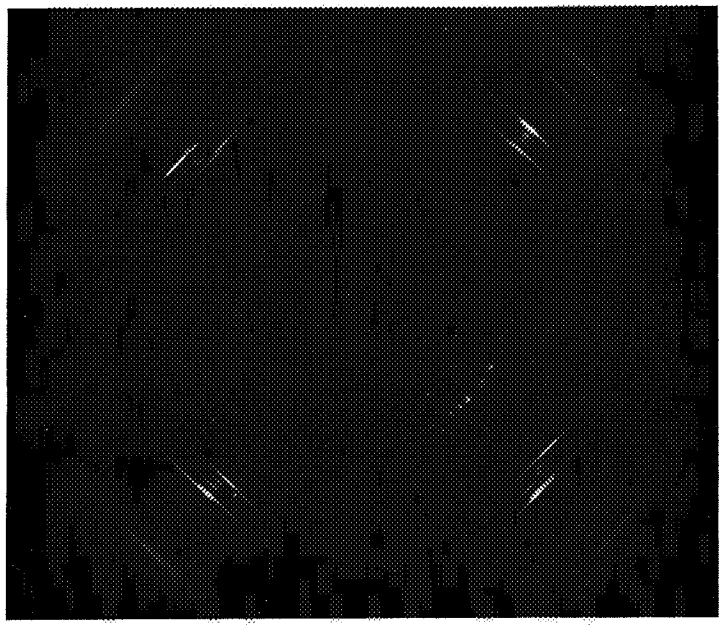

t = 0.000 second
(Initial Conditions, Normal Terrestrial Gravity)

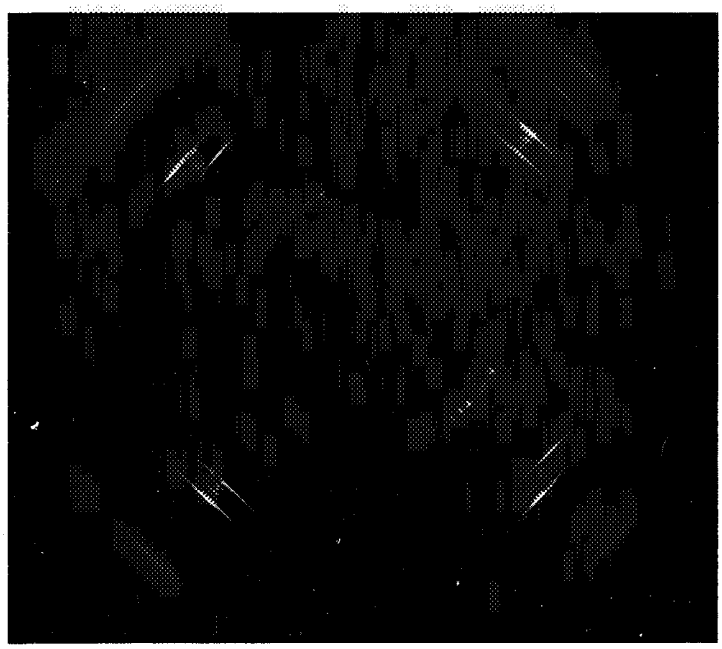

t = 0.005 second

FIGURE 27 a

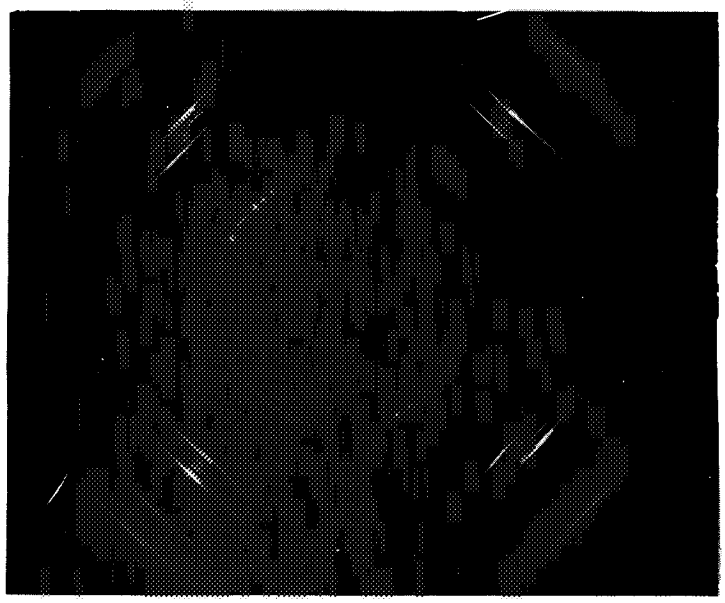

t = 0.010 second

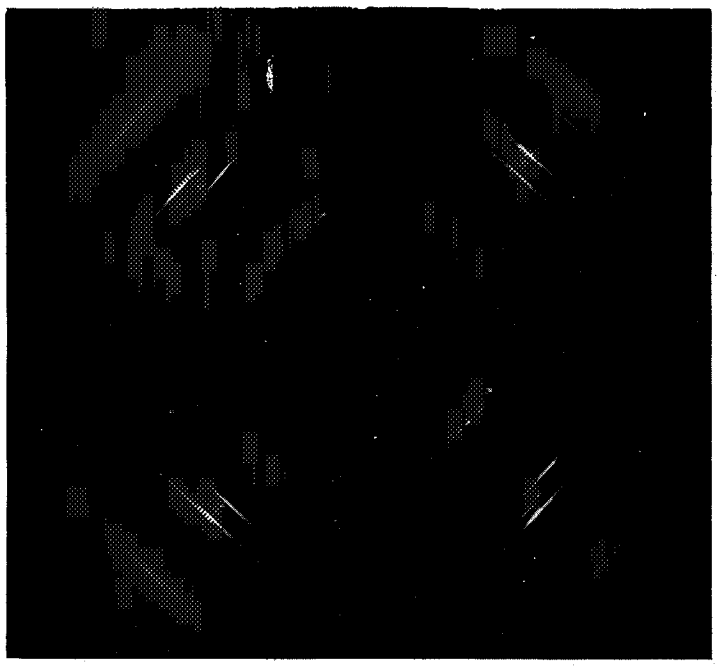

t = 0.015 second

FIGURE 27 b

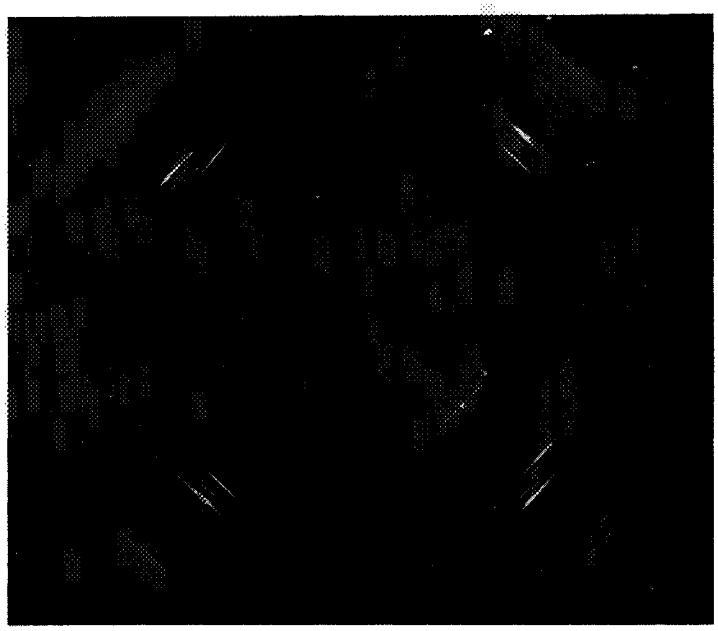

t = 0.020 second

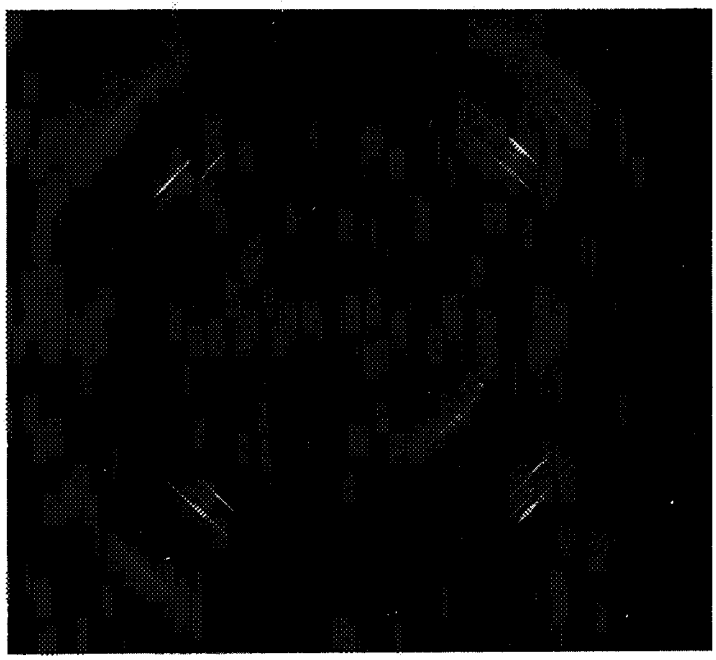

t = 0.025 second

FIGURE 27c

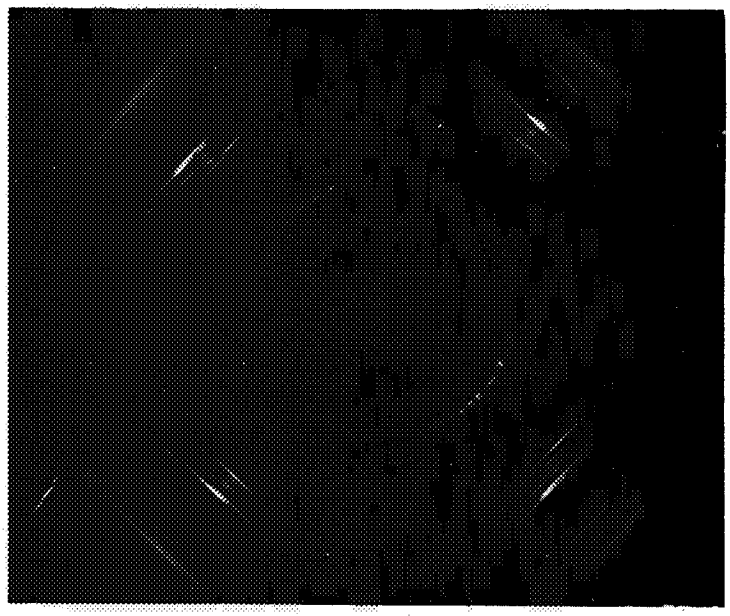

t = 0.030 second

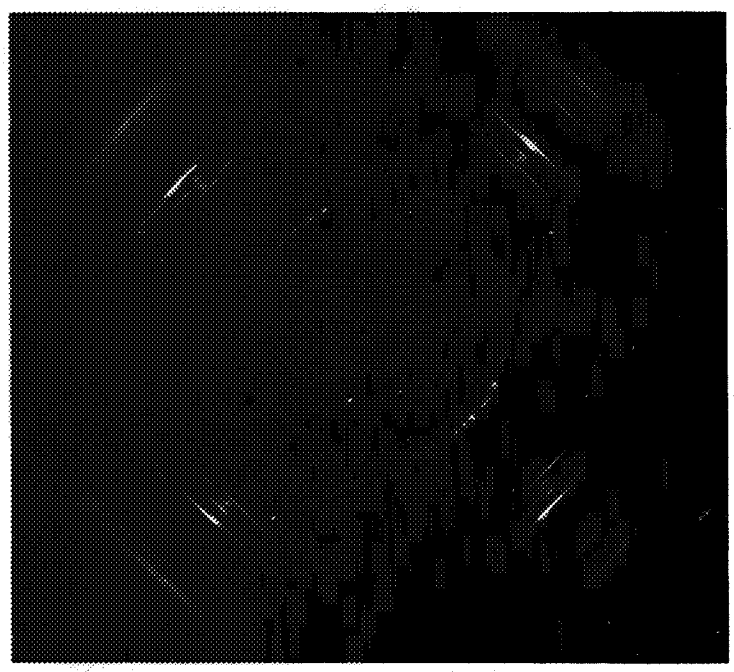

t = 0.035 second

FIGURE 27 d

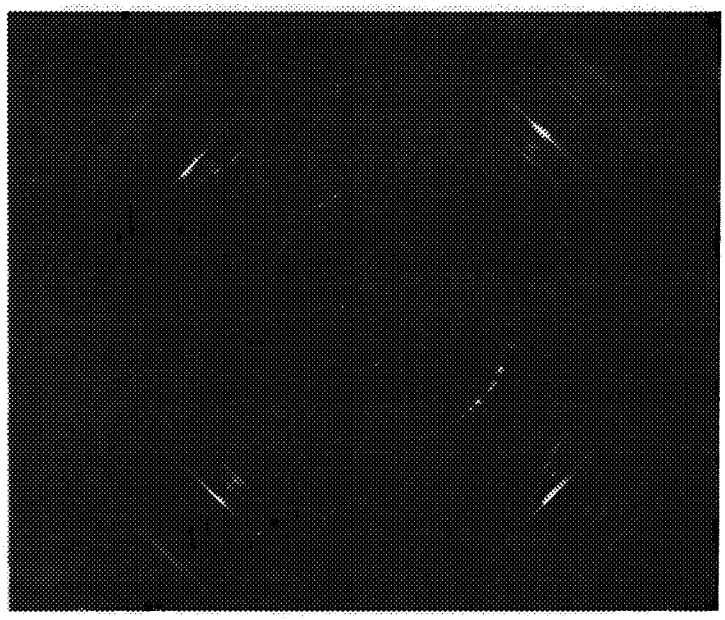

t = 0.040 second

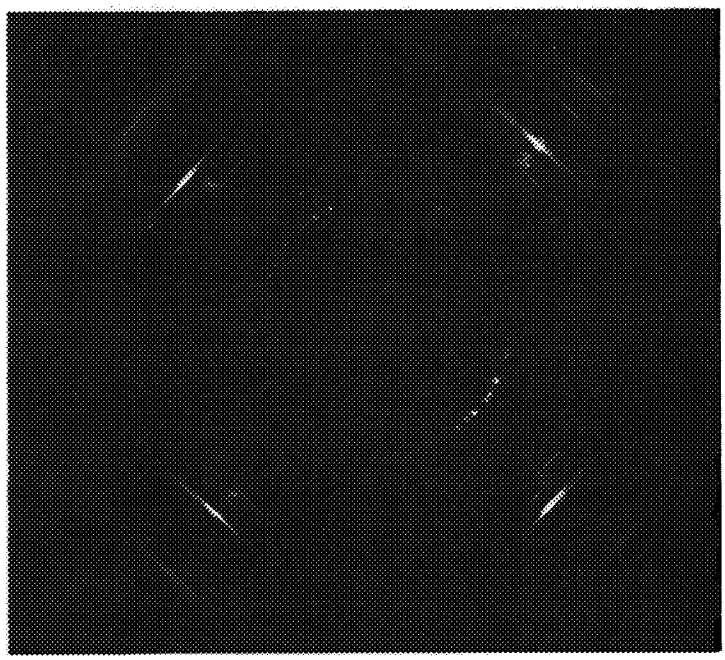

t = 0.045 second

FIGURE 27e

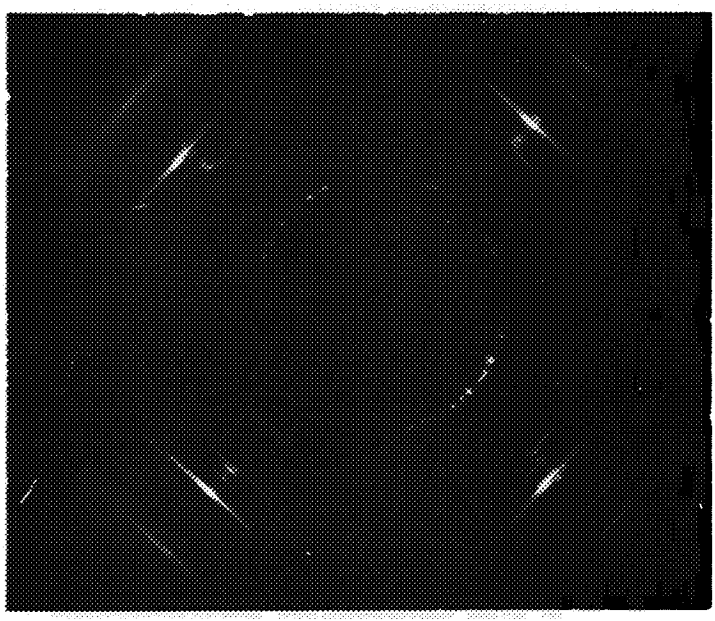

t = 0.050 second

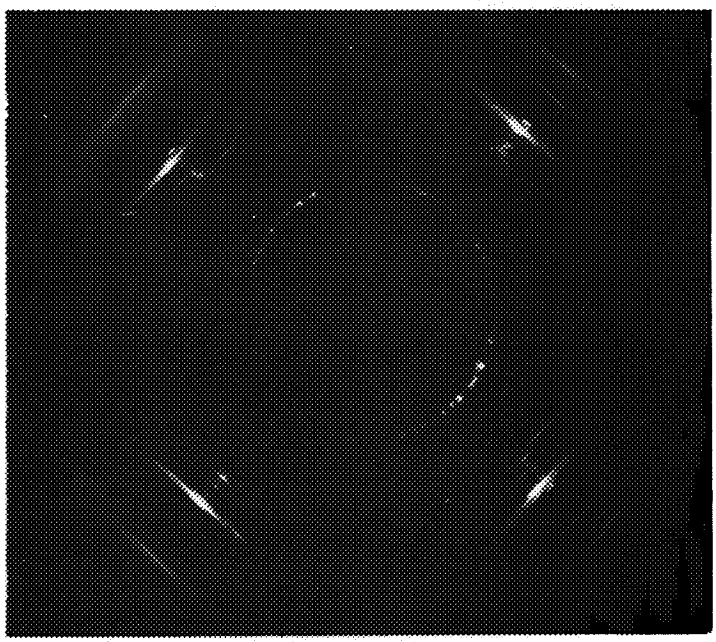

t = 0.055 second

FIGURE 27 f

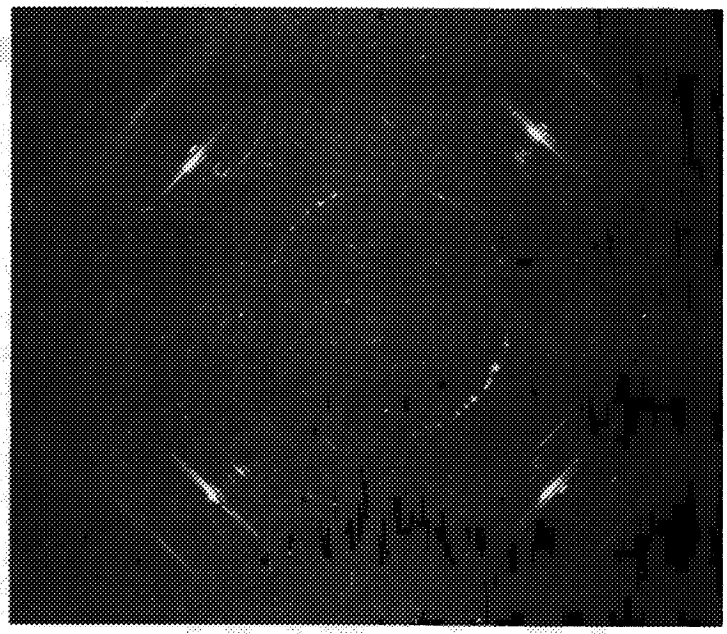

t = 0.060 second

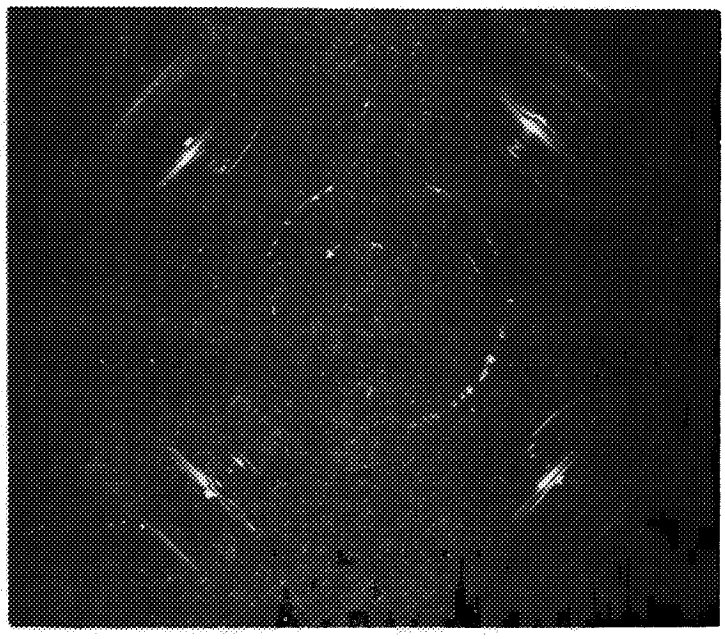

t = 0.065 second

FIGURE 27 g

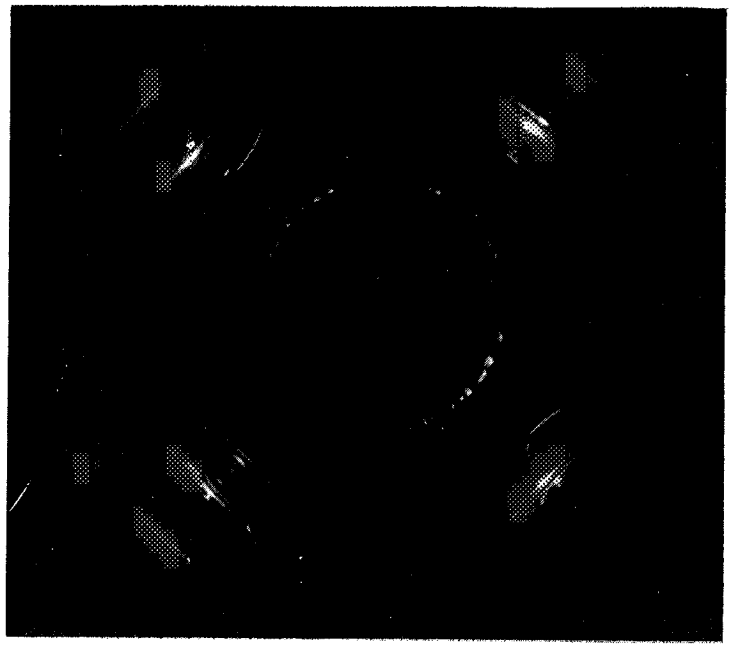

t = 0.070 second

t = 0.075 second

FIGURE 27 h

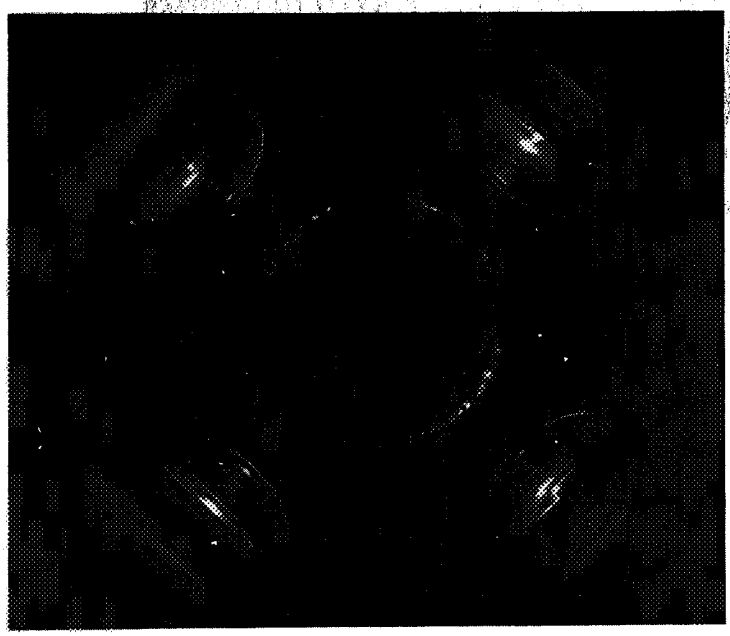

t = 0.080 second

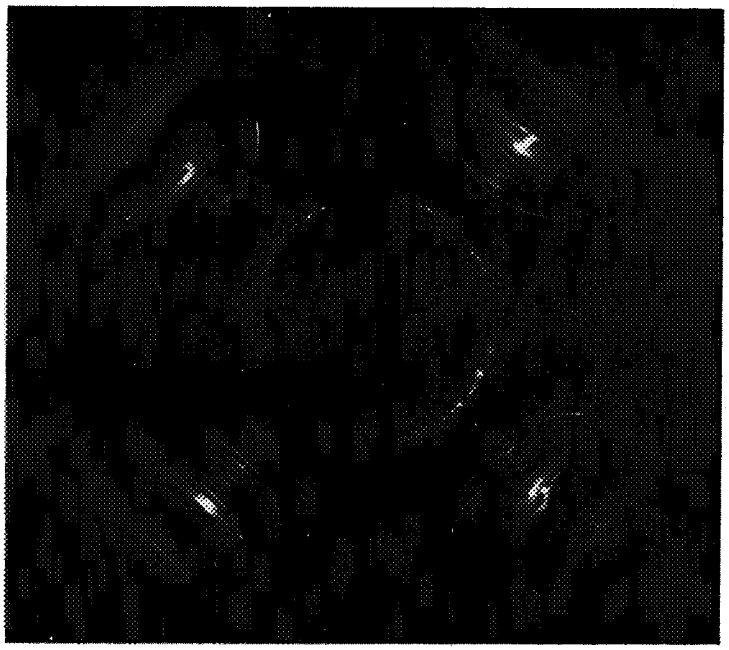

t = 0.085 second

FIGURE 27 i

t = 0.090 second

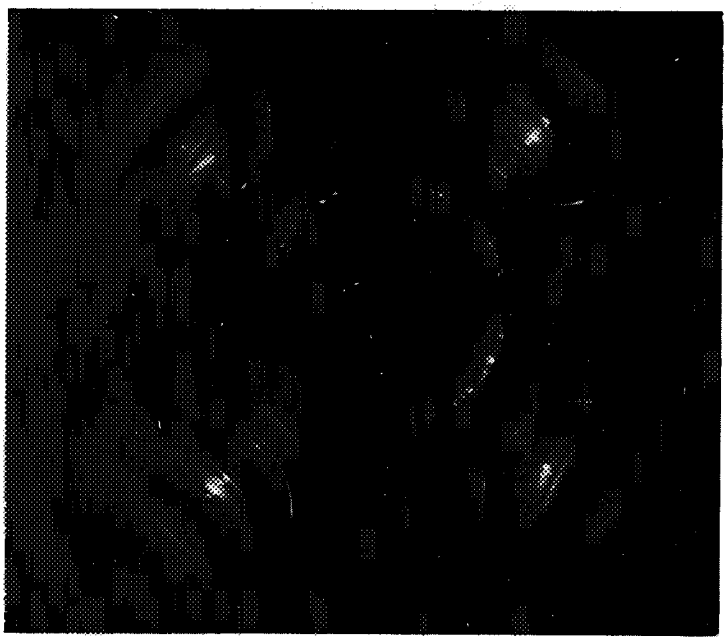

t = 0.095 second

FIGURE 27j

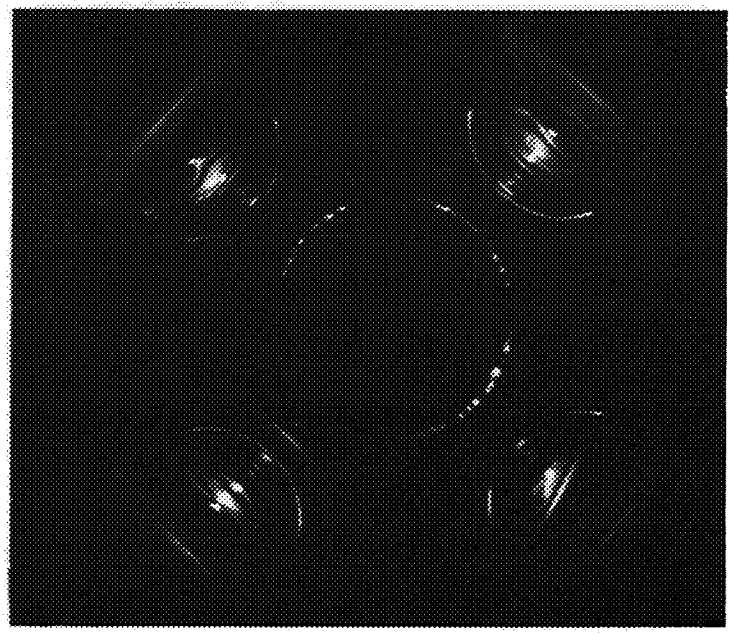

t = 0.100 second

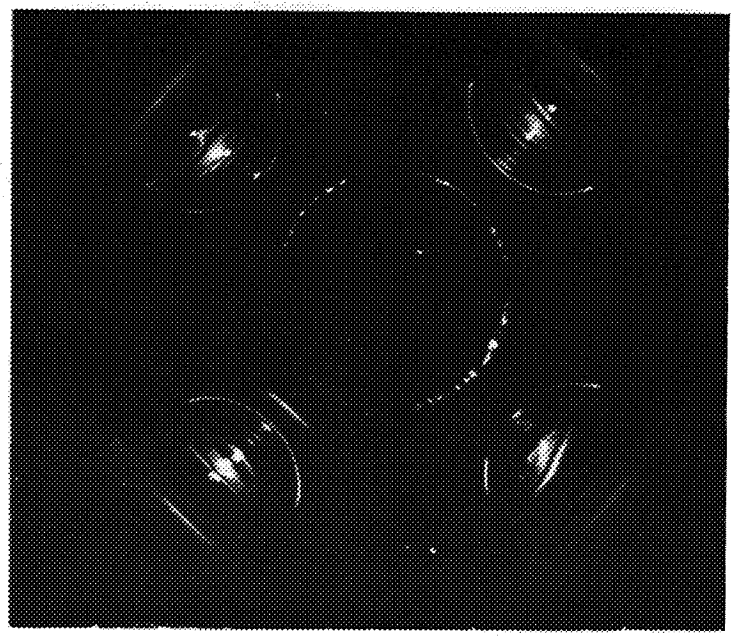

t = 0.105 second

FIGURE 27k

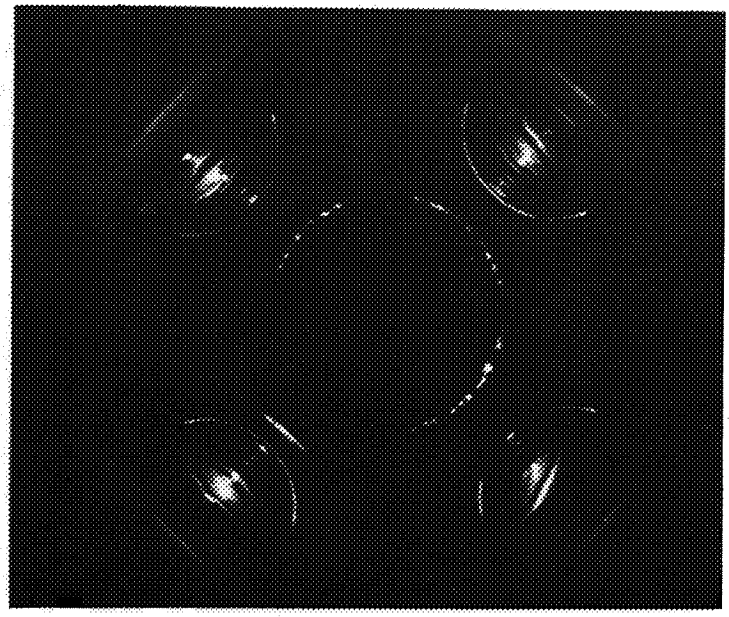

t = 0.110 second

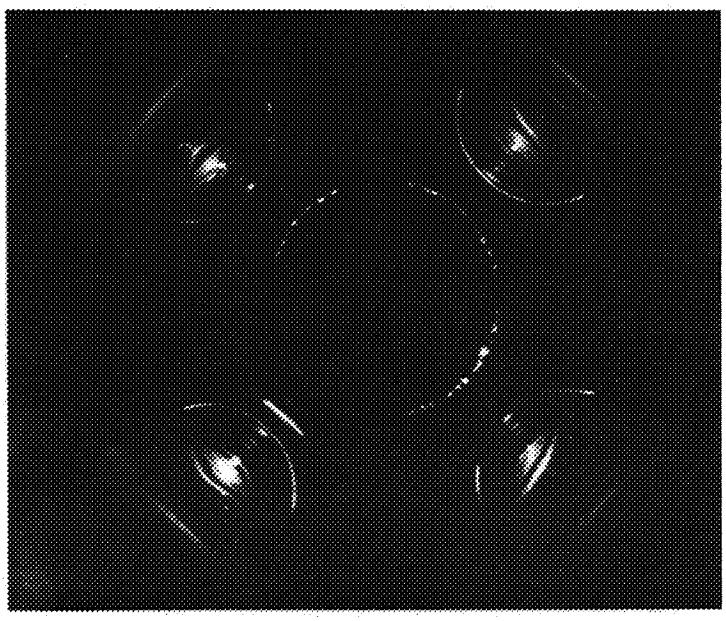

t = 0.115 second

FIGURE 27 1

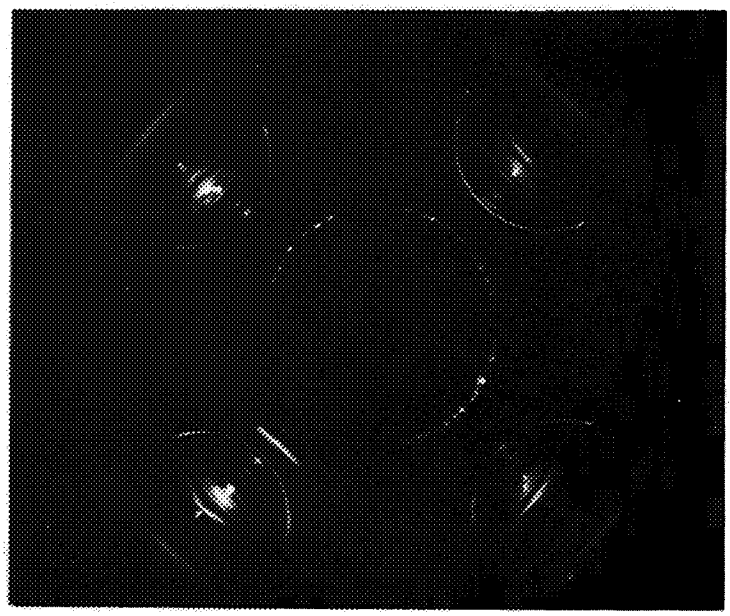

t = 0.120 second

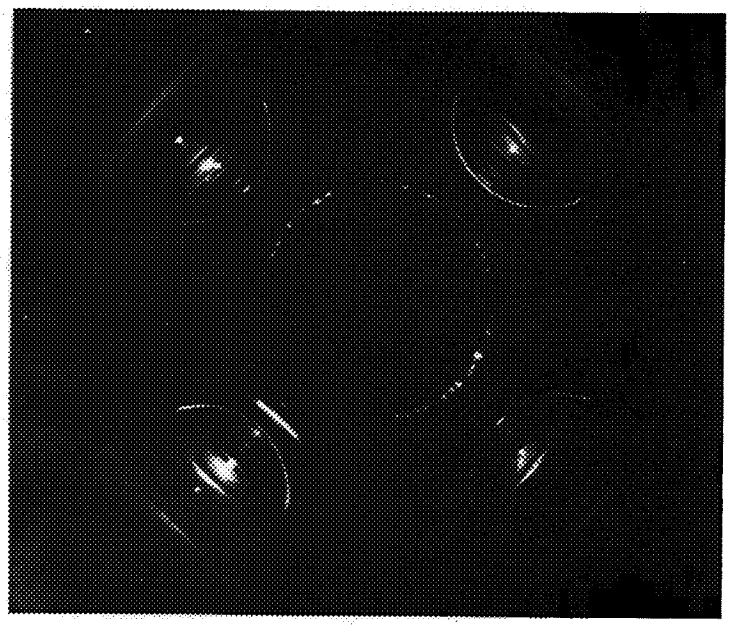

t = 0.125 second

FIGURE 27m

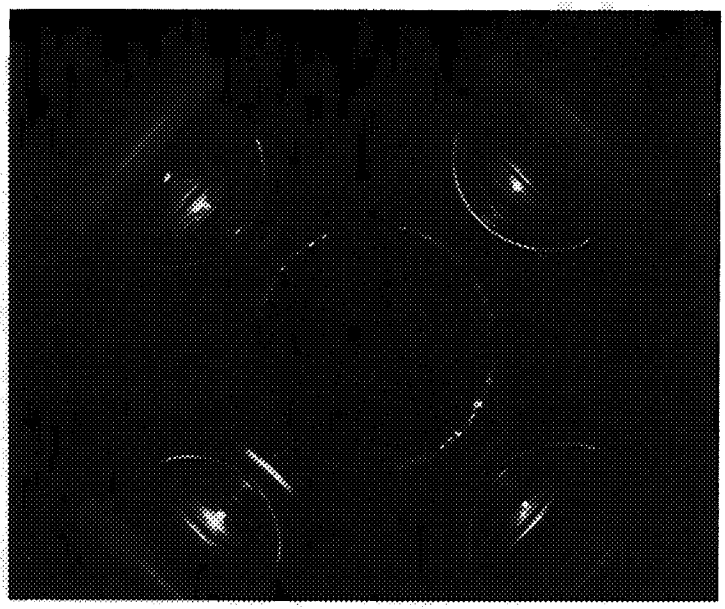

t = 0.130 second

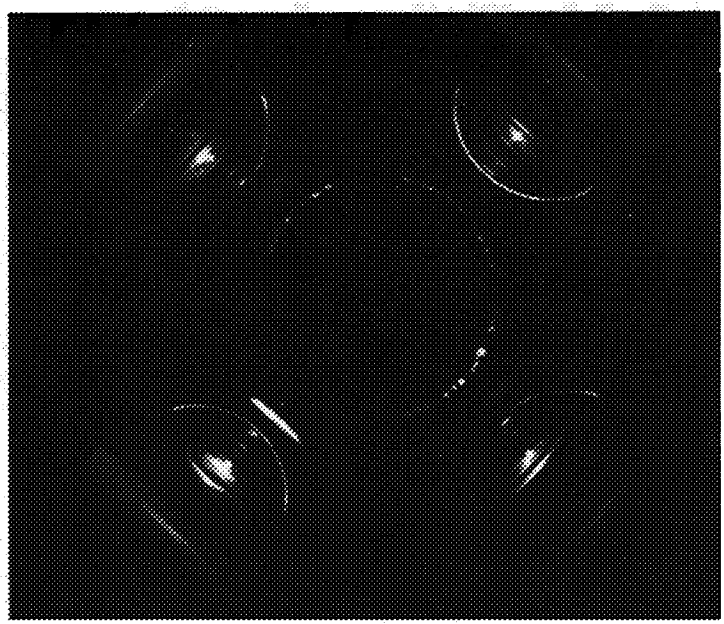

t = 0.135 second

FIGURE 27 n

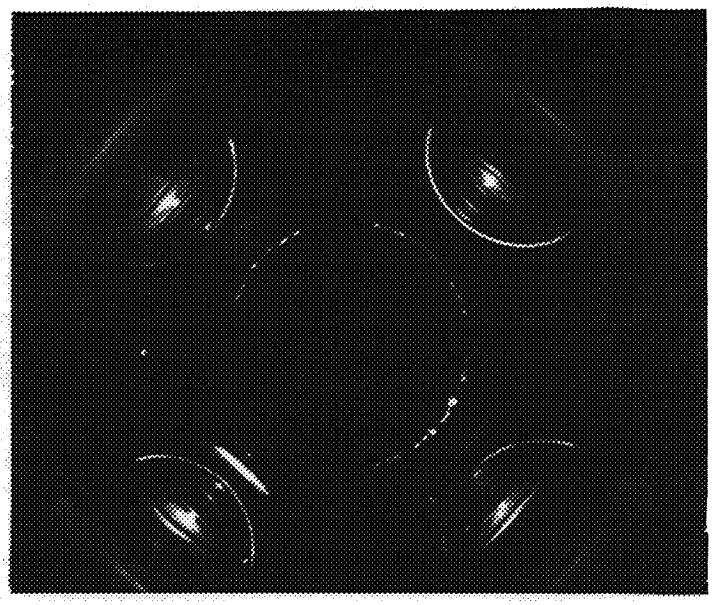

t = 0.140 second
(Zero Gravity Configuration)

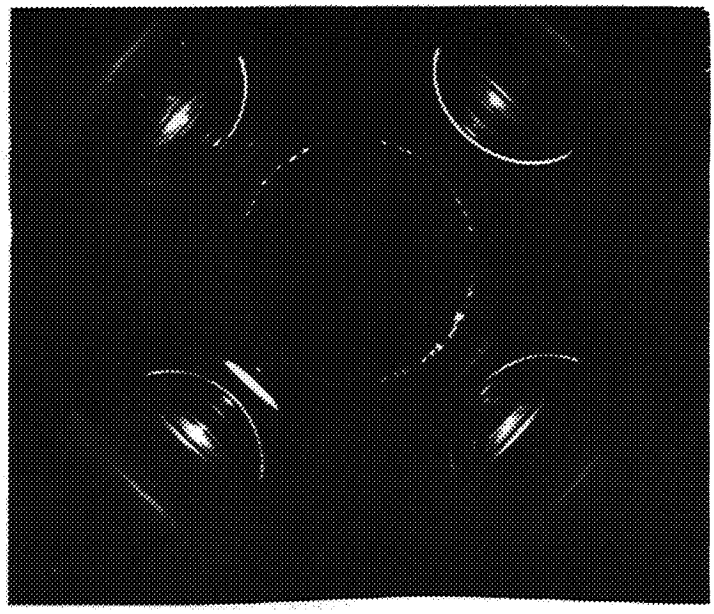

t = 0.145 second

FIGURE 27 o

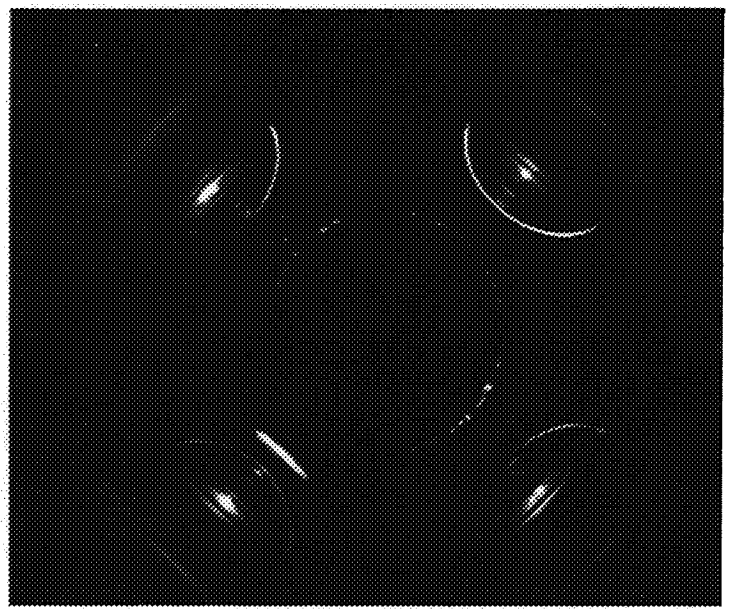

t = 0.150 second

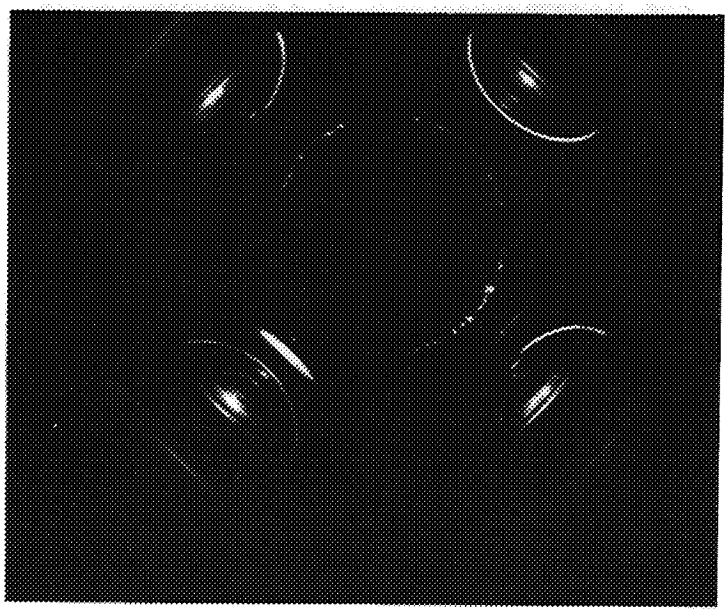

t = 0.155 second

FIGURE 27 p

CONCLUSIONS

The numerical and experimental results obtained were shown in Figures 24, 25, 26, and 27. Figure 24 consists of CRT plots of the numerically computed free surface configurations[1] expressed in the nondimensional variables ξ, ζ,[2] with the appropriate experimental surfaces superimposed upon them. From these curves, it appears that a comparison of experimental and computed results provides, within the computational accuracy maintained (5 percent), satisfactory agreement. It should be pointed out that when the initial equilibrium configuration, computed to an accuracy of less than one percent (Figure 26), is compared with the experimentally determined zero-g curve, exact agreement is attained. As a matter of fact, the value of the angle of contact (14 degrees) used in the computations is rigorously attained at the solid boundaries and, as shown in the previous analysis, is independent of the time. However, in the computed curves shown in Figures 24 and 25, this value does not appear to be attained at the solid boundaries due to an accumulation of truncation errors. The discrepancy is, in fact, an exact measure of the total error incurred.

It is interesting to note, from both the experimental and computed curves, that only a slight deformation occurs during the first quarter cycle. More precisely, the experimental curves[3] (Figures 24 and 27) indicate that the surface deformation is small during both the first and last quarters of the transition cycle, the major deformation occurring during the period 0.05 second to 0.09 second. The computed curves were, of course, determined to be within the prescribed accuracy in this region thereby ensuring complete verification of the mathematical procedure.

---

[1] These menisci are obtained using the zero-g configuration, for which we have an exact analytical expression, as an initial curve; thus, the time is reckoned from this point. The nondimensional variables are defined to be

$$\xi = r/\ell$$

$$\zeta = z/\ell$$

$$\text{where} \quad \ell = \sqrt{\epsilon/\rho n g_o} = \ell_o/\sqrt{n}$$

[2] Obtained by the method outlined at the end of the preceding section.

[3] An interesting feature of the photographs shown in Figure 27 is that the transition times from one to zero g (0.14 section) verifies the prediction based on the scaling laws derived in References 1 and 2.

To summarize, it appears that the mathematical method previously developed for the integration of the equations of epihydrodynamics is capable of providing (1) the time history of the free surface of a partially bounded liquid, (2) a method for prediction of the kinematics of liquids under low-gravity conditions, and (3) the solution to the low-g sloshing of liquids subjected to lateral and axial time-dependent forced translations.

REFERENCES

1. Benedikt, E. T. General Behavior of a Liquid in a Zero or Near Zero Gravity Environment, Weightlessness - Physical Phenomena and Biological Effects, Proceedings of the Symposium on Physical and Biological Phenomena Under Zero-g Conditions, Plenum Press, New York (1961).

2. Benedikt, E. T. Scale of Separation Phenomena in Liquids Under Conditions of Nearly Free Fall, J. Amer. Rocket Soc., 29 (1959).

3. Benedikt, E. T. and R. Lepper. Experimental Production of a Zero or Near Zero Gravity Environment, J. Amer. Rocket Soc., 29 (1959).

4. Benedikt, E. T. Production of a Near-Zero Gravity Environment in Rapid Falling Systems, Technical Memorandum of the Astro Sciences, ASG-TM-61-47, Northrop Corp. (June 1961).

5. Bendat, J.S., et al. Formulation and Numercial Solution of the Equations of Epihydrodynamics, Measurements Analysis Corporation report MAC512-02A (December 1965).

6. Propellant Behavior in Zero Gravity, Final Report, Contract No. NAS8-11097, NAA Report SID 64-1989 (2 November 1964).

7. Clark, John A. and Herman Merte, Jr. "Nucleate Transition and Film Boiling Heat Transfer at Zero Gravity," Physical and Biological Phenomena in a Weightless State, in Vol. 14, Advances in Astronautics, Edited by E. T. Benedikt and R. W. Halliburton, Los Angeles: Western Periodicals (1963).

8. Adelberg, M. and R. Jetter. "Effect of Gravity Upon Nucleate Boiling," Physical and Biological Phenomena in a Weightless State, in Vol. 14, Advances in Astronautics, Edited by E. T. Benedikt and R. W. Halliburton, Los Angeles: Western Periodicals (1963).

A STUDY OF PROPELLANT BEHAVIOR AT ZERO GRAVITY - FINAL REPORT, SID 66-286 (CONTRACT NAS8-11097)

ERRATA

1. Page 4, Equation (1-4), right-hand term should read $\frac{1}{2}\rho g_o \bar{z} \mathcal{V}$.

2. Page 5, footnote should indicate cube root: $\sqrt[3]{V/4\pi/3}$.

3. Page 10, first equation, last term should read $\lambda \dot{\mathcal{V}}$.

4. Page 11, third term on right-hand side of Equation (1-14) should read $+ \rho n g_o [\bar{z}]_*$.

5. Page 11, second equation, right-hand side should read $\vec{u}^o$.

6. Page 16, second equation, fraction in right-hand term should read $\frac{1}{\lambda_k}$.

7. Page 16, Equation (2-7'), numerator of fraction should read $2\lambda_j$.

8. Page 17, Equation (2-8'), delete sub-sub 1 from last λ_k term.

9. Page 20, Equation (2-15), insert term 2π at beginning, ahead of summation symbol.

10. Page 21, Equation (2-16), insert term 2π immediately following equal sign, ahead of summation symbol.

11. Page 21, first term on second line of Equation (2-16) should begin with λ_k (delete sub-h).

12. Page 21, Equation (2-18'), numerator of fraction should read $2\lambda_j$.

13. Page 22, right-hand term of first equation should read a_k/ℓ.

14. Page 24, Equation (2-27), numerator of fraction should read $2\lambda_j$.

15. Page 27, fourth line, numerator of fraction should read $\partial\hat{v}_{ji}$.

16. Page 35, sixth line, $Q_{n\ell}^{(II)(2,2)}$ should read $Q_{n\ell}^{(II)(1,2)}$.

17. Page 39, first line, denominator of first fraction should be ρ (delete P).

18. Page 39, last equation, right-hand term should read $\left(\frac{\partial \beta_{jh}^{(\alpha)}}{\partial A_{ik}^{(\alpha)}} \right)_{t=t_o}$.

19. Page 46, item 1, A Nose Piece, Figure 2 should read Figure 5.

20. Page 65, Figure 23, time from Camera Start to Specimen Cell Released should read 0.6 sec.